

Results of NRC-Sponsored Stellite 6 Aging and Friction Testing

Idaho National Engineering and Environmental Laboratory

**U.S. Nuclear Regulatory Commission
Office of Nuclear Regulatory Research
Washington, DC 20555-0001**



AVAILABILITY OF REFERENCE MATERIALS IN NRC PUBLICATIONS

NRC Reference Material	Non-NRC Reference Material
<p>As of November 1999, you may electronically access NUREG-series publications and other NRC records at NRC's Public Electronic Reading Room at http://www.nrc.gov/reading-rm.html. Publicly released records include, to name a few, NUREG-series publications; <i>Federal Register</i> notices; applicant, licensee, and vendor documents and correspondence; NRC correspondence and internal memoranda; bulletins and information notices; inspection and investigative reports; licensee event reports; and Commission papers and their attachments.</p>	<p>Documents available from public and special technical libraries include all open literature items, such as books, journal articles, and transactions, <i>Federal Register</i> notices, Federal and State legislation, and congressional reports. Such documents as theses, dissertations, foreign reports and translations, and non-NRC conference proceedings may be purchased from their sponsoring organization.</p>
<p>NRC publications in the NUREG series, NRC regulations, and <i>Title 10, Energy</i>, in the Code of <i>Federal Regulations</i> may also be purchased from one of these two sources.</p>	<p>Copies of industry codes and standards used in a substantive manner in the NRC regulatory process are maintained at—</p>
<ol style="list-style-type: none">1. The Superintendent of Documents U.S. Government Printing Office Mail Stop SSOP Washington, DC 20402-0001 Internet: bookstore.gpo.gov Telephone: 202-512-1800 Fax: 202-512-22502. The National Technical Information Service Springfield, VA 22161-0002 www.ntis.gov 1-800-553-6847 or, locally, 703-605-6000	<p>The NRC Technical Library Two White Flint North 11545 Rockville Pike Rockville, MD 20852-2738</p>
<p>A single copy of each NRC draft report for comment is available free, to the extent of supply, upon written request as follows:</p> <p>Address: Office of the Chief Information Officer, Reproduction and Distribution Services Section U.S. Nuclear Regulatory Commission Washington, DC 20555-0001</p> <p>E-mail: DISTRIBUTION@nrc.gov Facsimile: 301-415-2289</p>	<p>These standards are available in the library for reference use by the public. Codes and standards are usually copyrighted and may be purchased from the originating organization or, if they are American National Standards, from—</p> <p>American National Standards Institute 11 West 42nd Street New York, NY 10036-8002 www.ansi.org 212-642-4900</p>
<p>Some publications in the NUREG series that are posted at NRC's Web site address http://www.nrc.gov/reading-rm/doc-collections/nuregs are updated periodically and may differ from the last printed version. Although references to material found on a Web site bear the date the material was accessed, the material available on the date cited may subsequently be removed from the site.</p>	<p>Legally binding regulatory requirements are stated only in laws; NRC regulations; licenses, including technical specifications; or orders, not in NUREG-series publications. The views expressed in contractor-prepared publications in this series are not necessarily those of the NRC.</p> <p>The NUREG series comprises (1) technical and administrative reports and books prepared by the staff (NUREG-XXXX) or agency contractors (NUREG/CR-XXXX), (2) proceedings of conferences (NUREG/CP-XXXX), (3) reports resulting from international agreements (NUREG/IA-XXXX), (4) brochures (NUREG/BR-XXXX), and (5) compilations of legal decisions and orders of the Commission and Atomic and Safety Licensing Boards and of Directors' decisions under Section 2.206 of NRC's regulations (NUREG-0750).</p>

DISCLAIMER: This report was prepared as an account of work sponsored by an agency of the U.S. Government. Neither the U.S. Government nor any agency thereof, nor any employee, makes any warranty, expressed or implied, or assumes any legal liability or responsibility for any third party's use, or the results of such use, of any information, apparatus, product, or process disclosed in this publication, or represents that its use by such third party would not infringe privately owned rights.

**NUREG/CR-6807
INEEL/EXT-02-01021**

Results of NRC-Sponsored Stellite 6 Aging and Friction Testing

Manuscript Completed: October 2002
Date Published: March 2003

Prepared by
J.C. Watkins, K.G. DeWall

Idaho National Engineering and Environmental Laboratory
Idaho Falls, ID 83415

J. E. Jackson, NRC Project Manager

Prepared for
Division of Engineering Technology
Office of Nuclear Regulatory Research
Washington, DC 20555-0001
NRC Job Code W6593



**NUREG/CR-6807, has been reproduced
from the best available copy.**

ABSTRACT

This report describes a series of tests sponsored by the U.S. Nuclear Regulatory Commission and conducted by the Idaho National Engineering and Environmental Laboratory. The tests support research addressing the need to provide assurance that motor-operated valves are able to perform their intended safety function, usually to open or close against specified (design basis) flow and pressure loads. One of the parameters that affect gate valve operability is the friction between the disc seats and the valve body seats. In most gate valves, these surfaces are hardfaced with Stellite 6, a cobalt-based alloy.

The tests described in this report investigate the changes that occur in the friction as the Stellite 6 surfaces age and develop an oxide film. Stellite 6 specimens were aged in a corrosion autoclave, the oxide films were examined and characterized, and the specimens were subjected to friction testing in a friction autoclave. A very thin oxide film formed after only a few days of natural aging. Even a very thin oxide film caused an increase in friction. The surface structure of the oxide film was

dominated by a hard crystalline structure, such that the frictional response was analogous to rubbing two pieces of sandpaper together. The friction of the naturally aged specimens was observed to increase initially, but eventually stabilized.

Friction testing of specimens subjected to simulated in-service testing strokes at intervals during the aging process showed only a slight decrease in friction compared to other specimens. Results from specimens subjected to accelerated aging were inconclusive, because of differences in the structure and composition of the oxide films, compared to naturally aged specimens.

For the naturally aged specimens, the highest friction occurred on the first stroke. The first stroke smeared the oxide film and dislodged some of the granules, so that subsequent strokes saw lower friction values and less variation in the friction. This result underscores the importance of planning in-plant tests so that data are collected from the first stroke following a period of inactivity.

CONTENTS

ABSTRACT	iii
EXECUTIVE SUMMARY	xi
ACKNOWLEDGEMENTS.....	xiii
1. INTRODUCTION.....	1
2. DESCRIPTION OF THE TEST PROGRAMS.....	3
2.1 Overview of the Testing	3
2.2 Preparation of the Specimens	4
2.2.1 Phase I Friction and Characterization Specimens	5
2.2.2 Phase II Friction and Characterization Specimens.....	6
2.3 Aging the Specimens	9
2.3.1 Phase I Specimens	9
2.3.2 Phase II Specimens.....	13
2.4 Friction testing the Specimens	14
2.4.1 Phase I Friction Testing.....	14
2.4.2 Friction Testing at NIST.....	15
2.4.3 Phase II Friction Testing	16
3. RESULTS OF OXIDE FILM CHARACTERIZATION	19
3.1 Morphology	19
3.1.1 Naturally Aged Specimens.....	19
3.1.2 Accelerated Aged Specimens.....	25
3.2 Composition.....	25
3.2.1 Naturally Aged Specimens.....	30
3.2.2 Accelerated Aged Specimens.....	33
3.3 Oxide Film Thickness.....	36
3.3.1 Naturally Aged Specimens.....	37
3.3.2 Accelerated Aged Specimens.....	38
3.4 Accelerated versus natural aging	41
3.5 Known deviations in the experimental conditions.....	41
4. RESULTS OF FRICTION TESTING	47

4.1	Friction Testing Naturally Aged Specimens.....	48
4.1.1	Phase I Specimens.....	48
4.1.2	Phase II Specimens.....	50
4.2	Friction Testing Accelerated Aged Specimens.....	55
4.3	Changes in Friction Due to Aging of the Surface.....	59
4.4	Changes in Friction Due to Chemical Composition and Surface Structure.....	64
4.5	Changes in Friction with Stroking.....	65
4.6	Changes in Friction Due to Surface Contact.....	66
4.7	Changes in Friction Due to Valve Wedging.....	67
4.8	Changes in Friction Due to Temperature.....	67
4.9	Changes in Friction Due to Exposure to Air.....	69
4.10	Changes in Friction Due to Magnetite	70
5.	SUMMARY OF TEST RESULTS	73
6.	CONCLUSIONS	75
7.	REFERENCES.....	77

Figures

1.	MOV cross-section.....	1
2.	Sketch of the Phase II specimens, the contact regions are shown in blue.....	5
3.	Typical Phase I specimens prior to testing.....	7
4.	Typical Phase II specimens prior to testing	9
5.	Diagram of the initial Phase I corrosion autoclave	10
6.	Diagram of the in-service testing simulation rig	11
7.	Details of the simulated valve wedging fixture and loading configuration (top), and a photograph of the test fixture with dummy large specimens shown with stripes (bottom).....	12
8.	Photograph of the Phase II specimens mounted on the corrosion autoclave rack.....	13
9.	Diagram of the friction autoclave.....	14
10.	Typical variations in the normal load during a Phase II friction testing stroke.....	17

11.	Typical variations in the sliding load during a Phase II friction testing stroke	17
12.	Electron micrographs of the surface of a Phase I Stellite 6 specimen before exposure to aging	20
13.	Electron micrographs of the surface of a Phase I Stellite 6 specimen after 78 days exposure to natural aging conditions	21
14.	Electron micrographs of the surface of a Phase I Stellite 6 specimen after 78 days exposure to natural aging conditions with simulated in-service testing at 25 days and again at 50 days.....	22
15.	Electron micrographs of the surface of a Phase II Stellite 6 specimen before exposure to aging....	23
16.	Electron micrographs of the surface of a Phase II Stellite 6 specimen after 60 days exposure to natural aging conditions	24
17.	Electron micrographs of the surface of a Phase I Stellite 6 specimen after 11 days exposure to an anodic current density of 0.15 mA/cm^2	26
18.	Electron micrographs of the surface and cross section of a Phase I Stellite 6 specimen after 14 days exposure to an anodic current density of 0.35 mA/cm^2	27
19.	Electron micrograph of the surface of a Phase I Stellite 6 specimen after 19 days exposure to high-pH conditions; the large, zirconium-rich crystals are conspicuous	28
20.	Electron micrographs of the surface of a Phase I Stellite 6 specimen after 19 days exposure to high-pH conditions; the zirconium-rich crystals have been removed, but iron-rich crystals remain.....	29
21.	AES depth profile for Stellite 6 specimens after exposure to natural aging conditions	30
22.	XPS depth profile for a Phase I Stellite 6 specimen after 10 days exposure to natural aging conditions	30
23.	XPS depth profile for a Phase I Stellite 6 specimen after 20 days exposure to natural aging conditions	31
24.	XPS depth profile for a Phase I Stellite 6 specimen after 25 days exposure to natural aging conditions	31
25.	XPS depth profile for a Phase I Stellite 6 specimen after 40 days exposure to natural aging conditions	32
26.	XPS depth profile for a Phase I Stellite 6 specimen after 78 days exposure to natural aging conditions	32
27.	XPS depth profile of the chromium oxide in a Phase I Stellite 6 specimen exposed to natural aging conditions	34
28.	XPS depth profile of the oxygen in a Phase I Stellite 6 specimen exposed to natural aging conditions	34

29.	AES depth profile for a Phase II Stellite 6 specimen after 30 days exposure to natural aging conditions	35
30.	AES depth profile for a Stellite 6 specimen after 11 days exposure to an anodic current density of 0.15 mA/cm ²	35
31.	XPS depth profile for a Stellite 6 specimen after 19 days exposure to high-pH aging conditions	36
32.	Oxide film thickness versus time for Stellite 6, showing the data from the Phase I and Phase II natural aging tests and their data fits	39
33.	Oxide film thickness versus time for Stellite 6 from the Phase I and the Phase II testing, Type 304 Stainless Steel, and carbon steel.....	39
34.	Oxide film thickness versus time for Stellite 6, showing the data from the simulated valve wedging tests and the parabolic data fit of the Phase I naturally aged tests.....	40
35.	Electron micrographs of the surface of a Phase II Stellite 6 specimen after 30 days exposure to natural aging conditions and no exposure to water vapor.....	43
36.	Electron micrographs of the surface of a Phase II Stellite 6 specimen after 30 days exposure to natural aging conditions including exposure to water vapor	44
37.	AES depth profile for a Phase II Stellite 6 specimen after 30 days exposure to natural aging conditions, both with (lines with markers) and without (lines without markers) exposure to water vapor.....	45
38.	Contact regions between a gate valve disc and the valve seat	47
39.	A typical Phase I coefficient of friction trace.....	48
40.	Typical Phase I natural aging specimens before (top) and after (bottom) friction testing	49
41.	Maximum coefficient of friction for the Phase I naturally aged Stellite 6 specimens; versus stroke (top) and versus aging time (bottom)	51
42.	Nominal coefficient of friction for the Phase I naturally aged Stellite 6 specimens; versus stroke (top) and versus aging time (bottom)	52
43.	A typical Phase II coefficient of friction trace	53
44.	Typical Phase II natural aging specimens before (top) and after (bottom) friction testing	54
45.	Maximum coefficient of friction prior to the transition zone for the Phase II naturally aged Stellite 6 specimens; versus stroke (top) and versus aging time (bottom)	56
46.	Nominal coefficient of friction just prior to the transition zone for the Phase II naturally aged Stellite 6 specimens; versus stroke (top) and versus aging time (bottom)	57
47.	Nominal coefficient of friction immediately after the transition zone for the Phase II naturally aged Stellite 6 specimens; versus stroke (top) and versus aging time (bottom).....	58

48.	Coefficient of friction versus stroke for Phase I Stellite 6 specimens exposed to accelerated aging conditions; maximum values (top) and nominal values (bottom).....	60
49.	Coefficient of friction versus stroke for unaged and aged Phase I Stellite 6 specimens; maximum values (top) and nominal values (bottom).....	61
50.	Coefficient of friction (maximum) versus film thickness for naturally aged Stellite 6 specimens	62
51.	Change in the maximum coefficient of friction during the first stroke versus aging time.....	62
52.	Change in the coefficient of friction just prior to the transition zone during the first stroke versus aging time.....	63
53.	Change in the coefficient of friction after the transition zone during the first stroke versus aging time.....	63
54.	Coefficient of friction versus stroke for 20- and 40-day naturally aged and high-pH accelerated aging Phase I Stellite 6 specimens	65
55.	Coefficient of friction versus stroke for naturally aged Phase I Stellite 6 specimens and Phase I Stellite 6 specimens subjected to in-service testing; maximum values (top) and nominal values (bottom).....	68
56.	Change in the coefficient of friction of Phase II Stellite 6 specimens while hot and immediately upon cooldown.....	69
57.	Effect of temperature on the coefficient of friction of Stellite 6 following exposure to air.....	70

Tables

1.	Compositions of the Phase I Stellite 6 weld rods.....	5
2.	Compositions of the Phase I Stellite 6 friction testing specimens.....	8
3.	Compositions of the Phase II Stellite 6 weld rods.....	8
4.	Compositions of the Phase II Stellite 6 friction testing specimens	9
5.	Oxide film thickness on Phase I and Phase II Stellite 6 specimens exposed to natural aging	37
6.	Oxide film thickness on Phase I Stellite 6 specimens exposed to natural aging and simulated valve wedging loads	38
7.	Oxide film thickness on Phase I Stellite 6 specimens exposed to accelerated aging via an anodic current.....	40

EXECUTIVE SUMMARY

This report describes a series of tests sponsored by the U.S. Nuclear Regulatory Commission and conducted by the Idaho National Engineering and Environmental Laboratory. The tests support research addressing the need to provide assurance that motor-operated valves are able to perform their intended safety function, usually to open or close against specified (design basis) flow and pressure loads. One of the parameters that affect gate valve operability is the friction between the disc seats and the valve body seats. In most gate valves, these surfaces are hardfaced with Stellite 6, a cobalt-based alloy.

The tests described in this report investigate the changes that occur in the friction as the Stellite 6 surfaces age and develop an oxide film. Stellite 6 specimens were aged in a corrosion autoclave, the oxide films were examined and characterized, and the specimens were subjected to friction testing in a friction autoclave. The results of the aging tests show the presence of a very thin oxide film after very short exposure times of only a few days. The results of the friction tests show that even a very thin oxide film causes an increase in friction. Although the thickness of the oxide film may influence the friction, the key to being able to safely operate a valve is not necessarily based on the thickness or thinness of the oxide film, but rather on the mechanical properties of the oxide film as the Stellite 6 surface ages.

The results of both the Phase I and the Phase II testing shows that the friction increases as the specimens age. The friction during the Phase I testing showed no evidence of stabilizing after 78 days of aging. However, the friction during the Phase II testing did stabilize prior to 120 days of aging.

In general, the first stroke shows higher friction than succeeding strokes. The difference is greater for some specimens than for others. The decrease in the friction coefficient with continued stroking is probably caused by a change in the surface condition of the specimens due to plastic deformation or fracturing of the

crystals. The results indicate that the first stroke a valve experiences after it has been allowed to age and establish an oxide film will result in the highest coefficient of friction and therefore require the highest stem thrust to successfully operate the valve. This result has important implications for valves being subjected to in-plant testing: such in-plant tests need to collect data from the very first stroke a valve experiences following a period of inactivity, and data from subsequent strokes will be less relevant to valve operability and plant safety.

The results of the AFM and X-ray diffraction analyses at NIST indicate that the surface of the oxide film contains crystalline solids within an amorphous substrate. Crystalline solids in general are very abrasive and can result in high friction between the moving surfaces, analogous to rubbing two pieces of sandpaper together. Longer aging times correspond with larger crystalline grains and higher friction.

Although the single data point obtained in this study suggests that the simulated valve wedging would slightly decrease the expected friction, the difference is small. Before a definitive claim can be made as to either a small decrease in the friction, or no effect due to the simulated valve wedging, it would be prudent to obtain additional data to verify the direction and magnitude of the effect.

The composition and surface structure of the oxide films grown using acceleration techniques (anodic current and high pH) differ from those formed during natural aging. Large granular structures, iron enrichment, cobalt in the film, and additional oxide particles were observed in the accelerated tests. Considering these differences, oxide films produced by the acceleration methods are not representative of those produced by natural aging in the laboratory. However, the oxide films grown using acceleration techniques may be considered relevant to plant operations if highly oxidizing potentials can occur in the plant, if pH excursions can occur, or if magnetite or other

stray particles are deposited on and incorporated into the oxide films on the Stellite 6 sealing surfaces of the valves.

The results from the high-pH test indicate that precipitation of aging products on valve sealing surfaces from aging elsewhere can

increase the friction, a phenomenon that might occur in a plant environment. We know of no currently available data on film composition or thickness for in-plant Stellite 6 surfaces, but the presence of magnetite on the oxide film on valve hardfacing is possible and should be accounted for.

ACKNOWLEDGEMENTS

The authors wish to acknowledge Dr. Steven Shaffer and Dr. Anne-Claire Christiaen of the Battelle Memorial Institute for providing technical resources and insights to help make this work a success.

We thank Dr. Stephen Hsu of the National Institute of Standards and Technology who

reviewed our research and provided technical comments and insights.

We also thank Mr. Jerry Jackson and Dr. Gerald Weidenhamer of the NRC who patiently labored through the research that supports the basis for this report and for providing guidance, council, and suggestions.

Results of NRC-Sponsored Stellite 6 Aging and Friction Testing

1. INTRODUCTION

Under the sponsorship of the U.S. Nuclear Regulatory Commission (NRC), the Idaho National Engineering and Environmental Laboratory (INEEL) has been conducting research investigating the ability of motor-operated valves (MOVs) to function when subjected to design basis loads. That research included several recent tests addressing the friction characteristics of aged Stellite 6 disc and seat surfaces in gate valves. This report describes those aging and friction tests and compares and evaluates the results.

Methods exist to analytically predict the thrust needed to close (or open) motor-operated gate valves at specific flow and pressure conditions; however, the analyst must have a reasonably accurate, though conservative,

estimate of the coefficient of friction at the disc-to-seat interface (see Figure 1). In most gate valves, these surfaces are hardfaced with Stellite 6, a cobalt-based alloy. The results of the recent INEEL aging and friction research provide information to:

- Determine how aging can affect the performance of motor-operated gate valves.
- Determine the change in the disc-to-seat friction as a gate valve ages and whether the friction reaches a plateau.
- Determine the effect periodic gate valve cycling due to in-service testing has on friction.

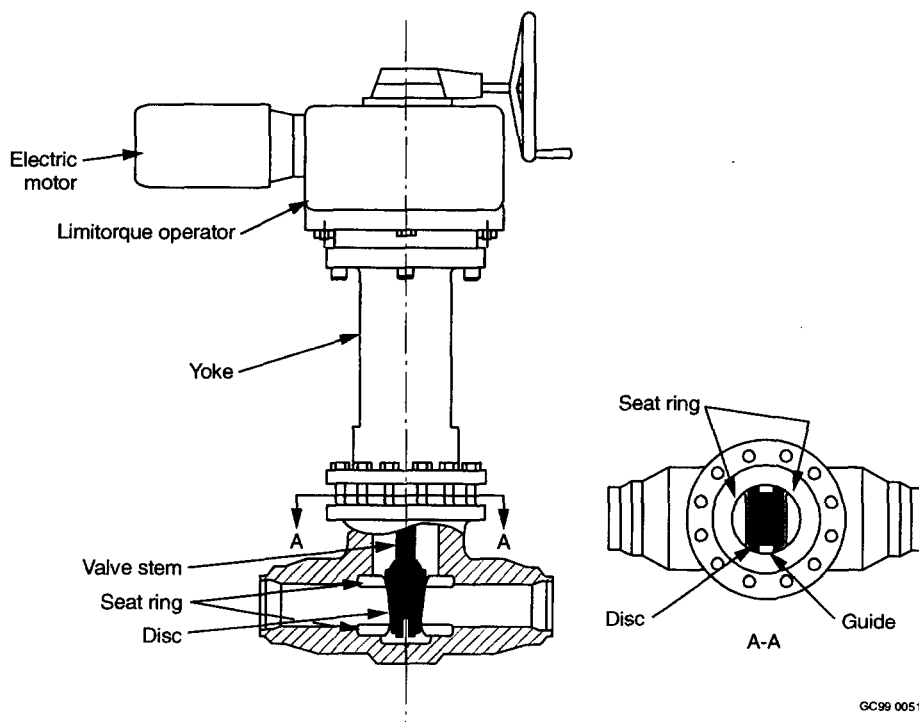


Figure 1. MOV cross-section.

This report presents the results from an INEEL research project designed to address these concerns. The project consisted of two sets of tests subjecting Stellite 6 specimens to an environment simulating boiling water reactor (BWR) coolant conditions, representing the conditions a typical reactor water clean-up (RWCU) isolation valve would experience, and inducing the accumulation of an oxide film. The tests included analysis of the resulting oxide film and testing to determine the coefficient of friction for specimens subjected to aging only and for specimens subjected to aging with periodic valve cycling.

The Battelle Memorial Institute in Columbus, Ohio performed the testing under a contract with the INEEL. Following the completion of the first phase of testing at Battelle, the Stellite 6 aging and friction research

results were peer reviewed by material science experts at NRC Headquarters. In addition, a corrosion and friction expert at the National Institute of Standards and Technology (NIST) performed an independent review of the work. This latter review evaluated the test methods, processes, and results and recommended that additional testing be performed. The results of this additional aging and friction testing, also performed by Battelle, are included in this report.

Two earlier, closely related INEEL test programs likewise produced an oxide film on Stellite 6 specimens and subjected the specimens to friction testing. The results of those tests are informative but somewhat inconclusive, for reasons explained later in this report. For completeness, this report includes a discussion of those tests.

2. DESCRIPTION OF THE TEST PROGRAMS

This report describes testing that investigated the aging and friction characteristics of Stellite 6. During the development of the Stellite 6 aging and friction testing program, the use of either full-size valves in a test loop or small specimen separate effects testing was discussed. The decision was made to use small specimens in a controlled laboratory environment. The use of a laboratory environment was determined to be preferable to testing full-size valves in a test loop provided the basic physics of the process being studied were understood. There are a number of reasons for this. For instance,

- The environment (pressure, temperature, chemistry, etc.) can be controlled more precisely and for longer periods of time than is possible with a typical full-size test loop,
- The instrumentation is typically more sensitive than the instrumentation in a typical full-size test loop, allowing researchers to obtain more accurate results and to monitor the impact of minor effects,
- The individual parameters can more easily be isolated, controlled, and studied which results in more accurate and applicable results rather than trying to separate the impact of a number of parameters,
- More data can be obtained in a given amount of time because several parameters can be processed simultaneously.
- The effect of misaligned or damaged equipment is greatly reduced, which in turn reduces the possibility of obtaining results that appear to be additional phenomena, and
- The laboratory environment is typically more resource efficient.

Based upon these reasons, the use of small specimens in a controlled laboratory environment was pursued.

2.1 Overview of the Testing

The Stellite 6 aging and friction testing was performed in two phases. The first phase, or the Phase I testing, consisted of four sets of tests. The first two Phase I tests focused on accelerating the growth of the oxide film on the Stellite 6 specimens. The reason for trying to accelerate the aging process was to produce in a few days or weeks an oxide film characteristic of what would be expected in a BWR coolant system after many months or years. One of these tests was very successful at accelerating the growth of an oxide film, while the other was less successful; however neither of the resulting oxide films was representative of the oxide film developed during natural aging. During the third Phase I test, specimens underwent natural aging at simulated BWR conditions, and both the oxide film growth and the resulting frictional response of the specimens were characterized as the specimens aged. The fourth Phase I test extended the time the specimens underwent natural aging and also quantified the effect periodic cycling of a valve would have on the growth of the oxide film and on the frictional characteristics of the specimens. The four sets of tests performed during the Phase I testing were:

1. Accelerated aging of specimens for 11 to 14 days using a small anodic electric current
2. Accelerated aging of specimens for 19 days using high-pH fluid conditions
3. Natural aging of specimens under normal BWR conditions for up to 40 days
4. Natural aging of specimens under normal BWR conditions for 78 days while subjecting some of the specimens to simulated valve wedging cycles (representing typical in-service testing) after 25 days and again after 50 days.

Following the Phase I testing, the Stellite 6 aging and friction research results were peer reviewed by material science experts at NRC

Headquarters. They reviewed the methods and processes used to make, age, and then friction test the Stellite 6 specimens. Their review concluded that the research was performed correctly and the conclusions were valid. However, because of the regulatory implications of the research, they requested that an independent corrosion and friction expert perform an additional peer review of the research. A corrosion and friction expert at NIST performed this additional peer review. Based on his review, he found the work to be technically sound and the results obtained with care. He also found that the quality of the data and the observed trends were consistent with good engineering practices. Finally, he found that the Stellite 6 surfaces were carefully prepared and the properties carefully measured. However, he felt that the results were not sufficient to base regulatory action on. To address these concerns, he recommended that additional testing be performed to extend the aging time, to include repeated friction testing at selected aging intervals, and to determine the impact of a second potential disc-to-seat contact mode on the friction.

Based on the peer review, Phase II testing was performed that consisted of making and then testing new Stellite 6 specimens. These specimens underwent natural aging at simulated BWR conditions for up to 120 days, and both the oxide film growth and the resulting frictional response of the specimens were characterized as the specimens aged. To address one of the concerns of the peer review (a second disc-to-seat contact mode and its effect on friction), the Phase II specimens were redesigned and are very different from the Phase I specimens.

During the Phase I testing, a small specimen started at one end of a large specimen, a load was applied to the specimens, and the two specimens were moved relative to each other such that the smaller specimen moved along the length of the larger specimen. Throughout the test, the two specimens were in continuous contact and the specimens were continuously loaded. Any corrosion products that were initially trapped between the two surfaces could

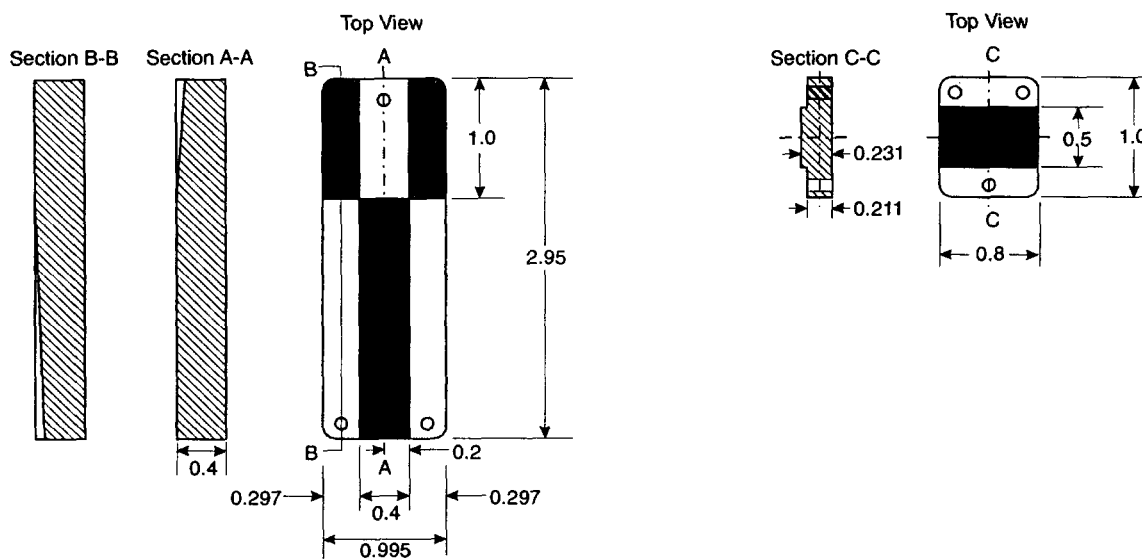
remain trapped and affect the frictional characteristics of the material.

During the Phase II testing, a second contact mode was introduced. In addition to testing specimens that were initially in contact with each other, we also wanted to test specimens that initially were not in contact with each other. This second contact mode allowed the specimens to come into contact with each other and push the corrosion products out of the way. This contact mode is similar to a valve disc coming into contact with a valve body seat and pushing the corrosion products out of the way. The frictional characteristics during this contact mode will be useful to estimate the potential impact aging can have on valve operability.

Figure 2 contains a sketch of the Phase II specimens. The blue region represents that portion of each specimen that came into contact with the other specimen. The smaller specimen was initially placed against the two-surfaced end of the larger specimen. During each friction test, the specimens were initially loaded and the two specimens moved relative to each other such that the smaller specimen traveled along the length of the larger specimen. When the smaller specimen reached the transition region of the larger specimen, where the two-surfaced region and the one surfaced region meet, two new surfaces came into contact. These two surfaces were under load and moving relative to each other. As such, they were also able to push the corrosion products out of the way if there was a tendency to do so. As the smaller specimen moved further along the larger specimen, the only region in contact represented surfaces that were initially not in contact.

2.2 Preparation of the Specimens

The Stellite 6 specimens that were used to determine the oxide film composition and the frictional characteristics during the Phase II testing were different from the specimens used during the Phase I testing. The preparation of the Phase I specimens will be discussed followed by the preparation of the Phase II specimens.



Dimensions in inches.

Figure 2. Sketch of the Phase II specimens, the contact regions are shown in blue.

2.2.1 Phase I Friction and Characterization Specimens

The Phase I testing consisted of four unique sets of tests. Each of the four sets of tests used several Stellite 6 "friction sets." Each friction set consisted of four specimens—two large inner specimens, and two small outer specimens—to accommodate the configuration of the friction testing autoclave described below. The specimens were prepared using methods typically used by valve manufacturers. The

Stellite 6 hardfacing was weld-deposited onto ANSI 1020 carbon steel blanks using the gas tungsten arc welding (GTAW) process. Uncoated weld rods of 0.125 inch and 0.094 inch diameter were used for the large inner and small outer friction specimens, respectively. The compositions of the weld rods, as specified by the manufacturer and by the American Welding Society (AWS), are shown in Table 1, along with a check of the major elements by Energy Dispersive Spectroscopy (EDS).

Table 1. Compositions of the Phase I Stellite 6 weld rods.

Element	AWS requirement (percent)	Composition of the small weld rod by EDS (percent)	Composition of the large weld rod by EDS (percent)
C	0.9 - 1.4	—	—
Mn	1.00 max	—	—
Si	2.0 max	1.1	1.4
Mo	1.0 max	—	—
Ni	3.0 max	1.8	2.5
Fe	3.0 max	1.8	2.4
W	3.0 – 6.0	5.4	4.8
Cr	26.0 – 32.0	28.1	27.4
Co	Balance (49-70)	61.9	60.6

The carbon steel blanks for the large inner specimens were 1.0 inch wide by 3.0 inch long, onto which a 0.5-inch wide strip of hardfacing was deposited along the length. The carbon steel blanks for the small outer specimens were 0.5 inch wide by 1.1 inch long, with the Stellite 6 footprint machined to either 0.25 inch wide by 1.1 inch long for the 10-ksi tests or 0.15 inch wide by 0.4 inch long for the 40-ksi tests. Almost all of the testing was performed with the 10-ksi specimens.

The hardfacing was deposited in three passes to achieve a thickness of at least 0.20 inch and to minimize iron dilution from the carbon steel substrate. The specimens were rough machined by electric discharge machining (EDM), with the final surface finish achieved through fine grinding to a finish of 16μ inch (arithmetic average) or better. For all specimens, the leading and trailing edges were chamfered to reduce the likelihood that any sharp edges would affect the friction testing.

All machining and cleaning operations were performed in a manner to avoid contamination. All machining was performed using water-based coolants. Cleaning consisted of scrubbing the specimens with a nylon bristle brush and ultrasonic cleaning using a 2% solution of a nonionic detergent with demineralized water, followed by ultrasonic cleaning in acetone and then ethyl alcohol. Typical Phase I specimens, after final cleaning and before aging, are shown in Figure 3. The sketch at the top of the figure shows the dimensions of the various Stellite 6 specimens. In addition to the large inner and small outer specimens described above, dummy specimens were included. These specimens were obtained by sectioning several of the large inner specimens. The Stellite 6 surface on these specimens was approximately 0.5 inch wide by 0.45 inch long and was used for oxide film characterization only. Following fabrication, the compositions of two of the large inner friction specimens and two of the small outer friction specimens were characterized. The compositions and hardness's of these specimens were within the range of properties typically found in

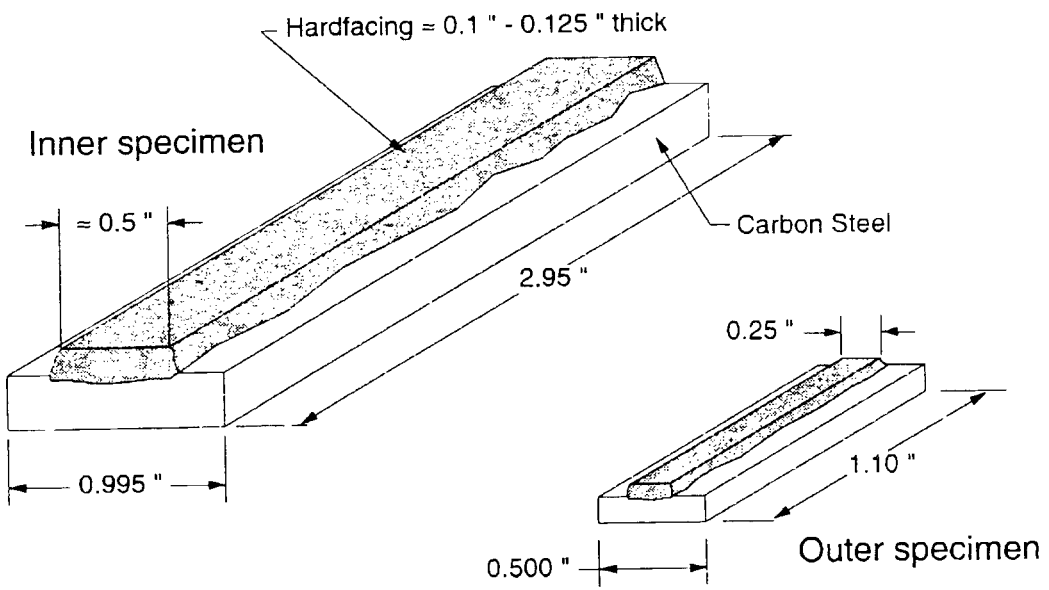
Stellite 6 valve hardfacing; Table 2 provides specific data.

2.2.2 Phase II Friction and Characterization Specimens

The Phase II testing consisted of a single test series that used several Stellite 6 "friction sets." Each friction set consisted of four specimens—two large inner specimens, and two small outer specimens—to accommodate the configuration of the friction testing autoclave described below. The specimens were prepared using methods typically used by valve manufacturers. The Stellite 6 hardfacing was weld-deposited onto a total of six 6-inch by 6-inch ASTM A36 carbon steel blanks that were 1-inch thick using the gas tungsten arc welding process. This is a 1018 carbon steel plate versus the 1020 carbon steel bar stock that was used to make the Phase I specimens. Both 0.125-inch and 0.094-inch diameter uncoated weld rods were used. The large inner specimens, the small outer specimens and the oxide film characterization specimens were then cut from the carbon steel blanks. The compositions of the weld rods, as specified by the manufacturer and by the American Welding Society are shown in Table 3.

The hardfacing was deposited in three passes to achieve a thickness of at least 0.20 inch and to minimize iron dilution from the carbon steel substrate. The specimens were rough cut using a band saw, machined to the required dimensions, and a final surface finish of 16μ inch (arithmetic average) or better was achieved through fine grinding. For all specimens, the leading and trailing edges were chamfered to reduce the likelihood that any sharp edges would affect the friction testing.

All machining and cleaning operations were performed in a manner to avoid contamination. All machining was performed using water-based coolants. Cleaning consisted of scrubbing the specimens with a nylon bristle brush and ultrasonic cleaning using a 2% solution of a nonionic detergent with demineralized water, followed by ultrasonic cleaning in acetone and then ethyl alcohol.



**Stellite 6 Friction Samples
Prior to Corrosion**

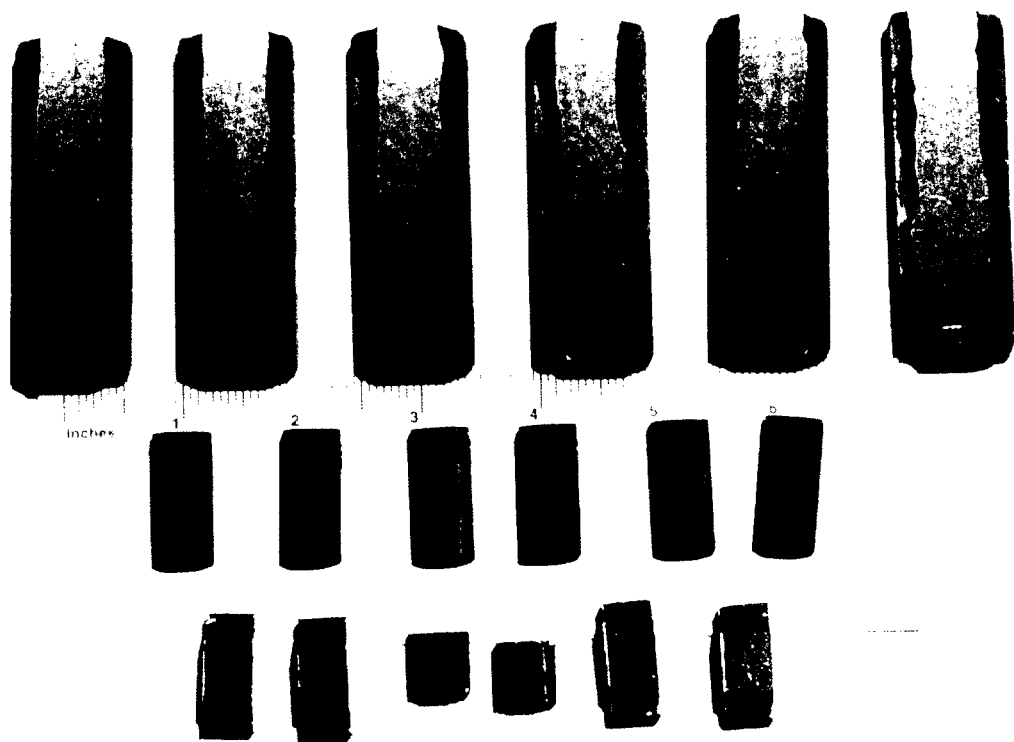


Figure 3. Typical Phase I specimens prior to testing.

Table 2. Compositions of the Phase I Stellite 6 friction testing specimens.

Element	Large Friction Specimen #1 (percent)	Large Friction Specimen #2 (percent)	Small Friction Specimen #28 (percent)	Small Friction Specimen #29 (percent)
Si	1.2	1.2	1.2	1.1
W	5.5	5.5	4.3	4.6
Ni	2.2	2.2	1.7	1.8
Fe	2.5	2.5	8.9	10.3
Cr	28.3	28.4	25.7	25.2
Co	60.3	60.4	58.4	57.1
Hardness (HRC)	44.0	44.7	41.8	41.0

Table 3. Compositions of the Phase II Stellite 6 weld rods.

Element	AWS requirement (percent)	Manufacturer specified composition of the small weld rod (percent)	Manufacturer specified composition of the large weld rod (percent)
C	0.9 - 1.4	1.2	1.1
Mn	1.00 max	—	—
Si	2.0 max	1.3	1.3
Mo	1.0 max	0.2	0.6
Ni	3.0 max	2.6	2.4
Fe	3.0 max	2.6	2.4
W	3.0 - 6.0	4.8	5.3
Cr	26.0 - 32.0	29.1	30.8
Co	Balance (49-70)	Balance (57.8)	Balance (55.7)

Typical Phase II specimens, after final cleaning and before aging, are shown in Figure 4. The unique shape of the large inner specimens is designed to address questions raised during the peer review. During friction testing, the small outer specimen initially rides on the dual surface region of the large inner specimen and then transitions to the single surface region.

In addition to the large inner and small outer specimens described above, dummy

specimens were included. The Stellite 6 surface on these specimens was approximately 0.5 inch wide by 0.5 inch long and they were used for oxide film characterization only. During fabrication, the compositions of selected specimens were characterized. The compositions of these specimens were within the range of properties typically found in Stellite 6 valve hardfacing. Table 4 provides specific data.

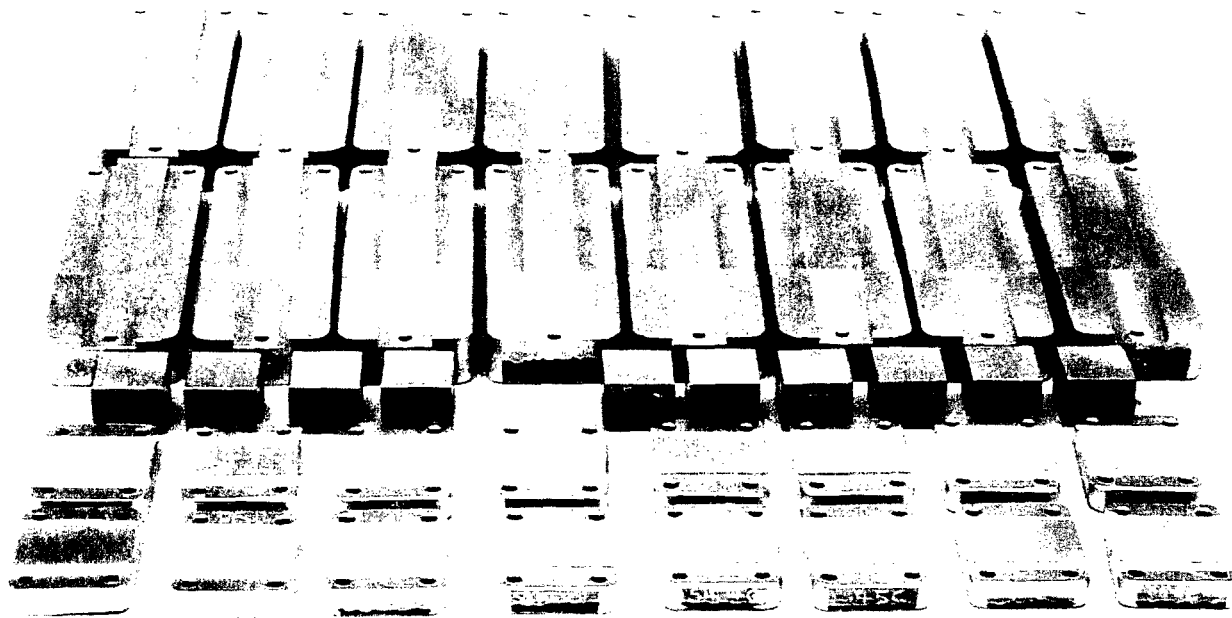


Figure 4. Typical Phase II specimens prior to testing.

Table 4. Compositions of the Phase II Stellite 6 friction testing specimens.

	Sample #1 (percent)	Sample #2 (percent)	Sample #3 (percent)	Sample #4 (percent)	Sample #5 (percent)	Sample #6 (percent)
Element	W	Ni	Fe	Cr	Co	
W	7.7	6.9	7.7	6.2	6.2	6.7
Ni	2.2	2.0	2.0	2.4	2.7	2.5
Fe	3.6	3.7	3.0	3.0	2.8	3.1
Cr	28.2	28.3	28.2	29.3	30.0	29.9
Co	58.3	59.1	59.1	59.2	58.3	57.9

2.3 Aging the Specimens

Both the Phase I and the Phase II specimens were aged at simulated BWR coolant conditions in a corrosion autoclave. The autoclave was attached to a reservoir of water in which the oxygen was controlled in the range of 100 to 200 ppb. Water from the reservoir was continuously supplied to the autoclave, with the temperature in the autoclave maintained at 550°F, and the pressure at 1050 psi, slightly above the saturated steam pressure, such that the water was about 10°F subcooled.

2.3.1 Phase I Specimens

The corrosion autoclave used during the first three Phase I tests was a five-gallon, flow-through, stainless steel "stirring" autoclave (Figure 5). The setup for the first test included a galvanostat and other provisions for supplying an anodic current to the specimens to accelerate the aging process. These provisions were excluded in the second and third tests. A different autoclave was used in the fourth test.

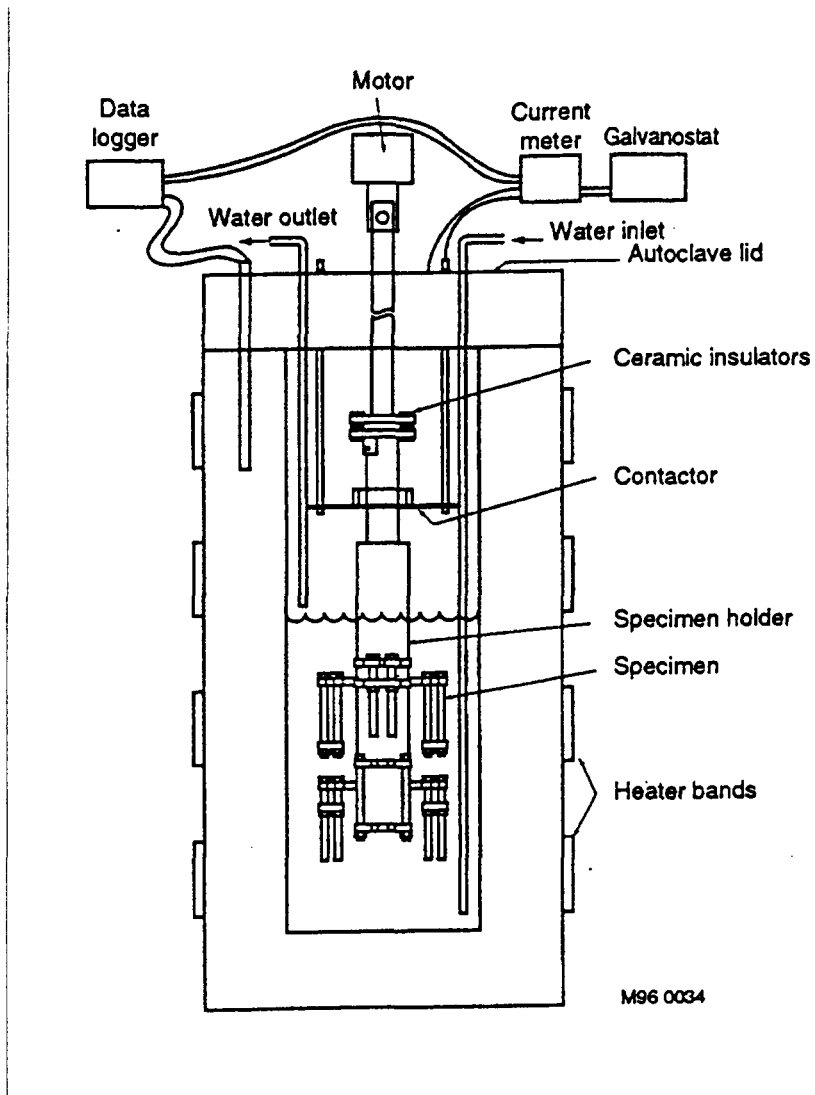


Figure 5. Diagram of the initial Phase I corrosion autoclave.

A replacement autoclave was necessary because the original autoclave failed during the initial heatup of the fourth test. A number of cracks were discovered in the autoclave that could not be repaired. The replacement autoclave was made of Hastelloy and was smaller, approximately 1 gallon in size, but still large enough to accommodate all the specimens. The replacement autoclave retained all the functional capabilities of the original autoclave.

In the original autoclave, the specimens were attached to a rack fabricated from zirconium and heat-treated to provide a non-conductive zirconium dioxide (ZrO_2) film. A

stirring unit was used to ensure adequate mixing during the aging process and to simulate flow past a valve in an RWCU system. Except for the accelerated aging tests using high pH fluid conditions, the pH was maintained at 6.5 to 7.0. The autoclave pressure and temperature were continuously recorded and the solution conductivity and dissolved oxygen concentration were recorded twice each day. The smaller autoclave used for the fourth test contained a rack made from Type 316 Stainless Steel, with Teflon sheeting to avoid direct contact between the rack and the specimens.

For the first test, specimens were exposed to simulated BWR conditions and a small anodic electric current applied to accelerate the aging. The following anodic currents were applied: (a) 0.15 mA/cm^2 for 11 days; (b) 0.15 mA/cm^2 for 11 days followed by 0.19 mA/cm^2 for 2.5 days; and (c) 0.35 mA/cm^2 for 14 days. The electrically insulating ZrO_2 film was removed from the corrosion autoclave rack at points where the specimens were attached, and the voltage was applied so that the anodic current flowed through the specimens to the autoclave wall (counter electrode). Following each exposure to an anodic electric current, the oxide films were characterized and friction testing was performed. A discussion of the results is presented later in this report.

For the second test (accelerated aging with high pH fluid conditions), specimens were exposed to simulated BWR conditions for 19 days with the pH of the fluid adjusted to 9.0 (instead of 6.5 to 7.0) using carbonate-free sodium hydroxide (NaOH). The rationale for the pH adjustment was based on solubility versus pH curves that indicate that increasing the pH of the fluid will increase the solubility of iron oxide

from other areas of the system. The iron oxide would then precipitate out on the surface of the Stellite 6. Consequently, it was expected that this technique would lead to thicker oxide films. Following the exposure to high pH fluid conditions, the oxide film was characterized and friction testing was performed. A discussion of the results is presented later in this report.

For the third test (natural aging), the oxide film was characterized following 2-, 10-, 20-, and 40-day exposure to simulated BWR conditions in the corrosion autoclave. Friction testing was performed on unaged specimens and on specimens following 2-, 10-, 20-, and 40-days in the corrosion autoclave. A discussion of the results is presented later in this report.

For the fourth test (natural aging plus simulated valve wedging), some of the specimens were removed from the corrosion autoclave and subjected to simulated valve wedging cycles at 25 days and again at 50 days. The simulated valve wedging cycles represent typical in-service testing (IST) conditions and used the IST simulation rig (Figures 6 and 7).

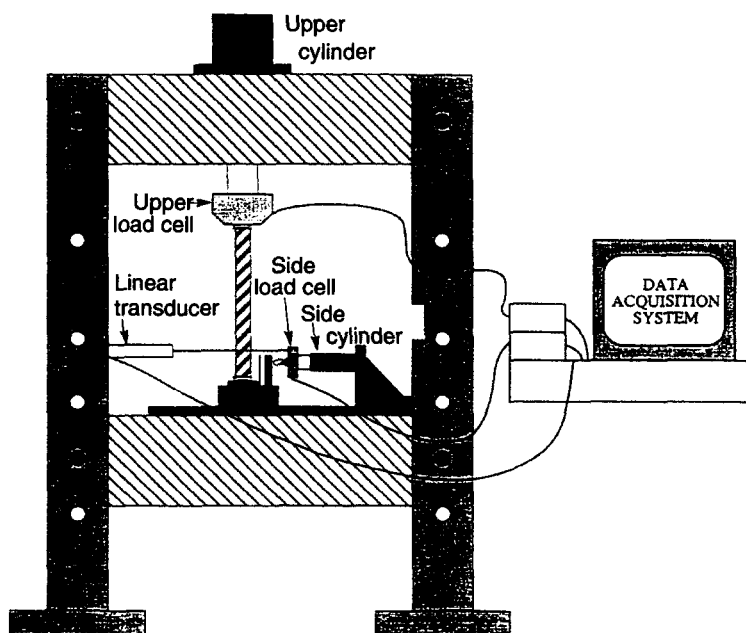


Figure 6. Diagram of the in-service testing simulation rig.

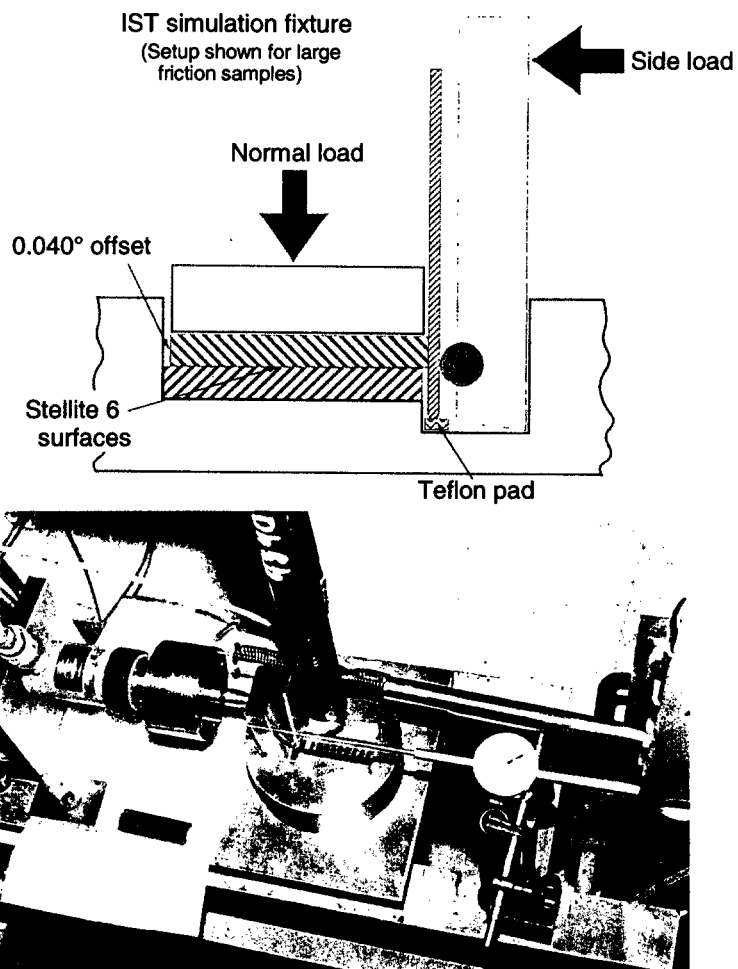


Figure 7. Details of the simulated valve wedging fixture and loading configuration (top), and a photograph of the test fixture with dummy large specimens shown with stripes (bottom).

The oxide film was characterized both before and after the simulated valve wedging cycles so that the effect the wedging had on the oxide film could be determined. Friction testing was performed following 78 days in the corrosion autoclave using specimens that had not undergone the simulated valve wedging, and with specimens that had undergone the simulated valve wedging at 25 days and again at 50 days. A discussion of the results is presented later in this report.

To subject the entire surface of each specimen to a simulated valve wedging, like-sized specimens were placed with their Stellite 6 surfaces face to face, a normal load of 20 ksi

applied, and then the specimens moved 0.040 inch (1 mm) relative to each other. Unlike the corrosion autoclave (described earlier) and the friction autoclave (described in the next subsection), the IST simulation rig subjected the specimens to a water bath at room temperature and atmospheric pressure rather than simulated BWR coolant conditions. (The high-temperature friction autoclave could not be used for the IST simulation, because it was not capable of generating the high normal loads on the like-sized specimens.) The like-sized face-to-face specimen pairs, the dimensions of the contact surface, and the force required to produce a contact stress of 20 ksi are:

- Large, inner friction specimens:
0.5-inch-wide by 3.0-inch-long, 30,000-lb normal force
- Small, outer 10 ksi friction specimens:
0.25-inch-wide by 1.1-inch-long, 5,500-lb normal force
- Dummy specimens for oxide film characterization:
0.5-inch-wide by 0.45-inch-long, 4,500-lb normal force. A stress level of 20 ksi was selected to approximate the stresses occurring during a valve wedging cycle of a typical RWCU system valve. The distance of 1 mm is based on the estimated valve disc motion during wedging based on testing performed by the

INEEL. Selected specimens were subjected to the simulated valve wedging after 25 days and again after 50 days of natural aging.

2.3.2 Phase II Specimens

The corrosion autoclave used during the Phase II testing was a five-gallon, flow through, stainless steel “stirring” autoclave, similar to the autoclave used during the initial Phase I testing. The specimens were attached to an internal rack (Figure 8) and naturally aged. The oxide film was characterized following 30-, 60-, 90-, and 120-day exposure to simulated BWR conditions in the corrosion autoclave. Friction testing was performed on unaged specimens and on specimens following 30-, 60-, 90-, and 120-days in the corrosion autoclave. A discussion of the results is presented later in this report.

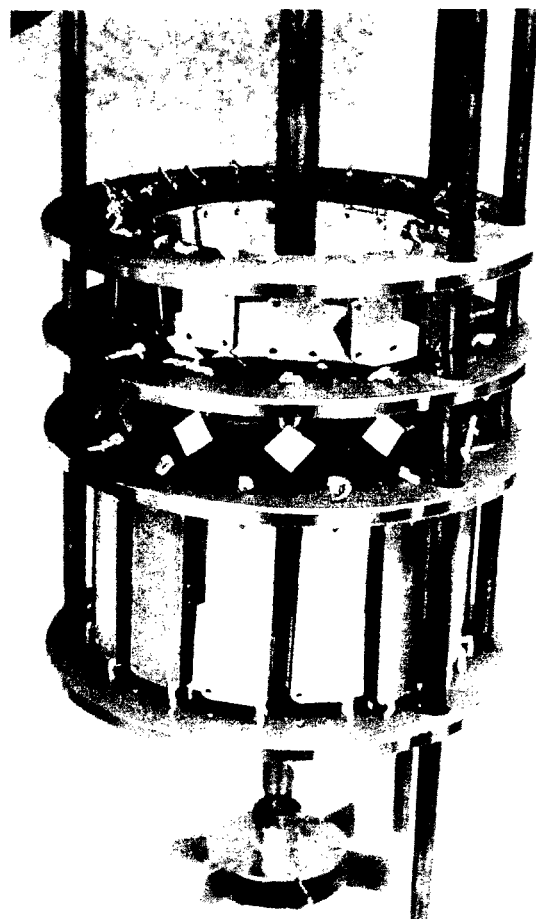


Figure 8. Photograph of the Phase II specimens mounted on the corrosion autoclave rack.

2.4 Friction testing the Specimens

2.4.1 Phase I Friction Testing

All of the Phase I friction testing that was performed at Battelle used the same friction autoclave. The friction autoclave (Figure 9), like the corrosion autoclave, was attached to a reservoir of water in which the oxygen was controlled in the range of 100 to 200 ppb. Testing was performed with the autoclave

heated to 550°F and pressurized to about 1050 psi. During each test, a specimen assembly (friction set) consisting of two small outer specimens and two large inner specimens was used. The small outer specimens were held in a stationary fixture, and the large inner specimens were attached to a carrier bar connected to a movable pull rod. Actuation of the pull rod caused the large inner specimens to slide between the small outer specimens at a relative velocity of 16 inch/min, a rate within the range expected for typical gate valves.

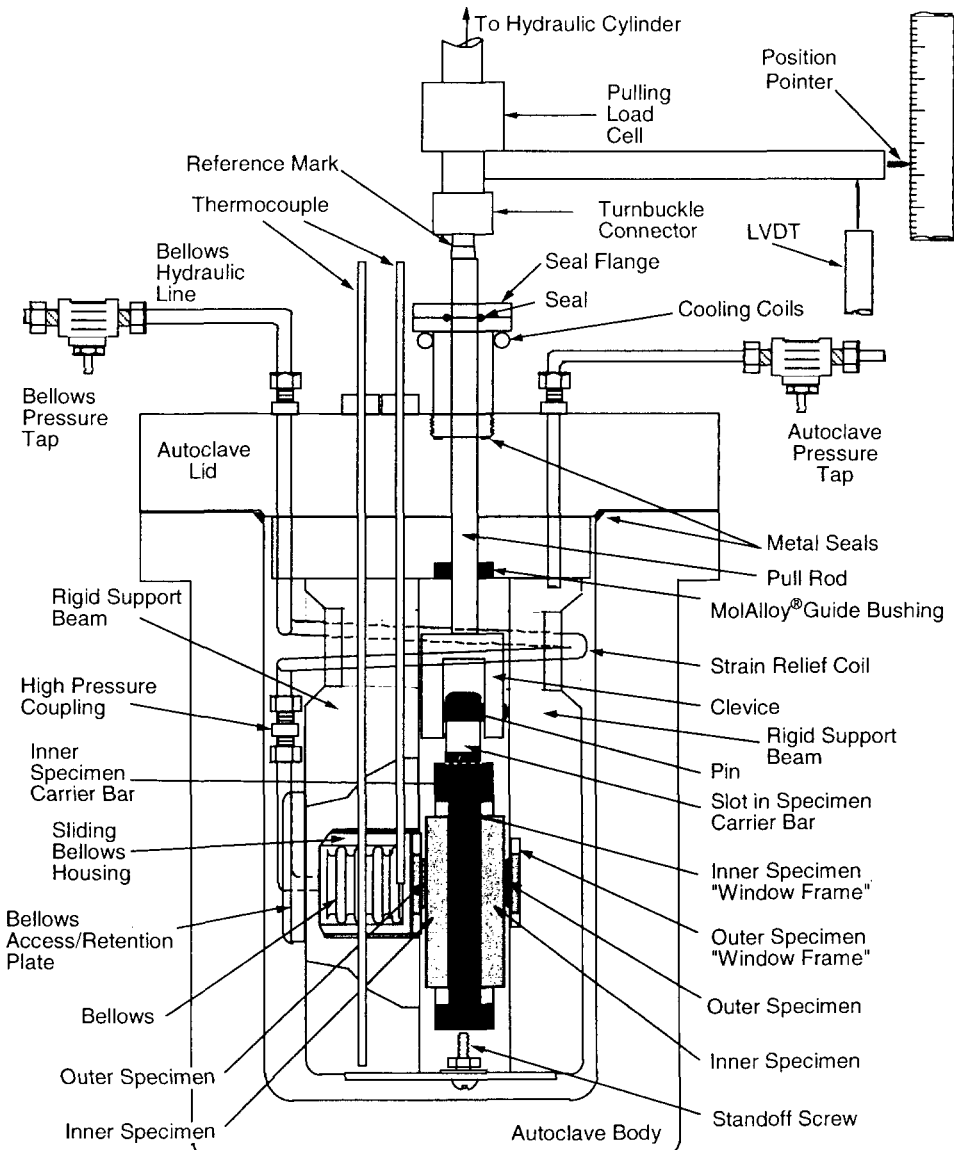


Figure 9. Diagram of the friction autoclave.

The friction-testing device is equipped with a bellows that can exert a force on one side of the specimen assembly. Pressurizing the bellows imposes a normal force on the specimens to produce the specified nominal contact stress of either 10 ksi or 40 ksi. The normal force required to achieve a 10-ksi nominal contact stress on the 0.25-inch-wide by 1.10-inch-long specimens is 2,750 lb. This contact stress was selected to approximate the stress level occurring during operation of typical RWCU system valves. (Assuming a uniform load distribution, the estimated contact stresses at the seats for typical 4-inch and 6-inch valves subjected to a differential pressure of 1,050 psi are 7.8 ksi and 12.6 ksi, respectively.) For the small 0.15-inch-wide by 0.40-inch-long specimens, a normal force of 2,400 lb. is required to achieve a nominal contact stress of 40 ksi.

With the friction coefficient (μ) defined in the usual manner, as the ratio of the sliding force to the normal force (i.e., $\mu = F_s/F_n$), the friction was determined by measuring the force applied by the bellows and the force required to move the inner specimens. Specifically, the friction coefficient was calculated using the following formula:

$$\mu = \frac{1}{2} \frac{F_s}{F_n}$$

Where

μ = coefficient of friction

F_s = sliding force ($f_{total} - f_{tare}$)

F_n = normal force (applied by the bellows)

f_{total} = total force measured while the specimens are moving

f_{tare} = force measured before the pull rod moves the specimens ($f_{seal} - f_{expulsion}$)

f_{seal} = force due to friction at the seal

$f_{expulsion}$ = force due to the fluid pressure in the autoclave trying to expel the pull rod.

The normal force (F_n) was determined using a known calibration between the effective bellows pressure and the resulting force exerted by the bellows. (The effective bellows pressure is the difference between the pressure inside the bellows and the pressure in the autoclave.)

The sliding force was determined from a load cell attached between the pull rod and the hydraulic cylinder that actuated it. A high pressure, low-friction seal on the top of the autoclave lid allowed the pull rod to be moved through the lid with minimal friction. As the pull rod was withdrawn during a friction test cycle, the first inch of stroke took up the slack in the pin-to-clevis assembly, thus allowing a measurement of the "tare" force (f_{tare}) resulting from the seal friction force (f_{seal}) less the expulsion force ($f_{expulsion}$) on the pull rod. In terms of forces on a valve, this represents the packing drag less the stem rejection load. After the pin reached the top of the clevis, the pull rod began pulling the large inner specimens between the small outer (stationary) specimens for a distance of approximately 2 inches. During this portion of the stroke, the load cell measurement less the previously determined "tare" force represents the force required to move the specimens. Dividing the sliding force (F_s) by two is necessary because the siding force is the result of friction at two interfaces, not just one. Thus, this formula gives the average friction value for the two sliding interfaces. Continuous measurements were taken during each friction test. The results are presented later in this report.

2.4.2 Friction Testing at NIST

Following the completion of the Phase I testing at Battelle, the results were peer reviewed by material experts at NRC Headquarters. The material experts reviewed the test methods, processes, and results. They concluded that the testing was performed

correctly and that the intent of the testing had been met. However, because of the regulatory implications of the work, they requested that an independent corrosion and friction expert perform an additional peer review.

A corrosion and friction expert at NIST was contacted and he agreed to perform the independent review. In addition to an evaluation of the test methods, processes, and results, the NIST review included examining and testing selected Stellite 6 specimens that had undergone aging at Battelle but had not been subjected to any friction testing. In particular, 10-day and 50-day specimens (from the third set of tests) were subjected to additional friction testing at NIST. Unlike the friction testing performed in the high-temperature, high-pressure autoclave at Battelle, the testing at NIST was performed at ambient temperature and pressure. The purpose of this testing was to investigate whether the configuration of the specimens in the friction autoclave at Battelle was representative of the way the Stellite 6 surfaces in a valve interact, or whether the resulting friction values contained any biases.

Unlike the friction testing performed at Battelle, the friction testing performed at NIST used a single Stellite 6 specimen and either a 0.5-inch steel ball or a 0.125-inch steel ball fixed on the end of a push rod. The ball and push rod assembly was loaded with a preset force, and then the assembly was moved across the Stellite 6 surface. During this testing, the force on the ball and the force required to slide the ball over the specimen were continuously recorded. Dividing the sliding force by the normal force results in the friction coefficient. The testing was then repeated using a small flat surface with a contact area of 1.8 mm^2 instead of a ball. Since the testing was not performed in an autoclave, correcting for pressure and seal loads

was not necessary. The results are presented later in this report.

2.4.3 Phase II Friction Testing

The Phase II friction testing used the same friction testing autoclave that was used during the Phase I testing. Like the Phase I testing, a specimen assembly (friction set) consisting of two small outer specimens and two large inner specimens was used. The bellows imposed a normal force on the specimens to produce the specified nominal contact stress of 10 ksi. The normal force required to achieve a 10-ksi nominal contact stress on the 0.8-inch-wide by 0.5-inch-long specimens is 2,000 lb., noting that only half the area of the small specimen is in contact with the large specimen at any given time. Like the Phase I testing, the contact stress was selected to approximate the stress level occurring during operation of typical RWCU system valves.

Continuous measurements of the sliding load and the normal load were taken during each friction test. The normal load was observed to vary during a stroke; however, the variation was less than 10% of the nominal 2000 lb. load. From test to test, the normal load was very repeatable. The sliding load exhibited large variations during a stroke in response to changes in the friction. From test to test, the sliding load also varied; again in response to changes in the friction. Typical normal load and sliding load traces are shown in Figures 10 and 11 and show not only the variation in load during a stroke, but also the variation in the load from stroke to stroke. Normal load and sliding load traces from other Phase II tests are similar. Although the normal load did vary during a stroke, the variation was small and the variation was accounted for when estimating the friction between the sliding surfaces. The results are presented later in this report.

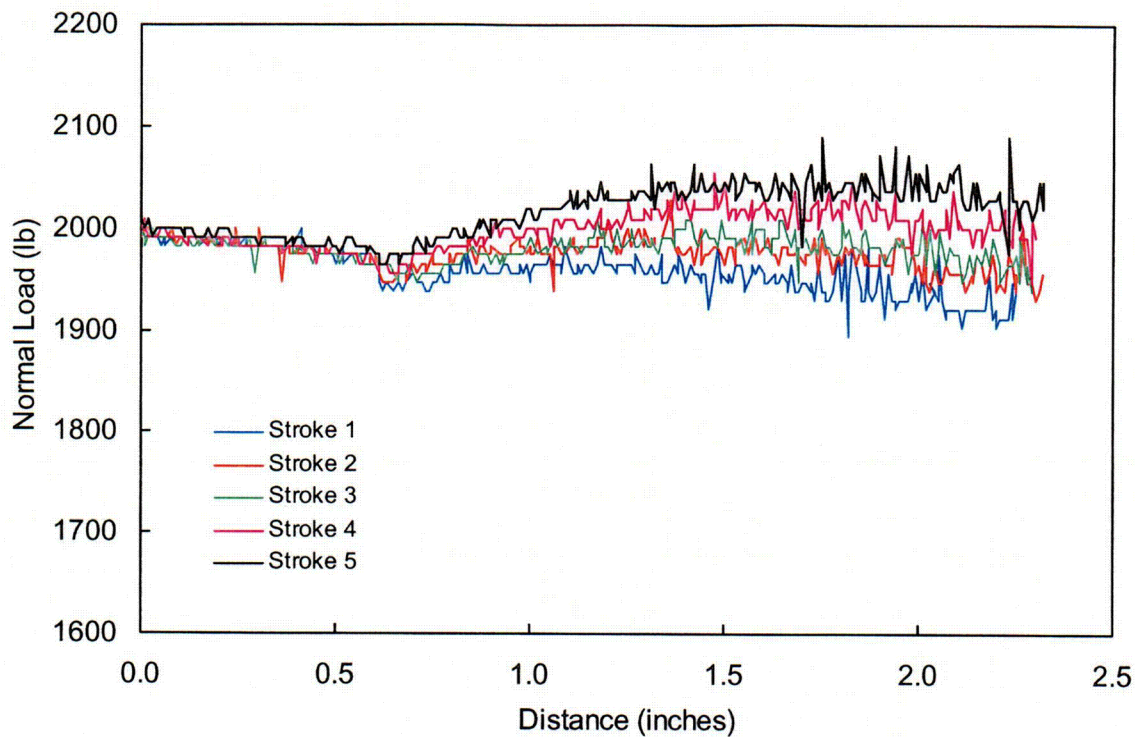


Figure 10. Typical variations in the normal load during a Phase II friction testing stroke.

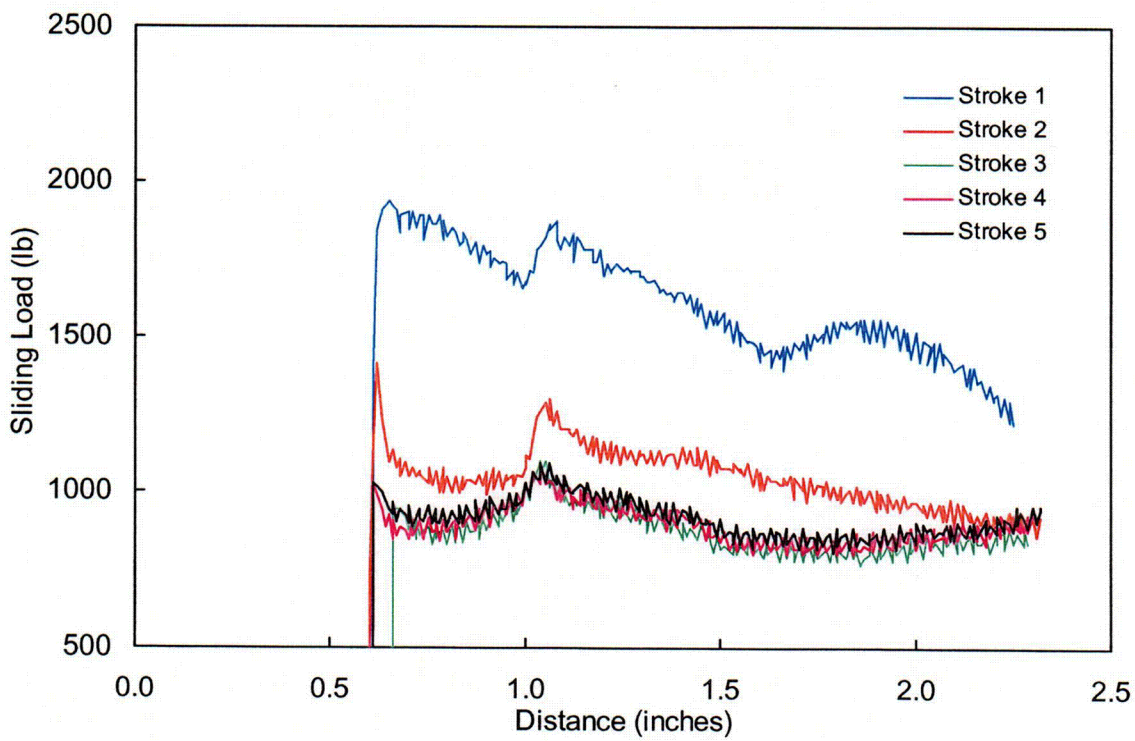


Figure 11. Typical variations in the sliding load during a Phase II friction testing stroke.

3. RESULTS OF OXIDE FILM CHARACTERIZATION

Following the corrosion of the Phase I and the Phase II specimens, the morphology, or physical structure, of the oxide films was evaluated by examining the electron micrographs of the oxide films. In addition, the surface topography of a few selected specimens was examined at NIST using an Atomic Force Microscope (AFM) and X-ray diffraction. The chemical composition of the oxide films was analyzed by Auger electron spectroscopy (AES) for some specimens and by X-ray photoelectron spectroscopy (XPS) for others (and both methods for a few specimens). The chemical composition analysis for the first two Phase I tests and the Phase II testing was performed at Evans East Laboratories, located in New Jersey. The chemical composition analysis for the last two Phase I tests was performed at Ohio State University.

With AES and XPS, the oxide film is incrementally sputtered away, and the elemental composition of planes in the oxide film determined. The results of these analyses are then plotted versus time (or depth, assuming an oxide film removal rate due to the sputtering) to provide a depth profile so that the relative elemental concentrations can be evaluated. The film thickness was determined from metallographic cross sections for specimens exposed to the anodic current. For the natural aging specimens and the high-pH specimens, the film thickness was determined from the AES and XPS results; this technique uses the change in chemical constituents versus depth (or sputter time) as an indication of film thickness. The following sections discuss each of these topics in more detail.

3.1 Morphology

The aging morphologies generated under natural aging conditions would be expected to mirror those found in service. However, it is likely that these films are not as thick as those found in service because of the relatively short duration of the natural aging times in the tests.

3.1.1 Naturally Aged Specimens

Figure 12 is an electron micrograph showing the surface of a Phase I Stellite 6 specimen before exposure to aging conditions. Note that the machining marks are visible on the surface, which is relatively smooth. Typical results after exposure of the Phase I Stellite 6 specimens to natural aging in the corrosion autoclave are shown in Figure 13 for a 78-day specimen. Note that the original machining marks are still visible on the surface. Evidence of sparsely distributed nodules exists on the outer surface, however these nodules were not sufficient to hide the surface imperfections from the original machining.

Figure 14 is an electron micrograph showing the surface of a Phase I Stellite 6 specimen that was subjected to an in-service test simulation. This specimen has undergone 78 days of natural aging, with simulated valve wedging cycles at 25 days and again at 50 days. Note that the surface shows evidence of deformation due to the simulated valve wedging loads, but only at local regions of contact. That is, the deformation occurs at the high spots that are the result of ordinary irregularities in the original machining of the surface during manufacture. The regions between the high spots were left relatively undisturbed. This is consistent with the visual observation made after the simulated in-service test, in which only a very small fraction of the surface (the high spots) appeared shiny and silver colored.

Figure 15 is an electron micrograph showing the surface of a Phase II Stellite 6 specimen before exposure to aging conditions. Note that the machining marks are visible on the surface, which is relatively smooth. Typical results after exposure of the Phase II Stellite 6 specimens to natural aging in the corrosion autoclave are shown in Figure 16 for a 60-day specimen. Note that like the electron micrograph for the aged Phase I specimen, the original machining marks are still visible on the surface. Evidence of sparsely distributed nodules exists on the outer surface, however these nodules

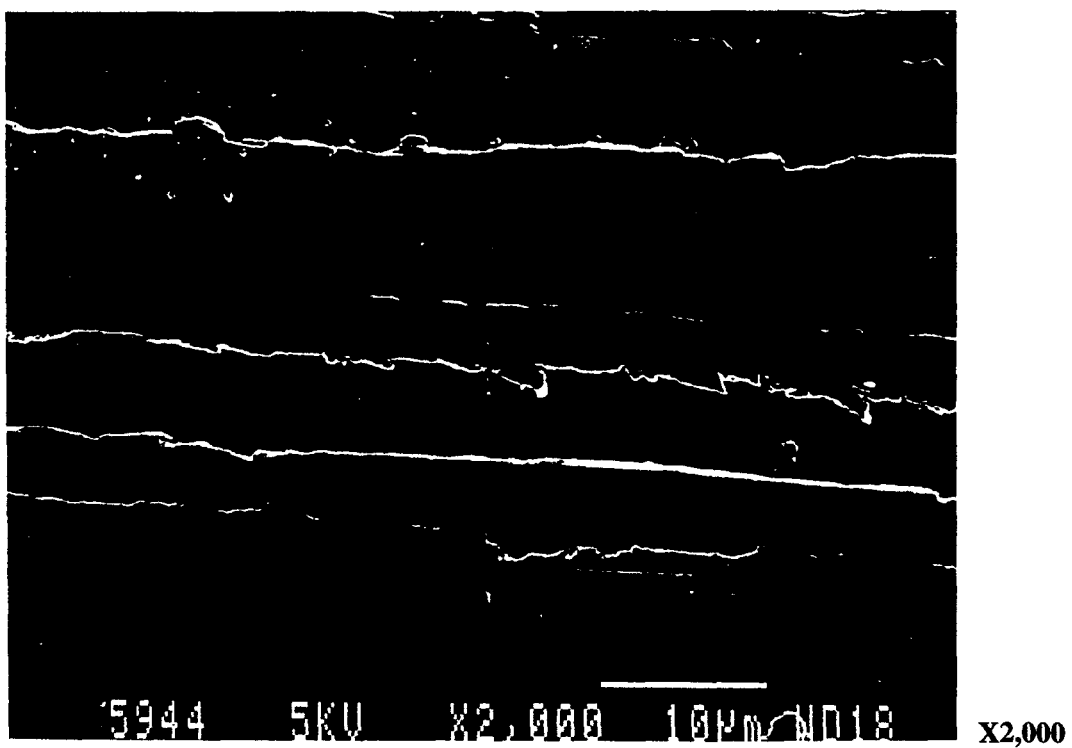
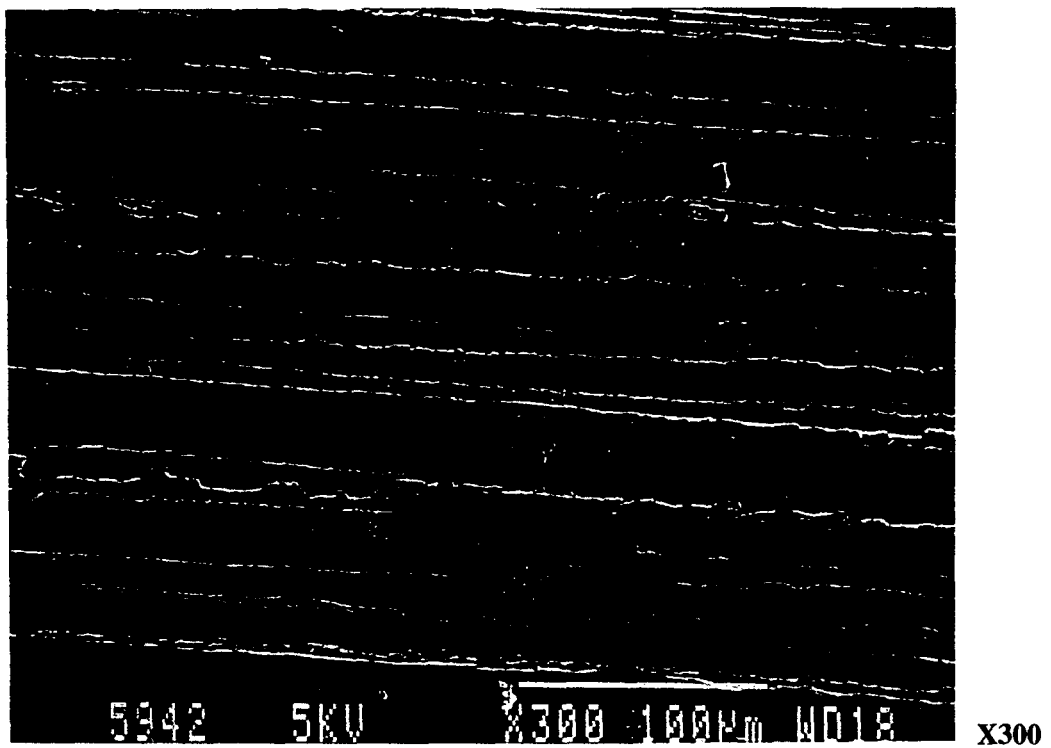
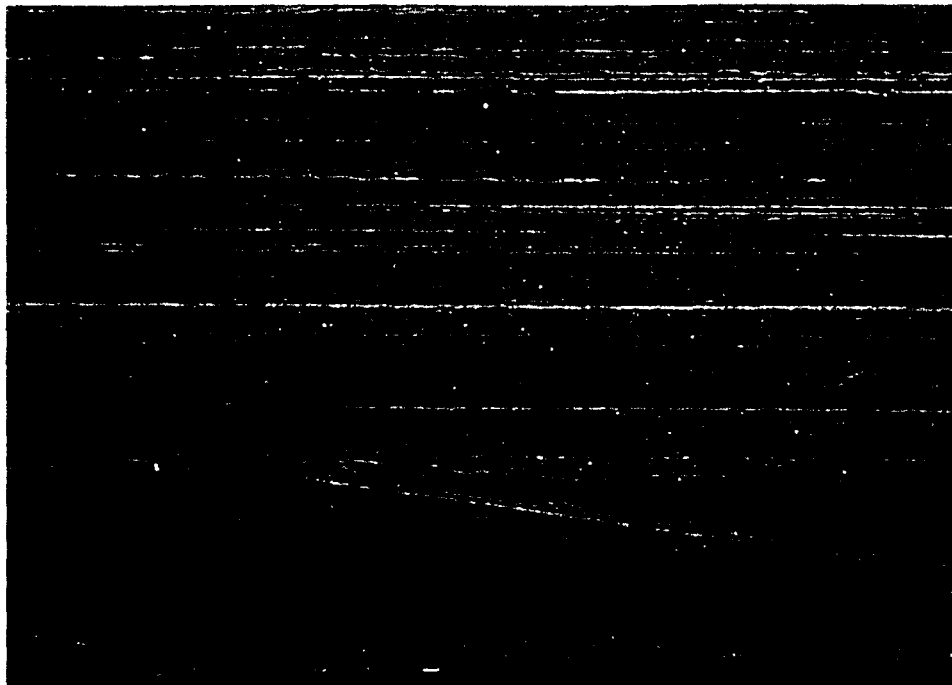


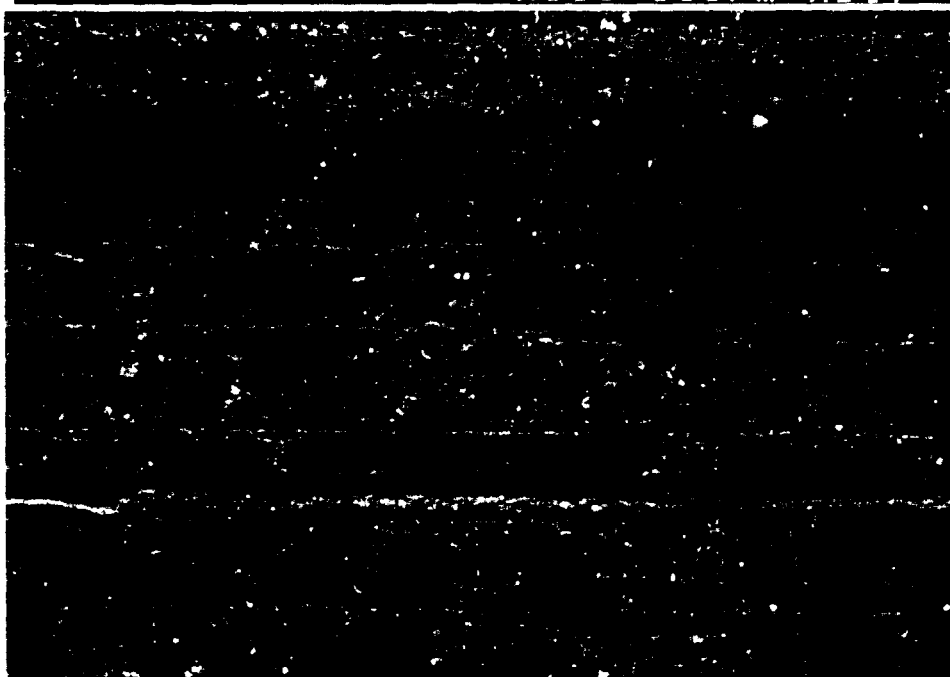
Figure 12. Electron micrographs of the surface of a Phase I Stellite 6 specimen before exposure to aging.



6285 10KV

X300 100μm WD17

x300

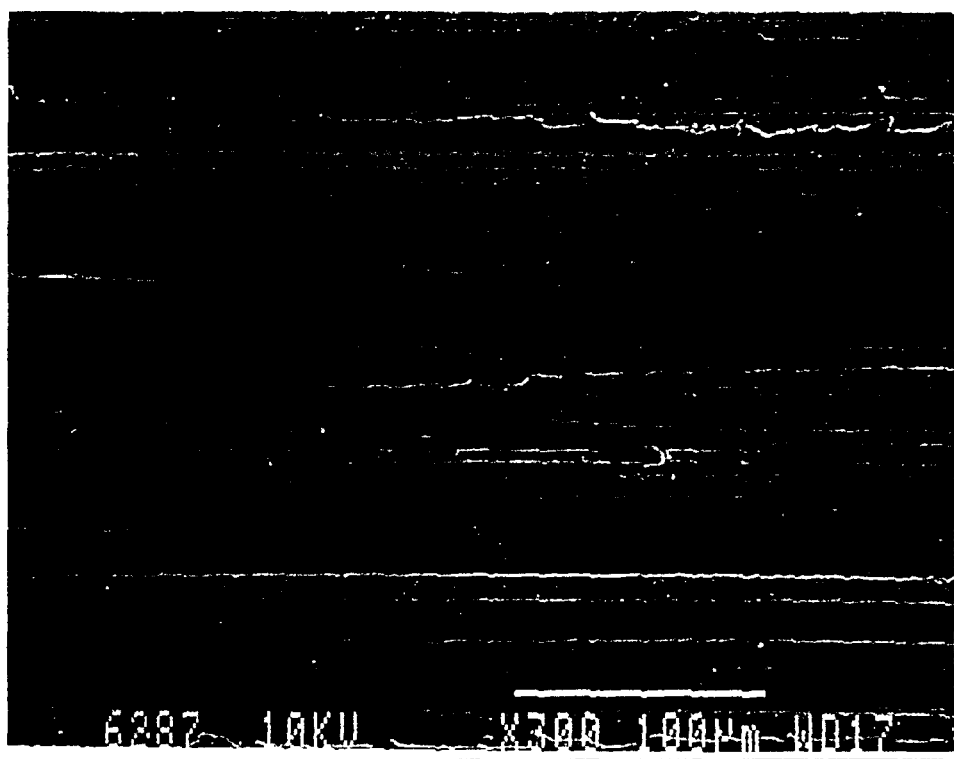


6286 10KV

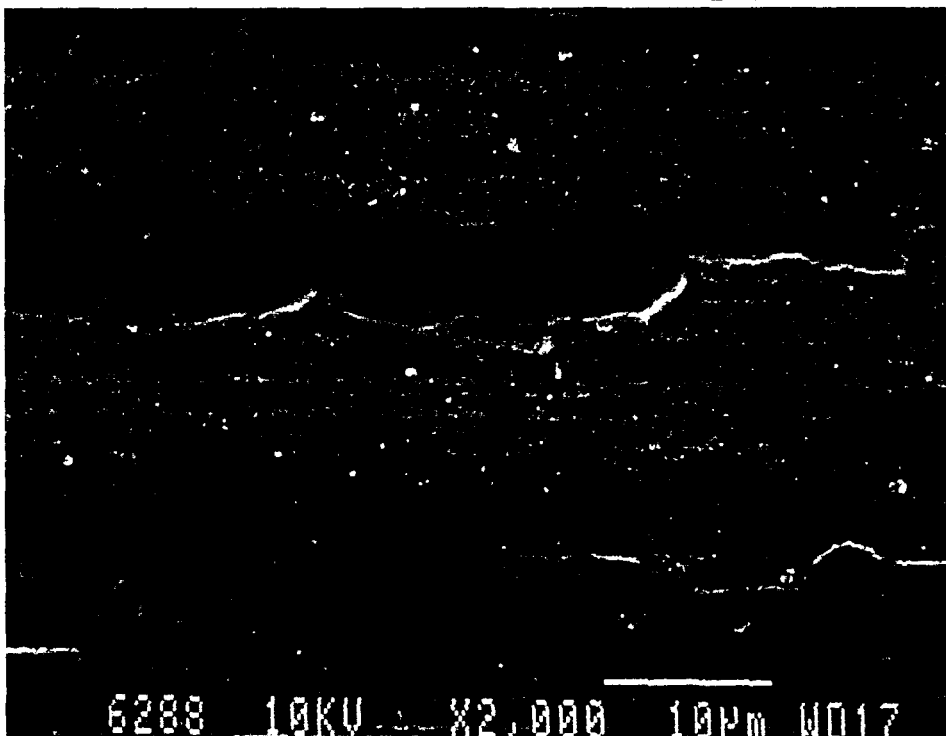
X2,000 10μm WD17

x2,000

Figure 13. Electron micrographs of the surface of a Phase I Stellite 6 specimen after 78 days exposure to natural aging conditions.

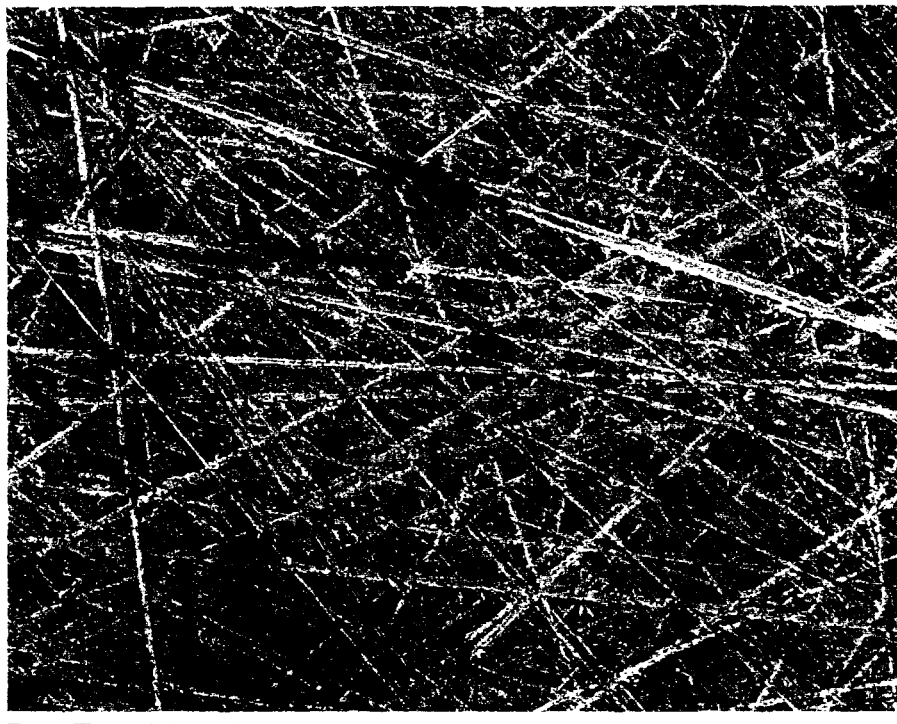


X300

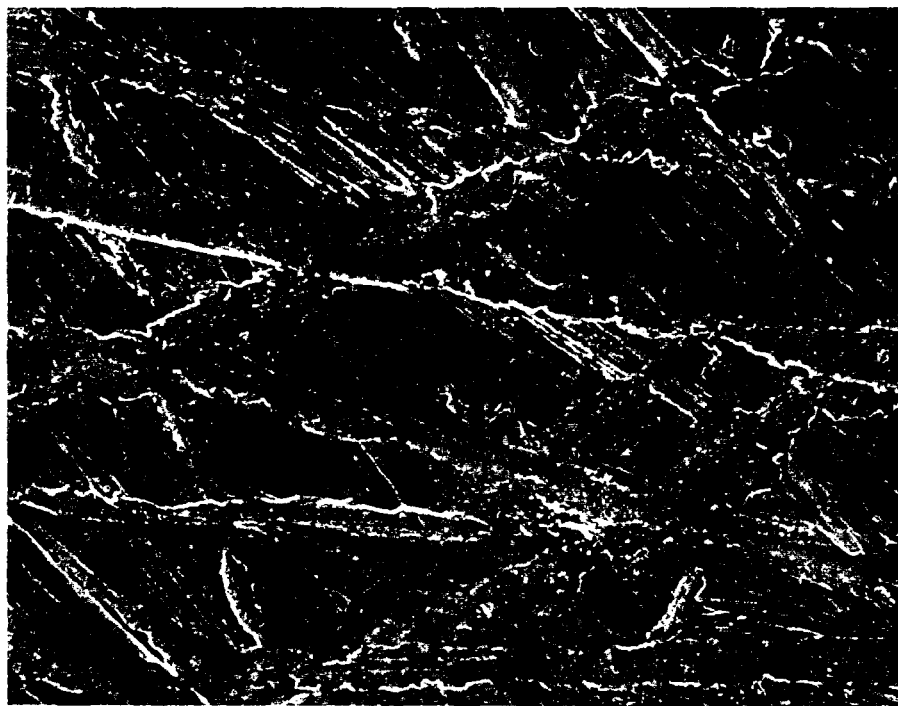


X2,000

Figure 14. Electron micrographs of the surface of a Phase I Stellite 6 specimen after 78 days exposure to natural aging conditions with simulated in-service testing at 25 days and again at 50 days.

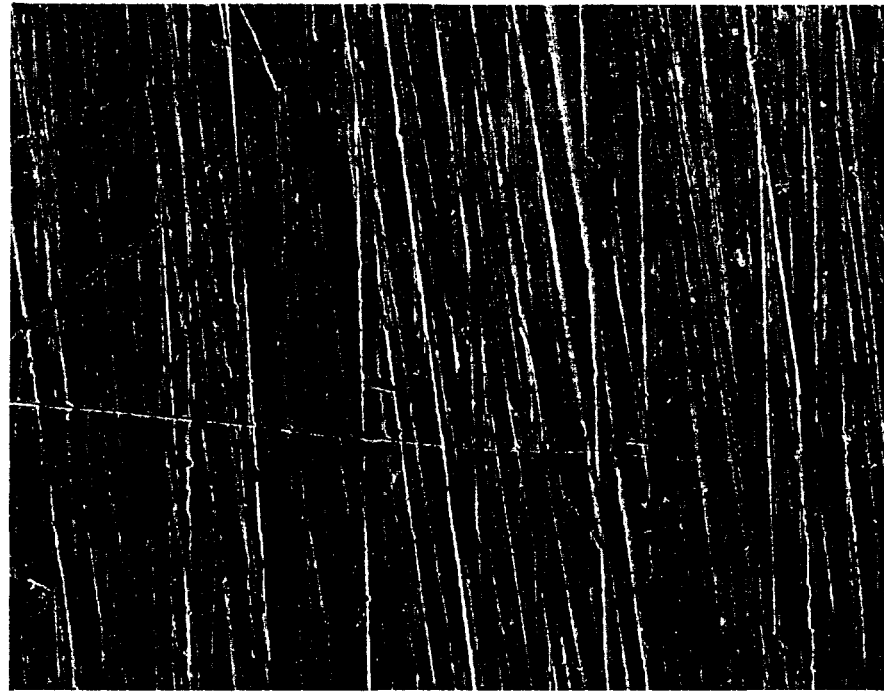


X300

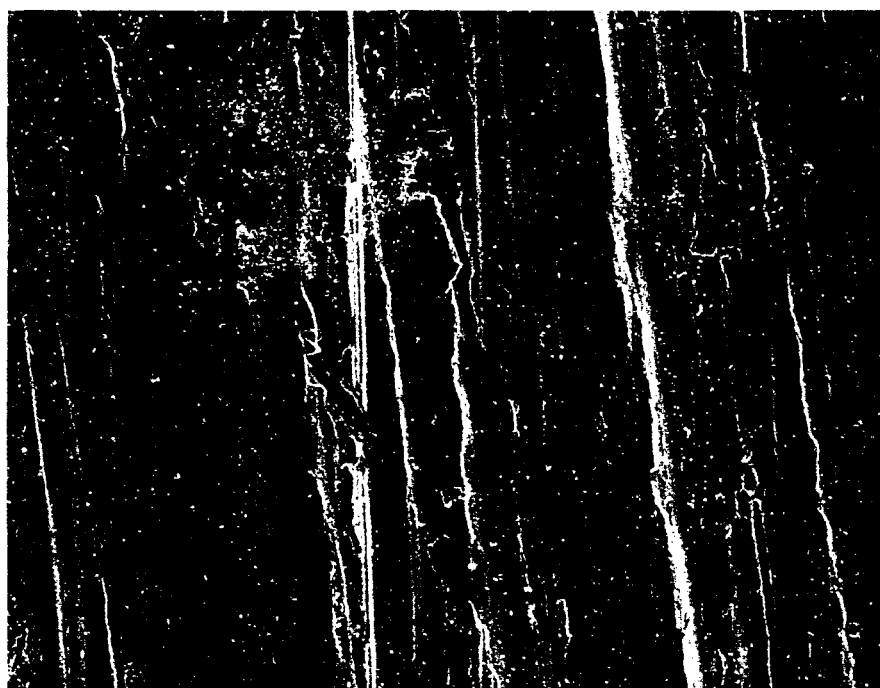


X2,000

Figure 15. Electron micrographs of the surface of a Phase II Stellite 6 specimen before exposure to aging.



X300



X2,000

Figure 16. Electron micrographs of the surface of a Phase II Stellite 6 specimen after 60 days exposure to natural aging conditions.

were not sufficient to hide the surface imperfections from the original machining.

3.1.2 Accelerated Aged Specimens

The surfaces of specimens subjected to accelerated aging (anodic current) are shown in Figures 17 and 18. Figure 17 provides a view of the surface after 11 days aging at an applied current density of 0.15 mA/cm^2 . Note that there are more and larger nodules present, compared to the natural aging. Nodule sizes were in the range of 0.1 to $1.0 \mu\text{m}$. The remnants of the machining marks are visible to a small extent, but the film appears thicker than with the natural aging.

Figure 18 presents images of the surface and the cross section of Stellite 6 after 14 days aging at an applied current density of 0.35 mA/cm^2 . Here, too, the surface shows a large number of nodules; these nodules might be characteristic of surfaces grown under applied currents. The cross section shows the base metal on the left; the right side is a section of the plastic coating applied to the specimen during sample preparation, and the oxide film is the thick line separating the two. The thickness of the oxide film is determined by measuring the apparent film thickness on this magnified image of the cross section. (Film thickness is discussed in more detail later in the report.) We also observed that this oxide film was cracked in several locations both parallel and perpendicular to the alloy surface.

The surface morphology from the accelerated high-pH aging test is shown in Figure 19. The large crystals apparent here were identified as ZrO_2 . The apparent source of the ZrO_2 was the specimen rack in the corrosion autoclave. We infer that the high pH (9.0) in this test either corroded the zirconium specimen rack or encouraged ZrO_2 in the coating to dissolve in the water, and that the ZrO_2 then precipitated on available surfaces when the water was cooled at the end of the test. These large crystals, which resided only at the surface of the film, were removed by cleaning the specimen with isopropyl alcohol. Smaller crystals remained. Figure 20 shows the specimen after cleaning, at two different magnifications. The appearance of

the small crystals contrasts significantly with the morphology of a natural aging oxide film, where the surface is typified by a more uniform coating. Energy Dispersive Spectroscopy (EDS) analysis of the large particle in the center of the frame of the lower photograph indicates that the crystals appear to be iron-rich and are most likely oxides.

Overall, the evaluation of the oxide film morphology showed that oxide films produced by accelerated aging via anodic current were rougher in surface structure than films produced by natural aging. Films produced by accelerated aging via high pH included the presence of metal/oxide crystals that are not present in films produced by natural aging. These differences are significant, and they cast doubt on the validity of using these aging acceleration methods to produce an oxide film with friction characteristics representative of oxide films occurring on Stellite 6 surfaces in BWR systems.

3.2 Composition

Figure 21 shows a typical AES depth profile of the oxide film after being exposed to natural aging conditions. Note that the chromium concentration is almost constant at the surface, through the oxide film, and into the base material. Conversely, the cobalt concentration is very low at the surface, rapidly rises between 1000 and 2000 Å, and remains constant through the base material. Also note that as the cobalt concentration is rapidly rising, the oxygen concentration is rapidly decreasing. This is characteristic of the transition zone between the oxide film and the base material. This depletion of the cobalt at the surface of the Stellite 6 is an indication that the cobalt has leached out of the oxide film and into the coolant. [One Angstrom (\AA) equals one ten-millionth (10^{-7}) of a millimeter.]

An XPS depth profile on the oxide film contains similar information. The biggest difference is that the AES depth profile displays the concentration of individual elements whereas the XPS depth profile displays the concentration of compounds.

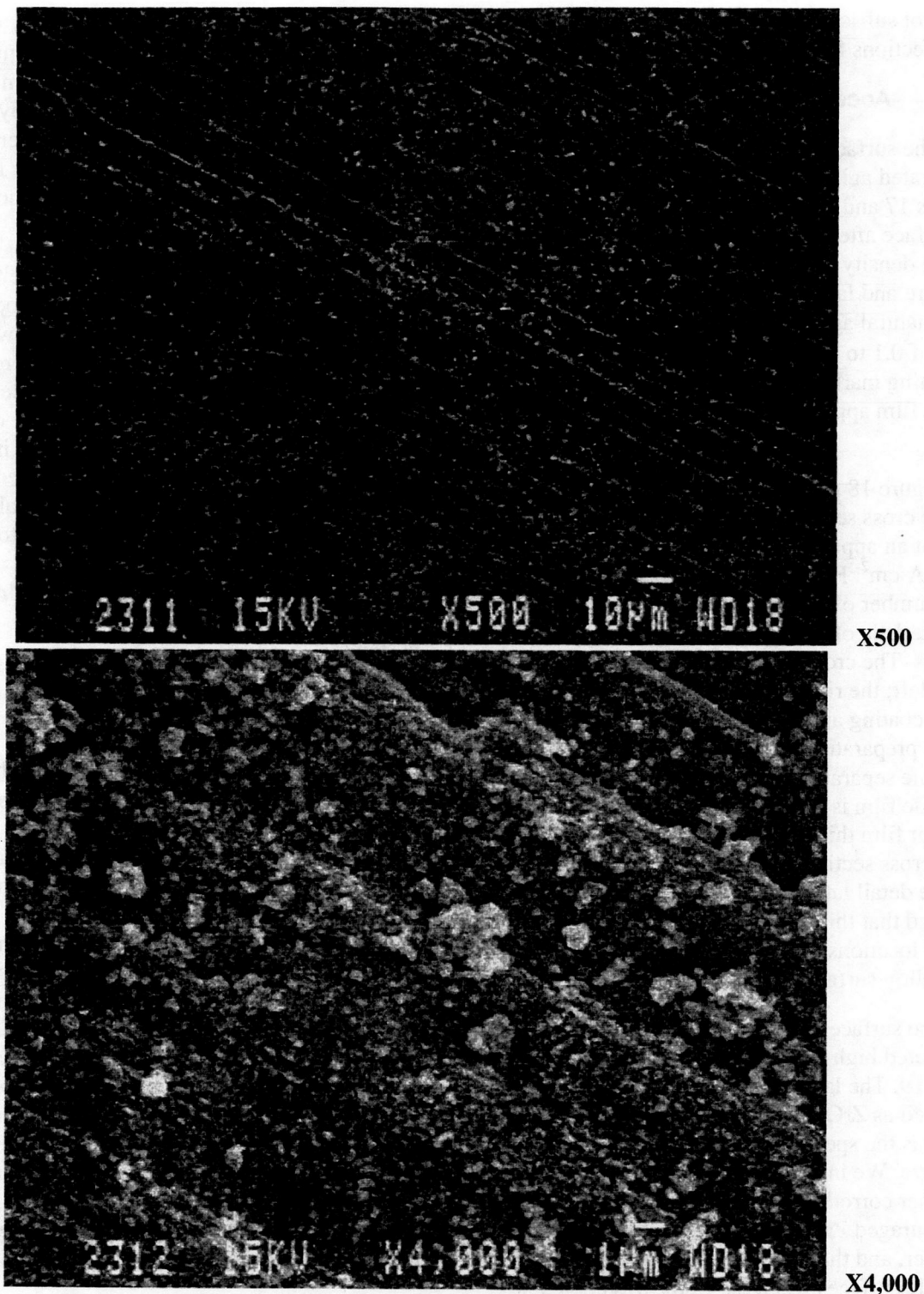


Figure 17. Electron micrographs of the surface of a Phase I Stellite 6 specimen after 11 days exposure to an anodic current density of 0.15 mA/cm^2 .

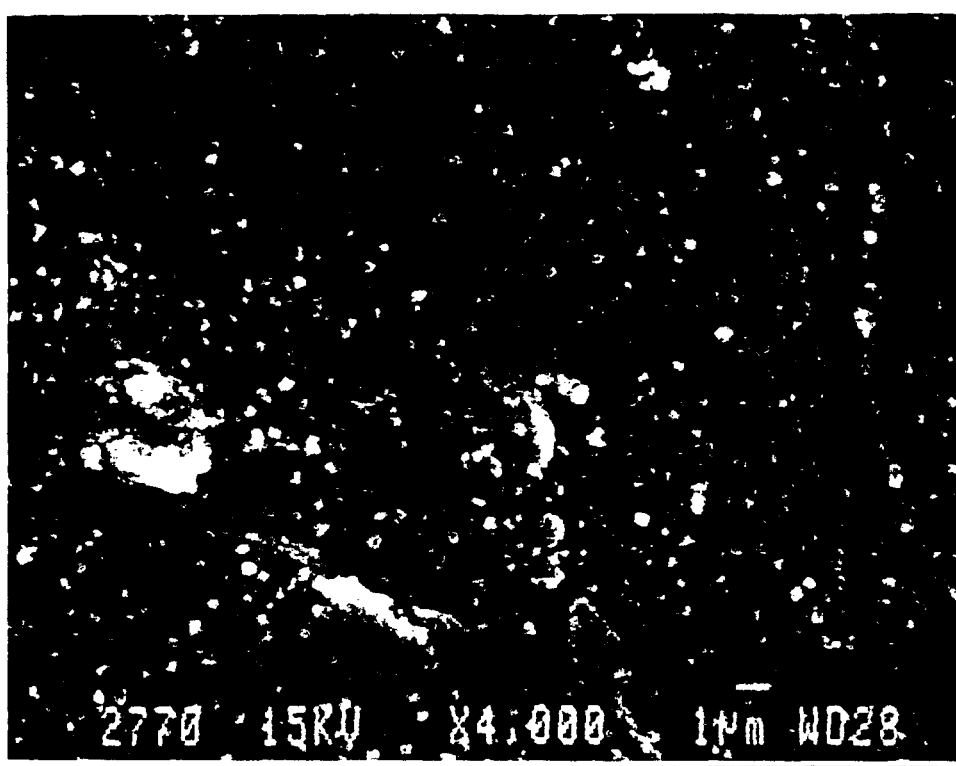


Figure 18. Electron micrographs of the surface and cross section of a Phase I Stellite 6 specimen after 14 days exposure to an anodic current density of 0.35 mA/cm^2 .

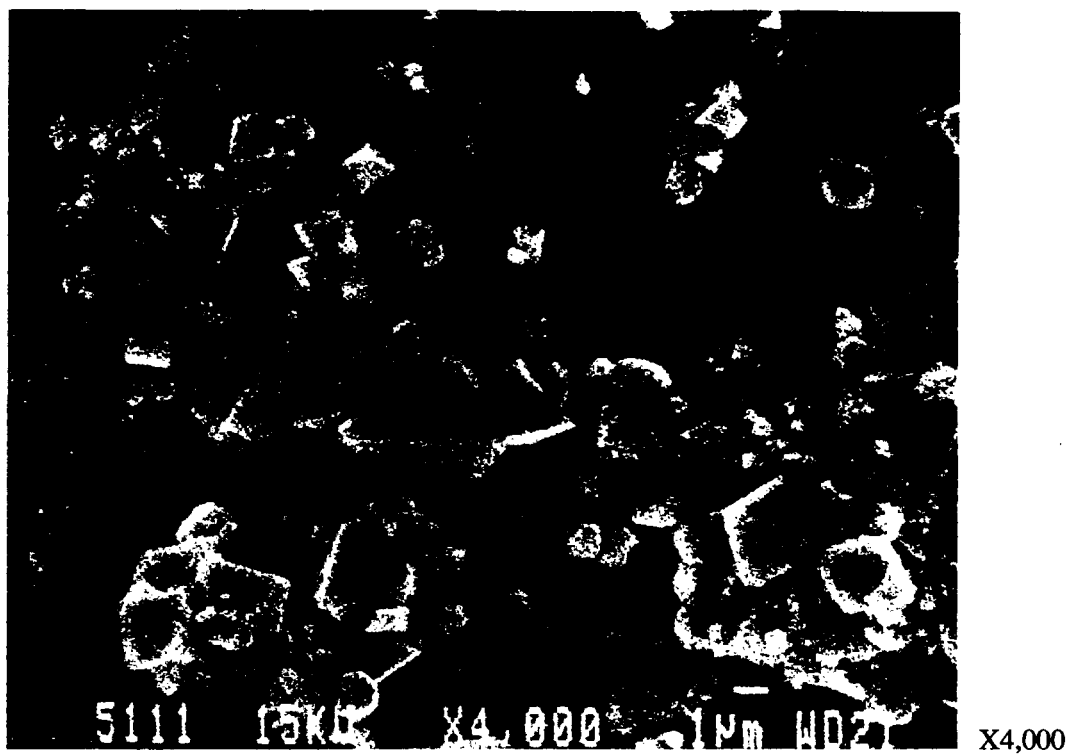
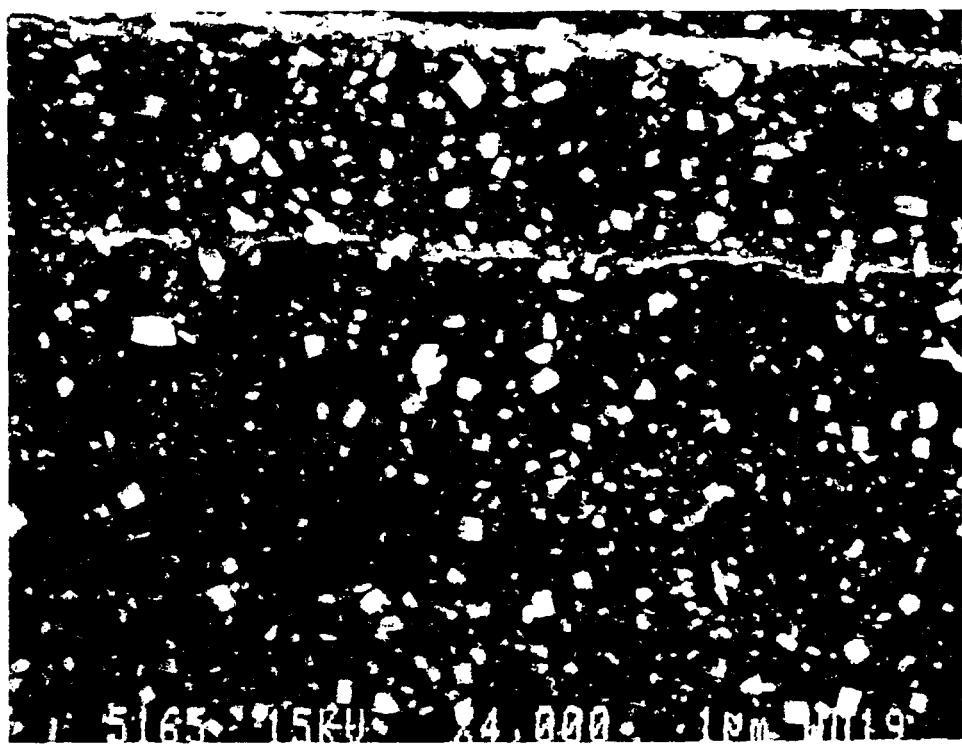
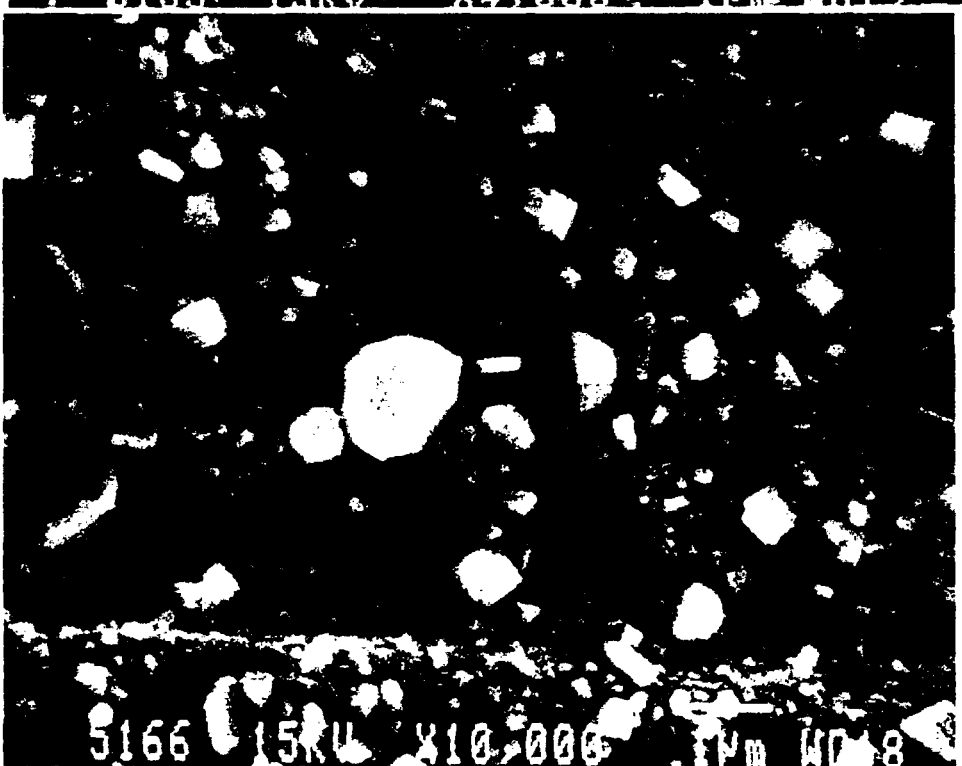


Figure 19. Electron micrograph of the surface of a Phase I Stellite 6 specimen after 19 days exposure to high-pH conditions; the large, zirconium-rich crystals are conspicuous.



X4,000



X10,000

Figure 20. Electron micrographs of the surface of a Phase I Stellite 6 specimen after 19 days exposure to high-pH conditions; the zirconium-rich crystals have been removed, but iron-rich crystals remain.

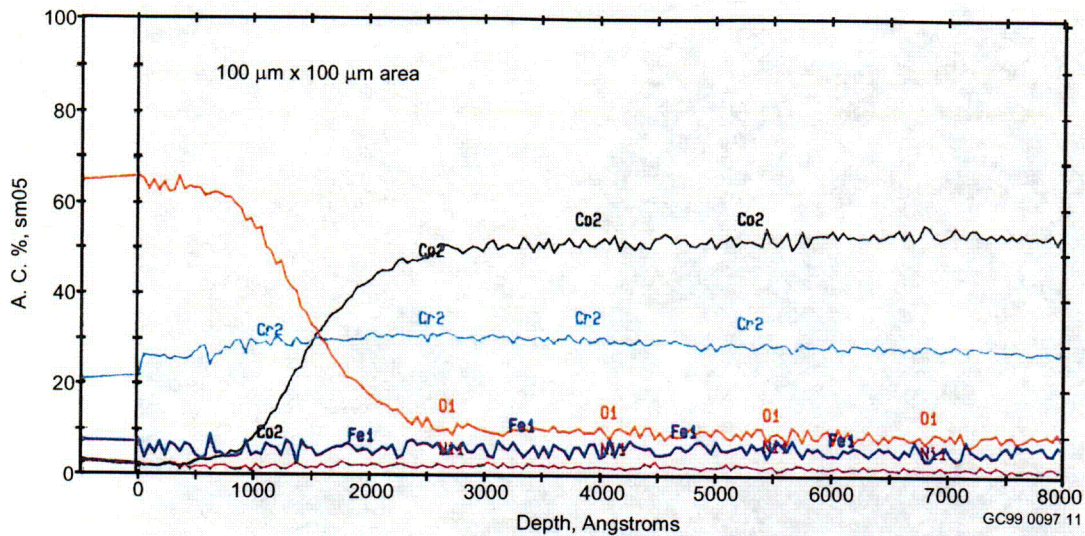


Figure 21. AES depth profile for Stellite 6 specimens after exposure to natural aging conditions.

3.2.1 Naturally Aged Specimens

Specimens from the Phase I natural aging tests were analyzed using XPS. Figures 22 through 26 show the concentrations for selected compounds in atomic percent, plotted against

sputtering time (which corresponds with depth, although the conversion between sputtering time and depth is not the same for each figure) for the 10-, 20-, 25-, 40-, and 78-day tests. (The 2-day specimen was also analyzed, but due to an equipment malfunction the plot is not available.)

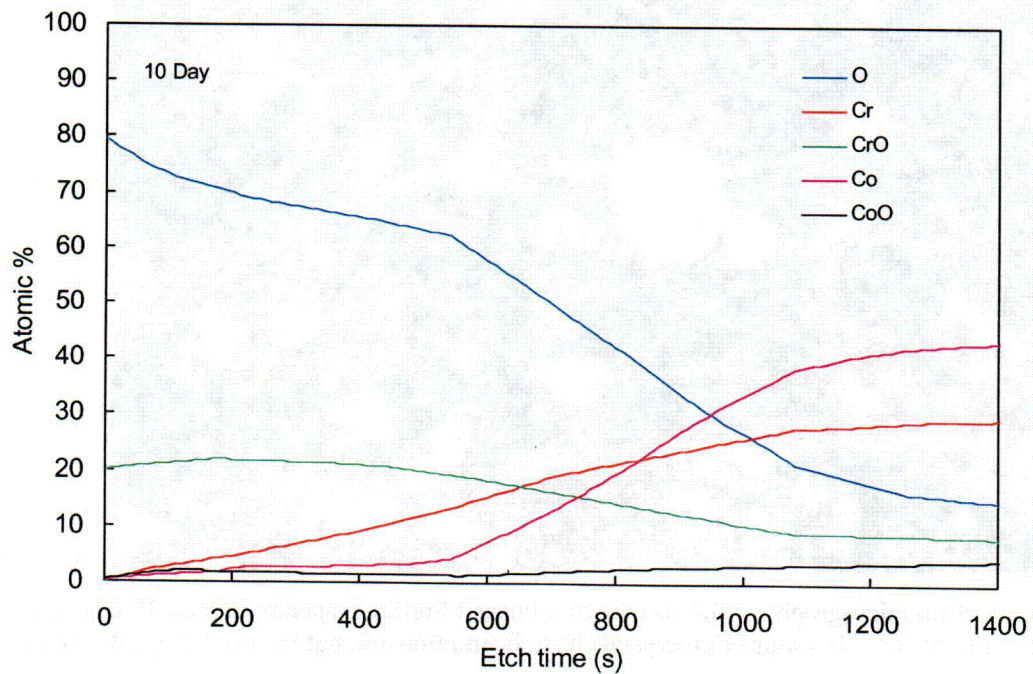


Figure 22. XPS depth profile for a Phase I Stellite 6 specimen after 10 days exposure to natural aging conditions.

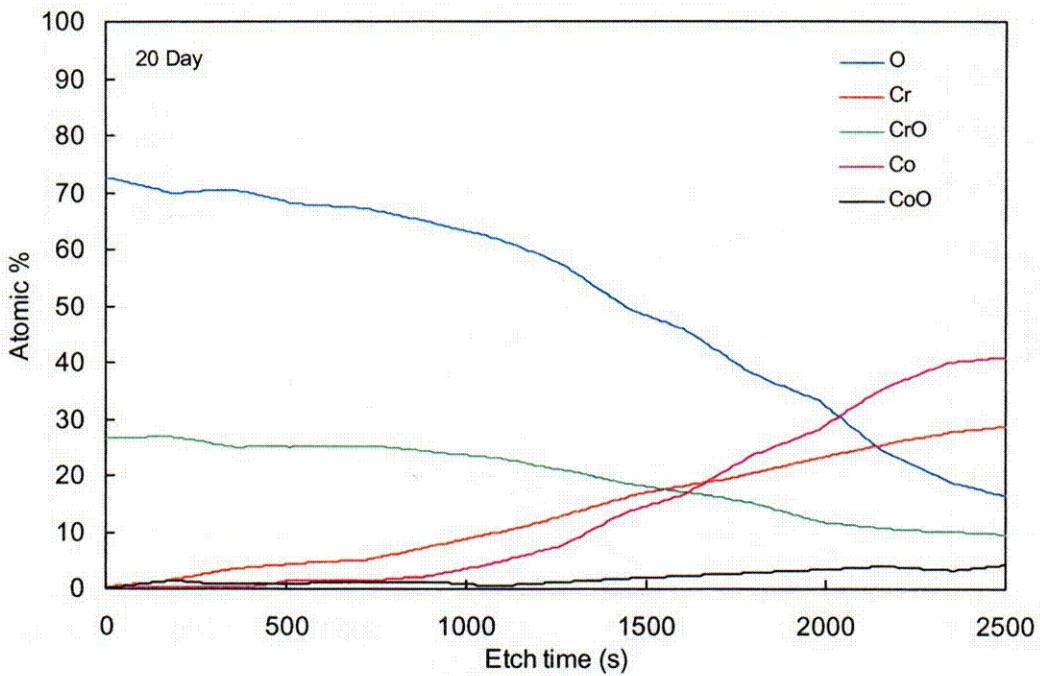


Figure 23. XPS depth profile for a Phase I Stellite 6 specimen after 20 days exposure to natural aging conditions.

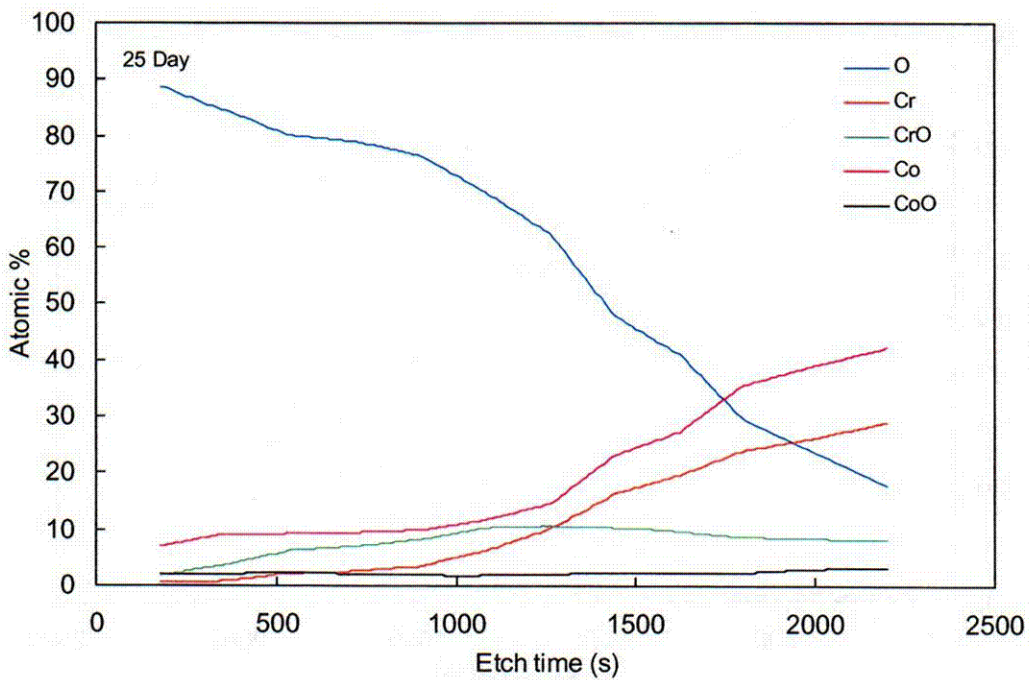


Figure 24. XPS depth profile for a Phase I Stellite 6 specimen after 25 days exposure to natural aging conditions.

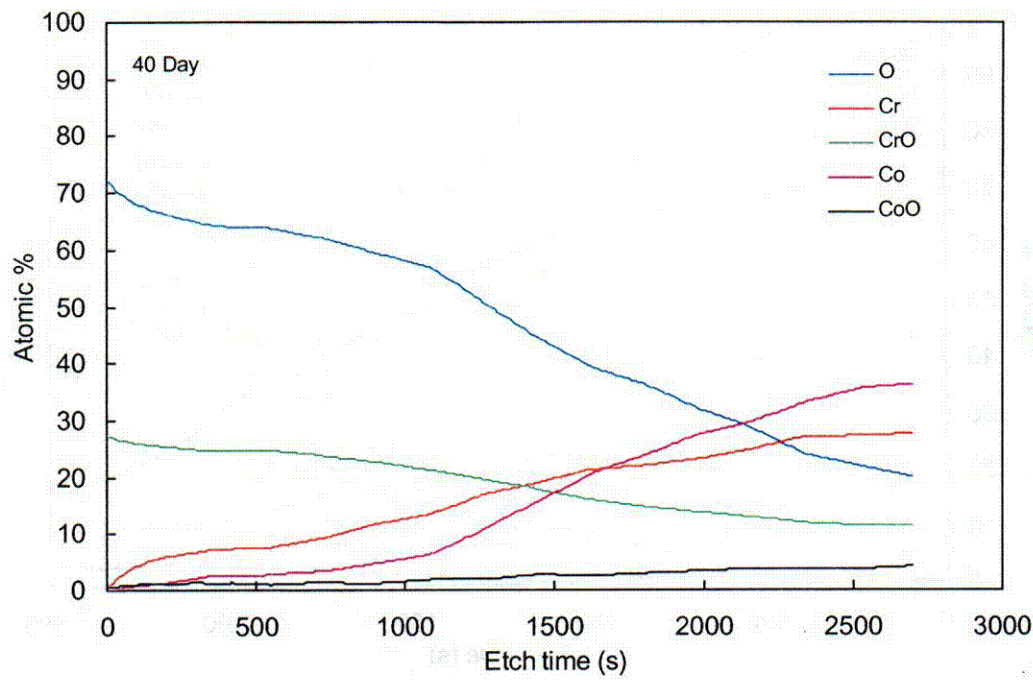


Figure 25. XPS depth profile for a Phase I Stellite 6 specimen after 40 days exposure to natural aging conditions.

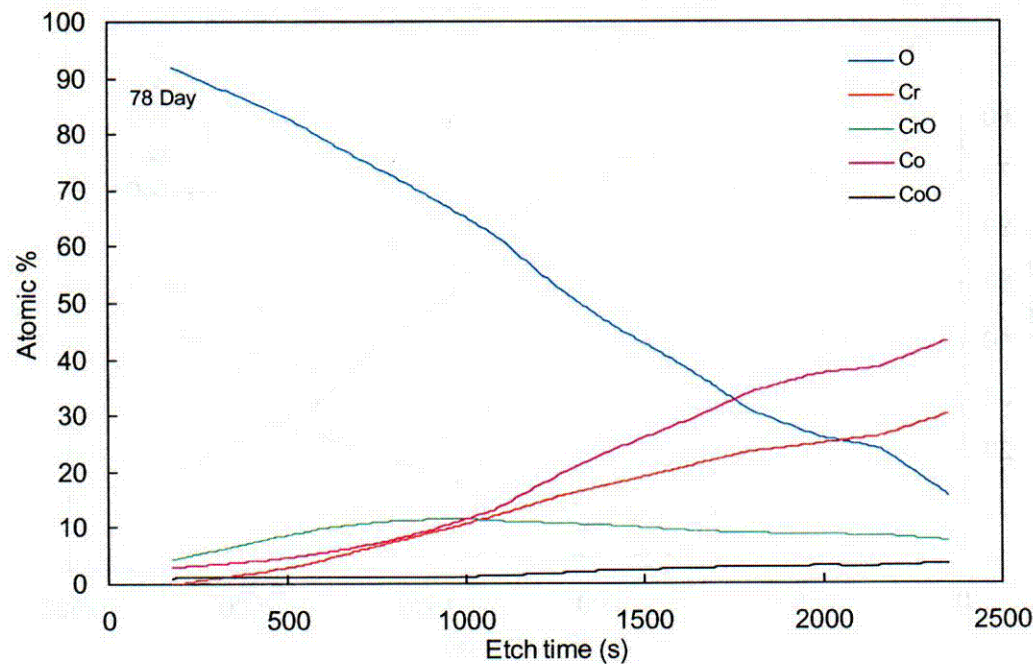


Figure 26. XPS depth profile for a Phase I Stellite 6 specimen after 78 days exposure to natural aging conditions.

Although the XPS profile is based on compound concentrations and the AES profile is based on elemental concentrations, the same trends are evident in each. The chromium concentration is relatively constant, although at the surface it takes the form of chromium oxide whereas in the base material it is free chromium. The cobalt concentration is low at the surface, rapidly rises through the transition zone, and is almost constant through the base material. The oxygen concentration is high at the surface, decreases through the oxide film, and is relatively low through the base material.

Figures 27 and 28 show similar information, but organized differently. In these figures, the concentration of the chromium oxides and of the oxygen for the 10-, 20-, 25-, 40-, and 78-day testing is shown. The 10-, 20-, and 40-day specimens were from the third set of Phase I tests and the 25- and 78-day specimens were from the fourth set of Phase I tests. These figures reveal an interesting trend. The concentration of the chromium oxides at the surface of the oxide film from the fourth set of Phase I tests (the 25-day and 78-day specimens) is 5% or less. However, the concentration of the chromium oxides at the surface of the oxide film from the third set of Phase I tests (the 10-day, 20-day, and 40-day specimens) is 20 to 30%. The concentration of oxygen at the surface of the oxide film shows similar differences. For the fourth test series, the oxygen concentration is about 90% at the surface, whereas for the third test series the oxygen concentration is 70 to 80% at the surface. These slight differences may be due to the two corrosion autoclaves that produced the oxide films on the specimens. However, the effect of these minor differences is not observed in the frictional behavior of the specimens.

The oxide films of two of these specimens (a 10-day and a 50-day specimen) were also analyzed at NIST using an Atomic Force Microscope and X-ray diffraction. The results indicate that the surface of the oxide film contains crystalline solids within an amorphous substrate. This type of surface can be likened to the surface of a piece of sandpaper in which the grains on the sandpaper are analogous to the

crystalline solids. As the surface of the Stellite 6 ages, the crystals become larger, similar to a piece of sandpaper with larger grains on it. The composition of the crystalline solids was not determined, but we expect them to be chromium oxide, cobalt oxides, or carbides. Such crystalline solids are, in general, very abrasive. When two such surfaces are placed against each other and one moved relative to the other, the friction can be quite high, especially during the first stroke. With subsequent stroking, the crystalline solids will either plastically deform or fracture as the two surfaces pass each other. As such, the friction would be expected to decrease with continued stroking until the friction of the bulk Stellite 6 material is reached. This would be comparable to two pieces of sandpaper rubbing against each other. During the first stroke, the surface grains are intact and offer the most resistance. As the surface grains are fractured, the resistance decreases until eventually just the two pieces of paper backing are rubbing against each other. The friction behavior of the oxide films is discussed in more detail later in the report.

Specimens from the Phase I natural aging tests that were subjected to simulated valve wedging cycles were also analyzed using XPS. Because the primary purpose of the XPS analysis was to determine the oxide film thickness, only the chromium and chromium oxide profiles were processed; detailed compositional profiles were not processed and plotted for all species.

Specimens from the Phase II natural aging tests were analyzed using AES. Figure 29 shows a typical elemental concentration profile for selected species in atomic percent, plotted against sputtering depth. The figure represents the elemental concentration profile after 30 days of aging; results for other aging times are similar.

3.2.2 Accelerated Aged Specimens

Figure 30 shows the oxide film composition from a specimen subjected to accelerated aging using an anodic current. This is an AES depth profile for a Phase I Stellite 6 specimen exposed to a current density of 0.15 mA/cm^2 for 11 days.

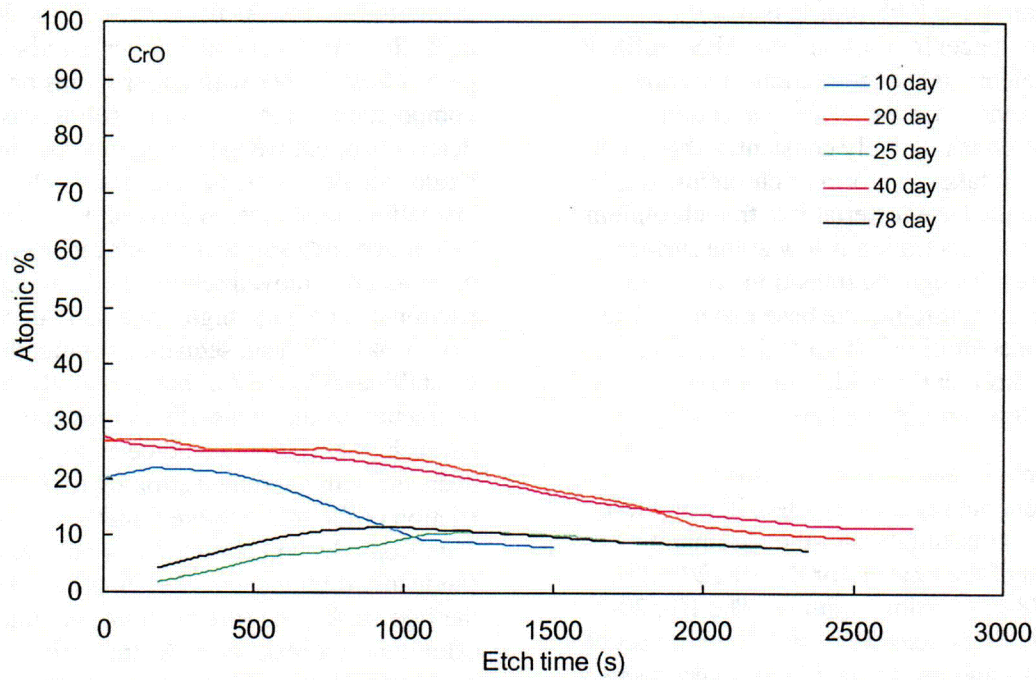


Figure 27. XPS depth profile of the chromium oxide in a Phase I Stellite 6 specimen exposed to natural aging conditions.

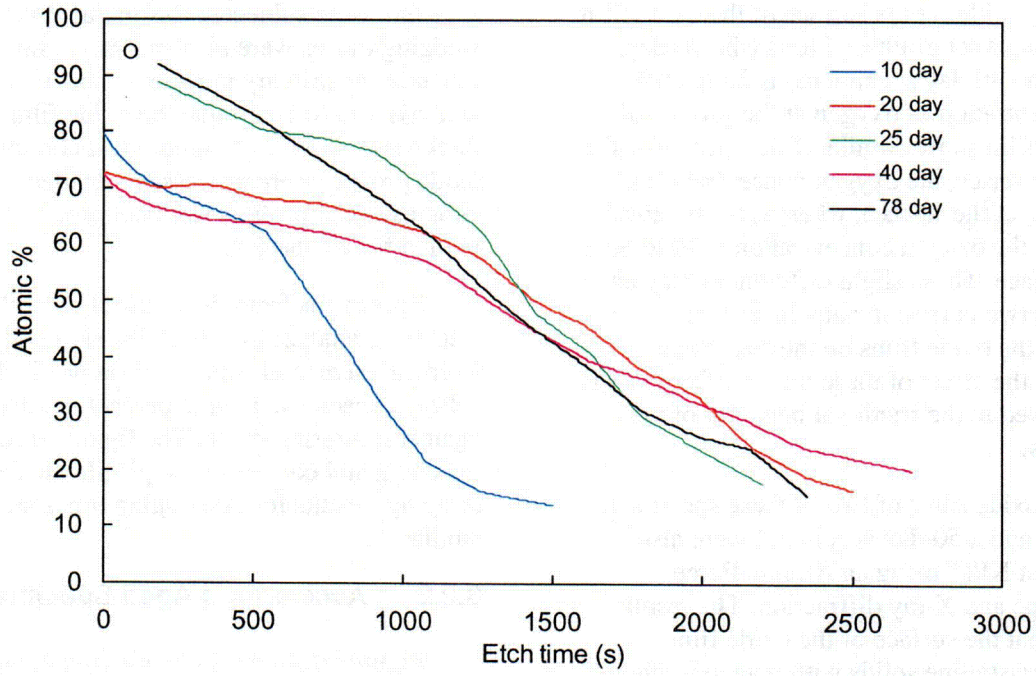


Figure 28. XPS depth profile of the oxygen in a Phase I Stellite 6 specimen exposed to natural aging conditions.

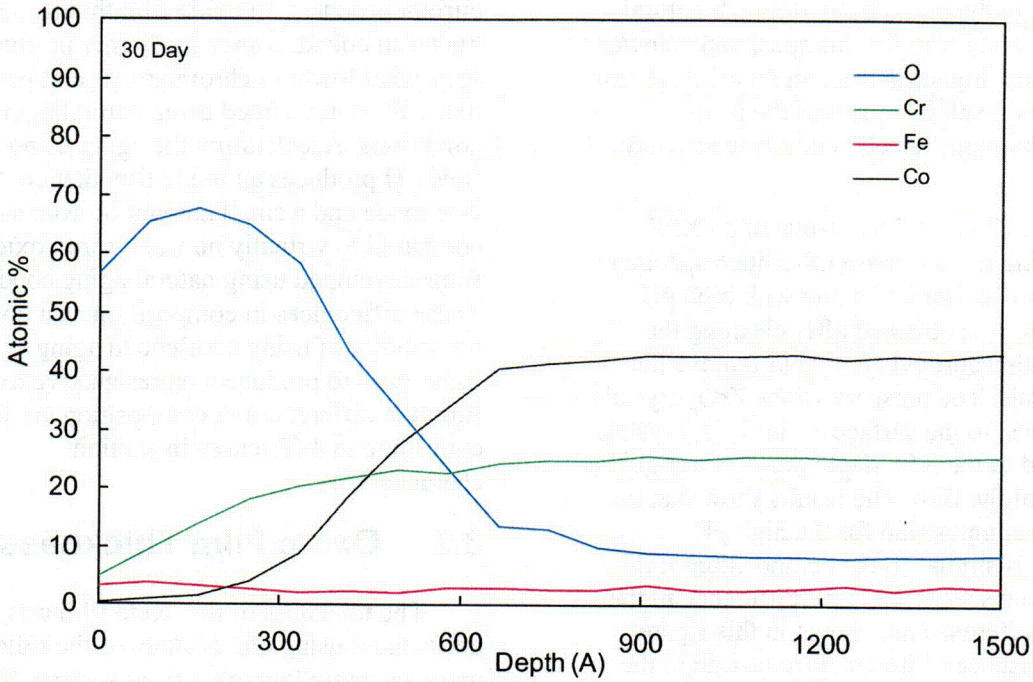


Figure 29. AES depth profile for a Phase II Stellite 6 specimen after 30 days exposure to natural aging conditions.

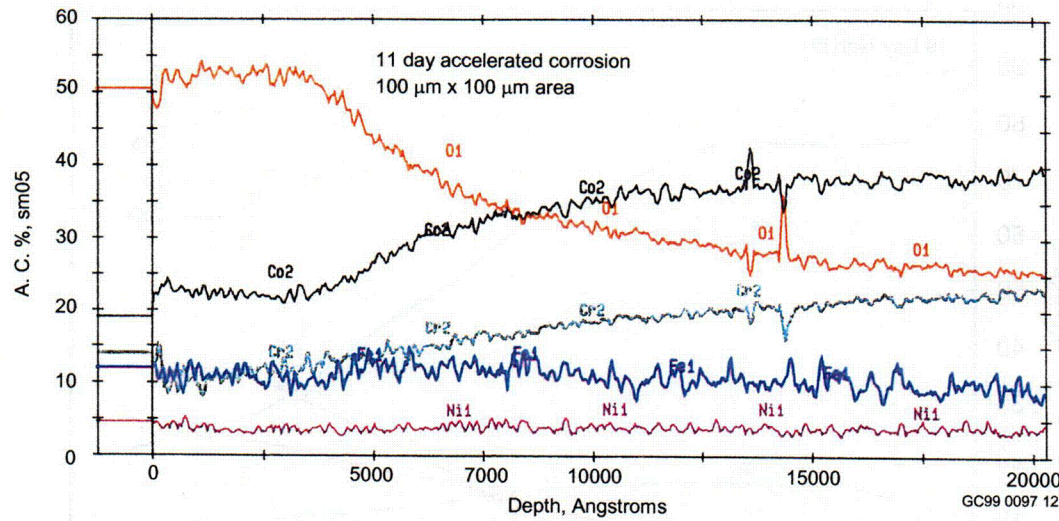


Figure 30. AES depth profile for a Stellite 6 specimen after 11 days exposure to an anodic current density of 0.15 mA/cm^2 .

Compared to the oxide films from the natural aging, the oxide film for this specimen is lower in chromium, higher in iron, and much higher in cobalt. This result is typical of the films produced by aging accelerated using an anodic current.

Figure 31 shows the results of an XPS depth profile from a Phase I Stellite 6 specimen subjected to accelerated aging with high pH. This profile was obtained after cleaning the surface with isopropyl alcohol to remove the ZrO_2 crystals. The presence of the ZrO_2 crystals was confined to the surface, as no ZrO_2 crystals were found in the XPS depth profile through the thickness of the film. The results show that the oxide film composition for the high-pH specimens is similar to the composition of the natural aging specimens. One difference in the results, a difference not shown in this figure, was the presence of iron and iron oxide in the film. The iron was fairly evenly distributed through the film thickness; the iron oxide content was higher near the surface of the film and lower at greater depth.

Overall, the XPS and AES results indicate that accelerating the aging using an anodic

current produces an oxide film that is much higher in cobalt, somewhat higher in iron, and somewhat lower in chromium, as compared to oxide films developed using natural aging conditions. Accelerating the aging using a high fluid pH produces an oxide film that contains iron oxide and a small amount of iron; as compared to virtually no iron or iron oxide in the films developed using natural aging conditions. These differences in composition cast doubt on the validity of using accelerated aging techniques to produce a representative oxide film; the differences in composition are likely to contribute to differences in friction characteristics.

3.3 Oxide Film Thickness

The thickness of the oxide film was determined using one or more of the following methods; metallographic cross section, XPS depth profiles, or AES depth profiles. The oxide film thickness was estimated using the XPS or the AES data because of the difficulty in resolving the oxide film boundary in the images from the scanning electron microscope (SEM).

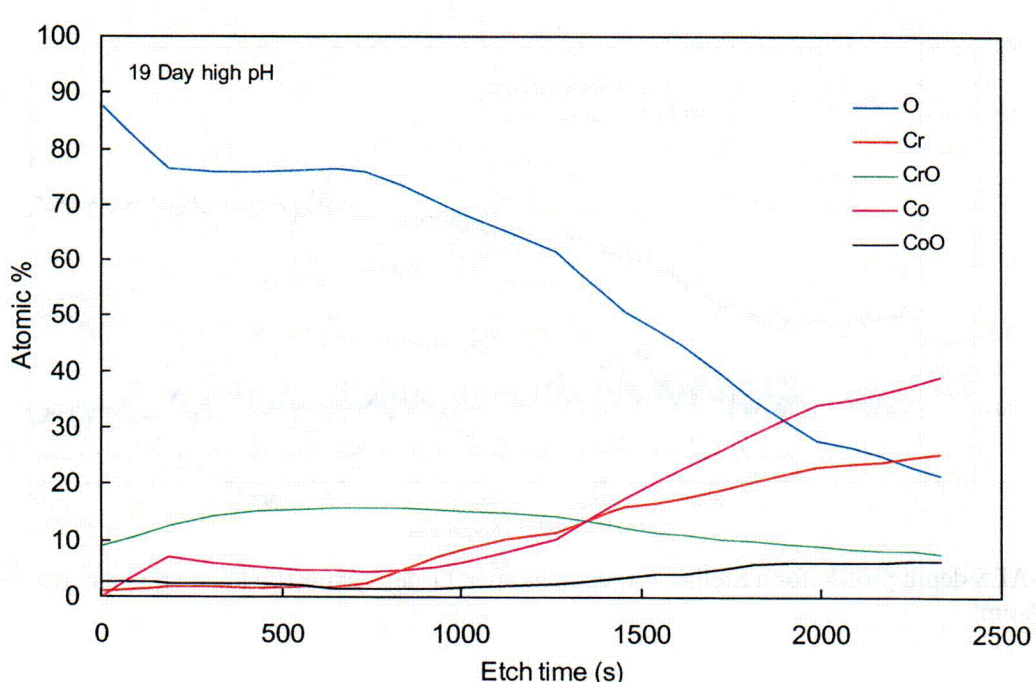


Figure 31. XPS depth profile for a Stellite 6 specimen after 19 days exposure to high-pH aging conditions.

Although more than one method may have been used on selected specimens, the estimated oxide film thicknesses presented in this report were based on:

- XPS data for the Phase I specimens that were naturally aged.
- XPS data for the Phase I specimens that were accelerated aged using a high-pH.
- Cross-section from an electron micrograph for the Phase I specimens that were accelerated aged using an anodic current.
- AES data for the Phase II specimens that were naturally aged.

3.3.1 Naturally Aged Specimens

Tables 5 and 6 present a summary of the thickness of the oxide film for the naturally aged

Phase I and Phase II specimens. The film thickness for the Phase I specimens was determined using XPS whereas AES was used for the Phase II specimens. To remove as many uncertainties as possible, all the XPS data from the Phase I testing were taken from the same source. The data in Table 5 are from naturally aged specimens that were not subjected to a surface load or deformation, whereas the data in Table 6 are from naturally aged Phase I specimens that were subjected to simulated valve wedging cycles. For this research, the thickness for the Phase I specimens was defined as that depth where the concentration of the chromium and the chromium oxide were equal in the XPS depth profiles. The thickness for the Phase II specimens was defined as the depth where the concentration of the oxygen and the cobalt were equal in the AES depth profiles.

Table 5. Oxide film thickness on Phase I and Phase II Stellite 6 specimens exposed to natural aging.

Time exposed to natural aging conditions (days)	Phase I Oxide film thickness (Å)	Phase II Oxide film thickness (Å)
2	N/A	
10	480	
20	1000	
25	1100	
30		528
		810
40	1085	
50	1350	
60		505
		638
78	1750	
90		658
120		579

Table 6. Oxide film thickness on Phase I Stellite 6 specimens exposed to natural aging and simulated valve wedging loads.

Time exposed to natural aging conditions (days)	Oxide film thickness (Å)
25	1100
25 + IST ^a	750
25 + IST ^a + 25	1800
25 + IST ^a + 25 + IST ^a	1350

a. Simulated in-service test wedging cycles.

Other researchers have used these methods to define the oxide film thickness, but they are not the only methods being used. For instance, some researchers define the oxide film thickness as the point where the oxygen concentration within the oxide film is reduced to one half the oxygen concentration at the surface. For our needs, consistent use of a method is more important than the selection of one method over another. Each of these thicknesses is the result of examining the composition of the oxide film from a single specimen, so we have no way to estimate the statistical variation at each exposure time. We recognize, however, that the statistical variation might be large.

Based on this oxide film thickness data, the thickness is plotted versus time and is shown in Figure 32, along with a best fit for each phase of testing. These results indicate that the oxide film growth rate for both the Phase I and the Phase II data appears to be parabolic. Even so, the thickness for the Phase II data appears to be constant, the thickness appearing to have reached a plateau. By comparison, the work of Honda et al. (1987) investigated the oxide film growth characteristics of Type 304 Stainless Steel and of carbon steel. Figure 33 shows that the oxide film growth rate of Stellite 6 from either the Phase I or the Phase II testing is slower than that of the Type 304 Stainless Steel and much slower than the growth rate for carbon steel.

Part of the Phase I work that was performed at Battelle included testing to determine whether

the simulated valve wedging affected the oxide film thickness, and if so, how additional exposure to BWR conditions affects the subsequent growth of the oxide film. Figure 34 presents the results of this testing and shows the effect a simulated valve wedging cycle has on the long-term growth characteristics of the oxide film. The oxide film thickness before the in-service test wedging cycle (boxes) is compared to the oxide film thickness after an in-service test wedging cycle (triangles); included for comparison is the data fit of the Phase I naturally aged, undisturbed oxide film thickness. The resulting film thickness after 25 days and after 50 days appears to follow the general thickness trend observed for specimens that were allowed to age during the Phase I testing without being disturbed.

3.3.2 Accelerated Aged Specimens

The oxide film thicknesses for the accelerated anodic aging tests were determined from metallographic cross sections. The results are summarized in Table 7. The oxide films are much thicker than those formed under natural aging conditions.

The film thickness for an accelerated high-pH aging specimen was determined from the XPS plot in Figure 31 as the depth at which the chromium and chromium oxide concentrations were equal. The oxide film thickness as defined by this method is 1100 Å for this 19-day specimen, which is similar to that measured on the 20- to 40-day natural aging specimens from

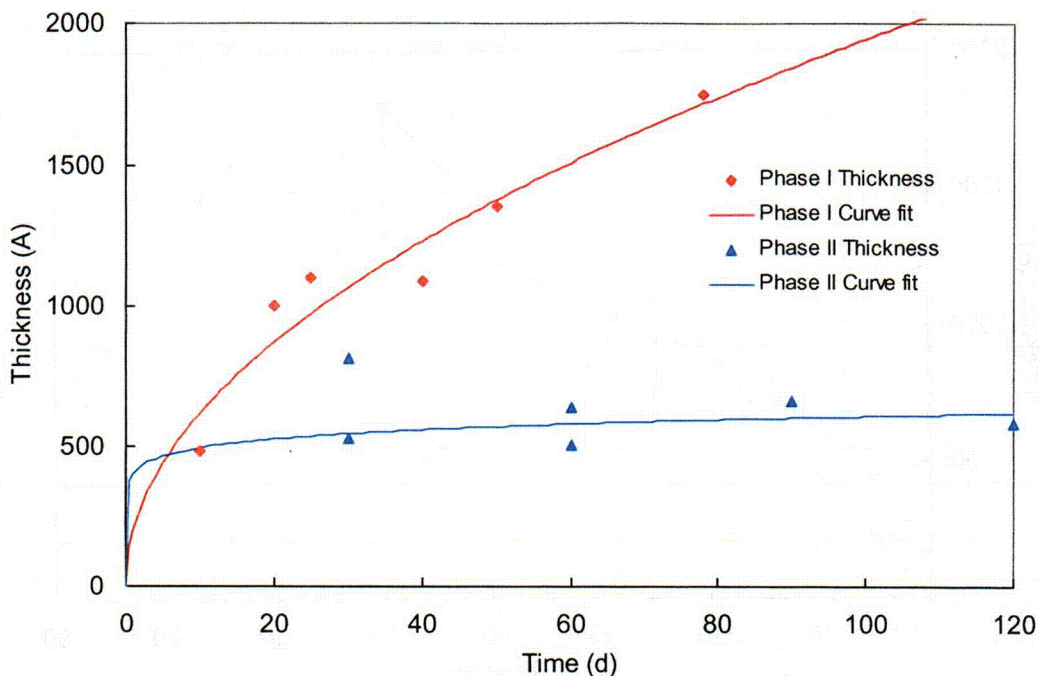


Figure 32. Oxide film thickness versus time for Stellite 6, showing the data from the Phase I and Phase II natural aging tests and their data fits.

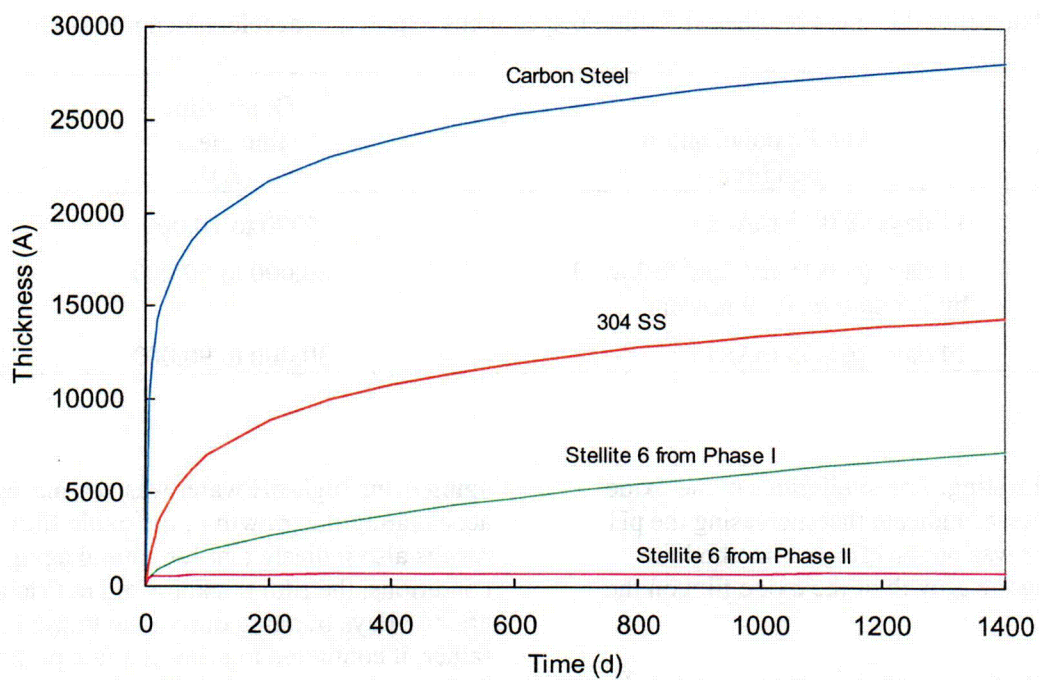


Figure 33. Oxide film thickness versus time for Stellite 6 from the Phase I and the Phase II testing, Type 304 Stainless Steel, and carbon steel.

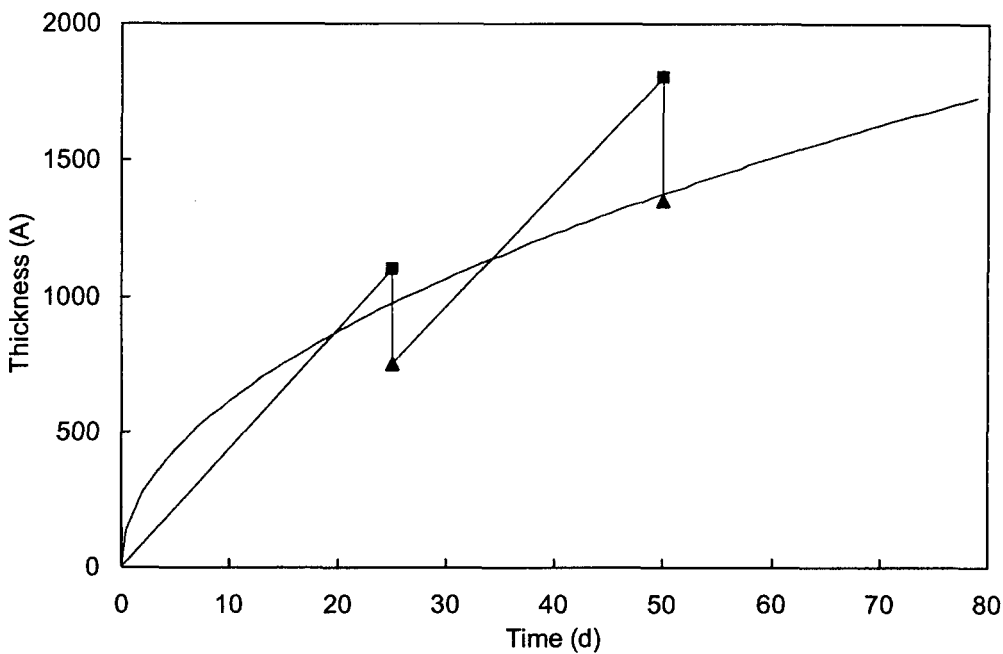


Figure 34. Oxide film thickness versus time for Stellite 6, showing the data from the simulated valve wedging tests and the parabolic data fit of the Phase I naturally aged tests.

Table 7. Oxide film thickness on Phase I Stellite 6 specimens exposed to accelerated aging via an anodic current.

Anodic polarization conditions	Oxide film thickness (Å)
11 days @ 0.15 mA/cm ²	5000 to 10,000
11 days @ 0.15 mA/cm ² followed by 2.5 days @ 0.19 mA/cm ²	30,000 to 50,000
14 days @ 0.35 mA/cm ²	30,000 to 90,000

the Phase I testing. The similarities in the oxide film thicknesses indicate that increasing the pH of the water was not an effective method for accelerating the growth of the oxide film on the specimens.

Overall, the results show that accelerated aging using an anodic current was successful at producing a thicker oxide film in a shorter time, as compared with natural aging. Accelerated

aging using high-pH water was not successful at accelerating the growth of the oxide film. The results also indicate that for natural aging conditions, the film thickness did not stabilize after 78 days of aging during the Phase I testing; rather, it continued to grow at a rate proportional to the square root of time. However, the Phase II testing indicates that for natural aging conditions, the film thickness appears to have stabilized. The review effort performed by NIST

supports the concept that the thickness of the oxide film will increase as a function of exposure time, although the growth rate may decrease over time. Even though the thickness of the oxide film may continue to increase, the ability to safely operate a valve is not necessarily affected by the thickness or thinness of the oxide film, but rather on the mechanical properties of the oxide film as it ages. In particular, the friction of the oxide film as the material ages is of particular interest to assessing valve operability concerns.

3.4 Accelerated versus natural aging

The results described here provide an indication of the difficulty that can be encountered in using accelerated aging techniques to grow oxide films typical of the composition and structure expected in a reactor environment. The accelerating techniques attempted in this test project suffer from either having no significant effect on the thickness of the oxide film, or from possible confounding effects on friction by altering the film composition or surface structure.

Specifically, the use of a small anodic current to accelerate the aging was successful in producing a thick film in a short time. However, the surface structure (the presence of nodules) and chemical composition (higher cobalt, lower chromium) of the film were significantly different than for films produced by natural aging. The use of high pH to accelerate the aging did not produce a thick film in a short time, and the surface structure (the presence of small iron-rich metal/oxide crystals) and chemical composition (presence of iron and iron oxide) were somewhat different than for films produced by natural aging. These differences, together with the corresponding differences in the friction results (reported in the next section of the report), indicated that these aging acceleration methods are not suitable for producing oxide films that are representative of films produced over longer periods of time under natural (normal BWR) conditions.

3.5 Known deviations in the experimental conditions

During the Phase II testing, the specimens were naturally aged in a corrosion autoclave at BWR coolant conditions. The corrosion autoclave is designed to maintain pressure and temperature conditions for an extended period of time. Unfortunately, twice during the corrosion process, the water level in the corrosion autoclave dropped and the specimens were exposed to water vapor instead of liquid water. The first exposure to water vapor occurred during the 30 to 60 day corrosion cycle; the second occurred during the 90 to 120 day corrosion cycle which also contained specimens undergoing their 0 to 30 day corrosion cycle. Although the temperature and pressure were maintained, the concern is that the corrosion film formed while in a steam environment may not be representative of the corrosion film formed while fully submerged in water.

To determine if the corrosion film would be affected by the exposure to water vapor, high temperature and high-pressure corrosion experts were sought for their insights. Several experts were contacted, namely Dr. Ian Wright at Oak Ridge National Laboratory, Ian Inglis and Dr. Victor Murphy at Atomic Energy Canada Ltd., and Professor Margaret Stack of the University of Strathclyde, in Scotland. They each indicated that they knew of no data that could be used for a direct comparison of oxides formed in steam versus oxides formed in water. Although no detailed characterization was conducted, work conducted by AECL in stress relieving materials in 400°F steam indicated that there was no visual evidence of differences in the oxide formed on carbon steel or zirconium alloy compared with the oxide formed during water exposure.

To determine if the specimens were affected by the exposure to water vapor, two sets of specimens were examined. One set of specimens contained 30 days of natural aging and were exposed only to liquid water. The other set of specimens also contained 30 days of natural aging, however these specimens were exposed to water vapor in addition to liquid

water. To determine if they were affected, electron micrographs of each surface were compared. In addition, the oxide film composition and the estimated oxide film thickness of each were evaluated.

Figures 35 and 36 contain the electron micrographs of the 30-day specimen that was exposed to water vapor and the 30-day specimen that was not exposed to water vapor, respectively. These figures show that the oxide film does not obliterate the initial machining marks and that the surfaces are smooth with sparsely distributed nodules. Both figures are typical of electron micrographs from naturally aged specimens shown earlier.

Next, the composition and thickness of each oxide film were evaluated. Figure 37 shows an AES depth profile of each. Although slight differences can be seen, these differences are more reflective of a slight variation in the thickness of the oxide film rather than a variation in the composition of the oxide film.

Based on the similarity of the electron micrographs, the composition of the oxide film, and on the relative thickness of the film, we do not believe that the oxide film was adversely impacted by the exposure to water vapor during the corrosion.

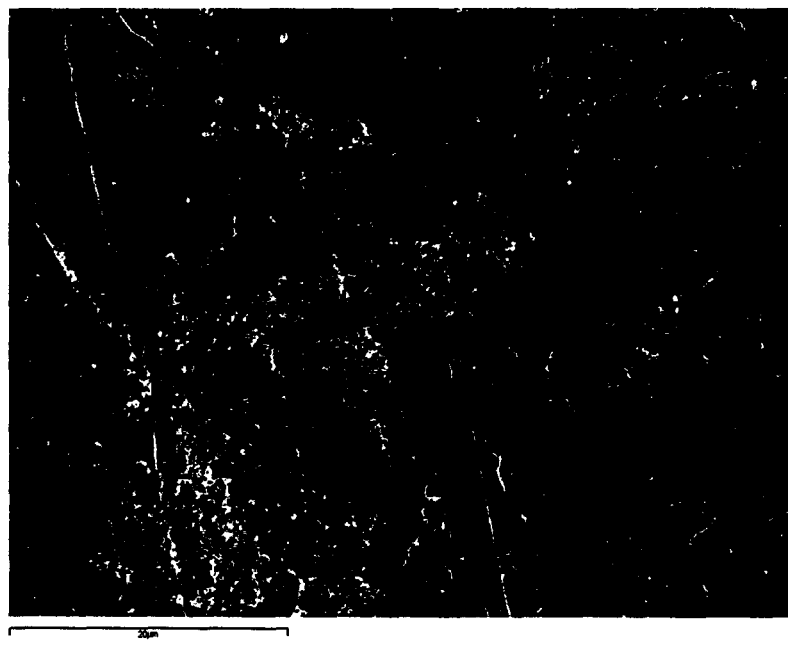
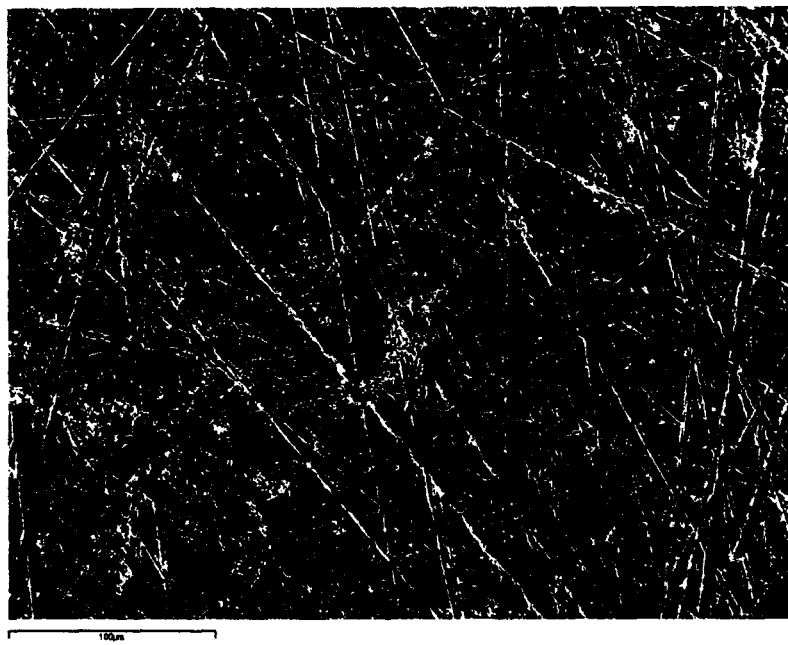


Figure 35. Electron micrographs of the surface of a Phase II Stellite 6 specimen after 30 days exposure to natural aging conditions and no exposure to water vapor.

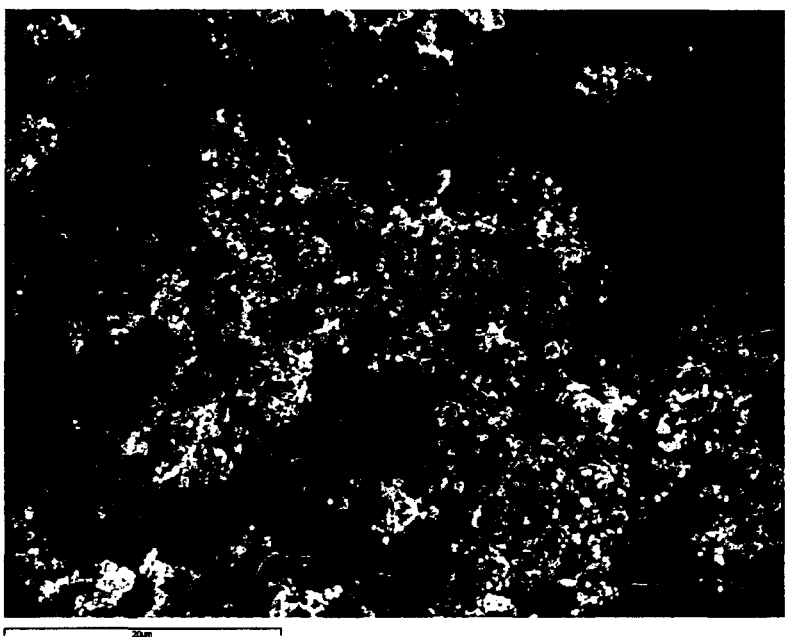
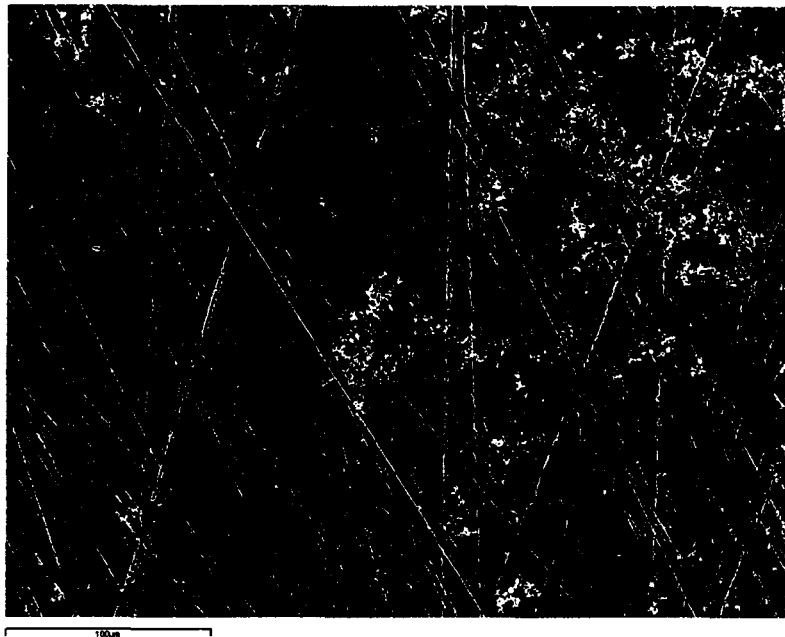


Figure 36. Electron micrographs of the surface of a Phase II Stellite 6 specimen after 30 days exposure to natural aging conditions including exposure to water vapor.

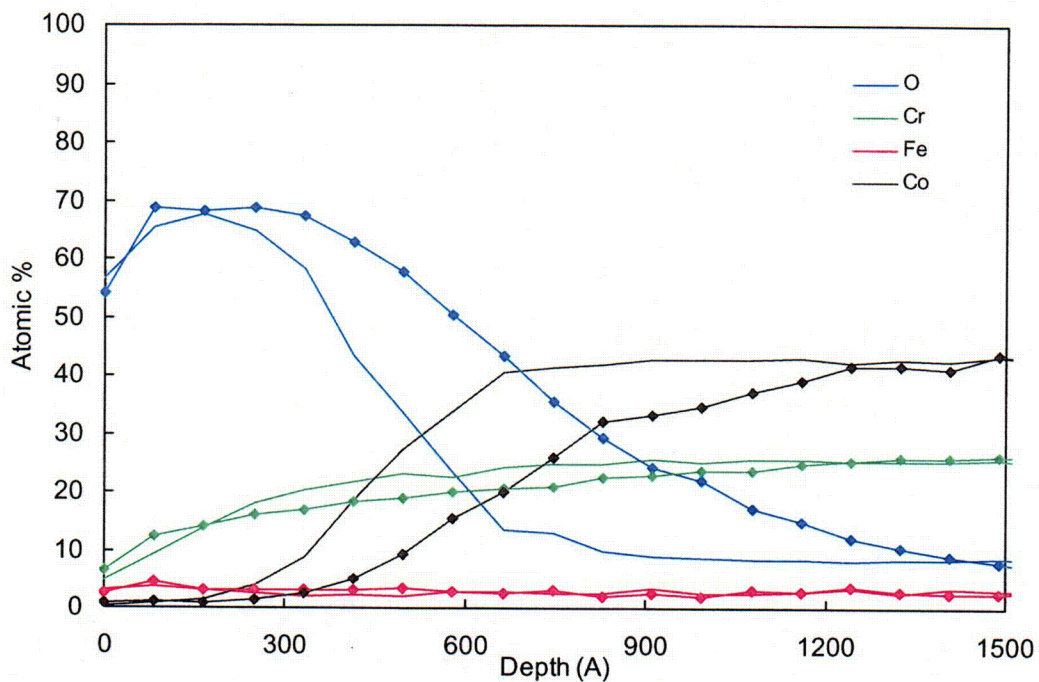


Figure 37. AES depth profile for a Phase II Stellite 6 specimen after 30 days exposure to natural aging conditions, both with (lines with markers) and without (lines without markers) exposure to water vapor.

4. RESULTS OF FRICTION TESTING

During the friction testing performed at Battelle, the sliding force at the pull rod and the normal force applied by the bellows were continuously monitored so that a running trace representing the coefficient of friction was produced for the entire stroke. Because of the differences between the Phase I and the Phase II specimens, the shape of these friction traces are different. Even though the shapes of the friction traces appear different, the evaluation of both the Phase I and the Phase II friction testing can be related to the friction between the disc and the valve seats during selected portions of the valve stroke. Prior to the start of a valve closure, the disc and seat are not in contact. As the valve closes, the disc and the seat eventually contact; the timing of the contact can be different for a parallel disc gate valve versus a flex wedge gate valve. In general though, both valves exhibit disc to seat contact that can range from the two

surfaces contacting and trapping any corrosion products between the surfaces to contacting such that the corrosion products are pushed away from the contact zone.

Once disc to seat contact occurs, further motion of the disc results in previously untouched surfaces of the disc coming into contact with previously untouched surfaces of the seat. This concept is shown in Figure 38 where two similar sized circles represent the seating surfaces of the disc and the valve seat. Moving the center of one circle towards the center of the other circle represents valve motion; the resulting intersection of the edge of the circles is similar to the intersection of a disc and a seat ring. While there is continual disc to seat, or circle to circle contact throughout the stroke, the contact between any given portion of

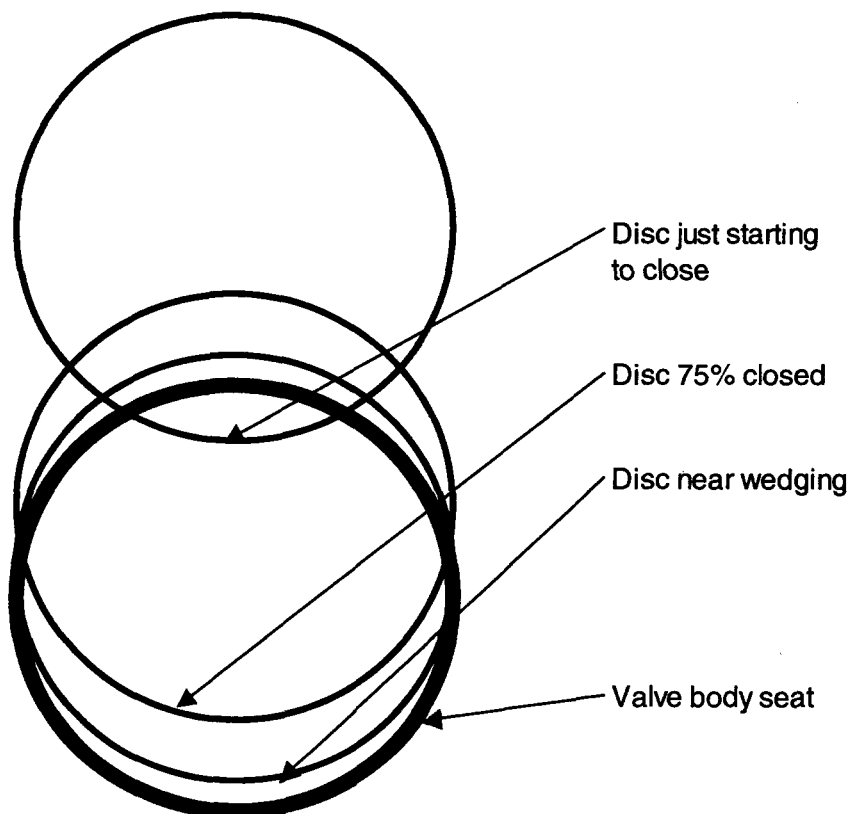


Figure 38. Contact regions between a gate valve disc and the valve seat.

the disc or seat is relatively brief. The only region where any sustained motion occurs between the disc and the seat is at the horizontal edges; from the time the valve is about 75% closed to full closure.

The contact between a disc and a seat can be related to selected portions of the friction-testing stroke. The friction testing always begins with two stationary specimens in contact with each other. In general, this contact mechanism is not typical of the contact mechanisms of a valve that is initially open but it does represent an upper bound to the friction. As the friction testing specimens begin to move, the surface of the larger specimen exposes a new surface to the contact zone, the surface of the smaller specimen does not. The initial portion of the stroke of the Phase I or the Phase II specimens is similar to the contact between a disc and a seat where the disc drops directly onto the seats, trapping the corrosion products. The post transition portion of the stroke of the Phase II specimens is similar to the contact between a disc and a seat where the disc is at a slight angle such that the corrosion products can be pushed away from the contact zone.

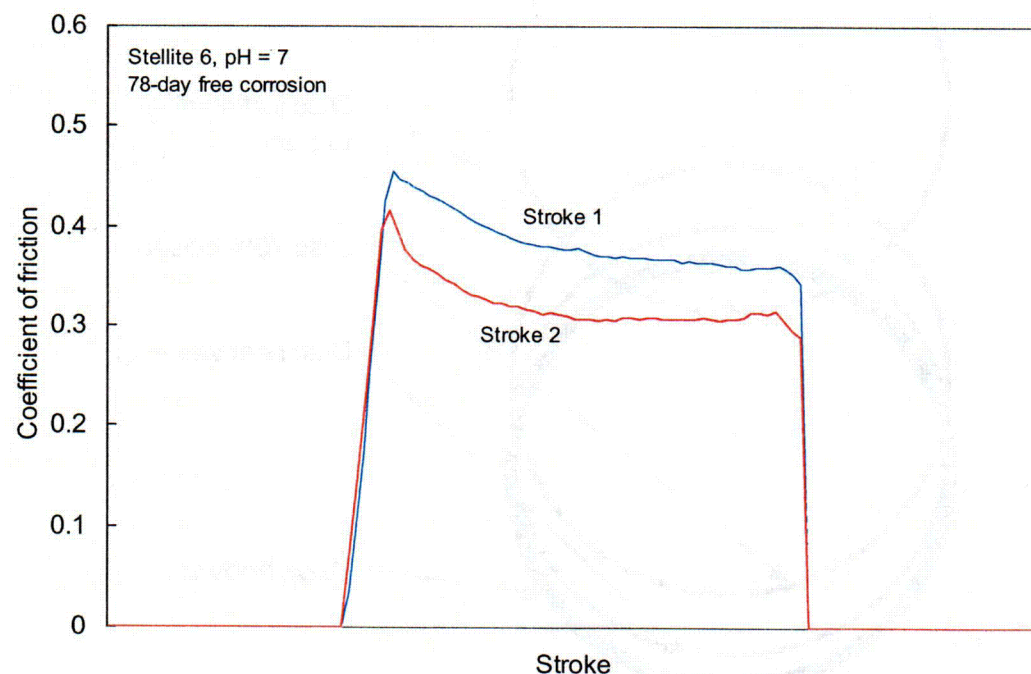


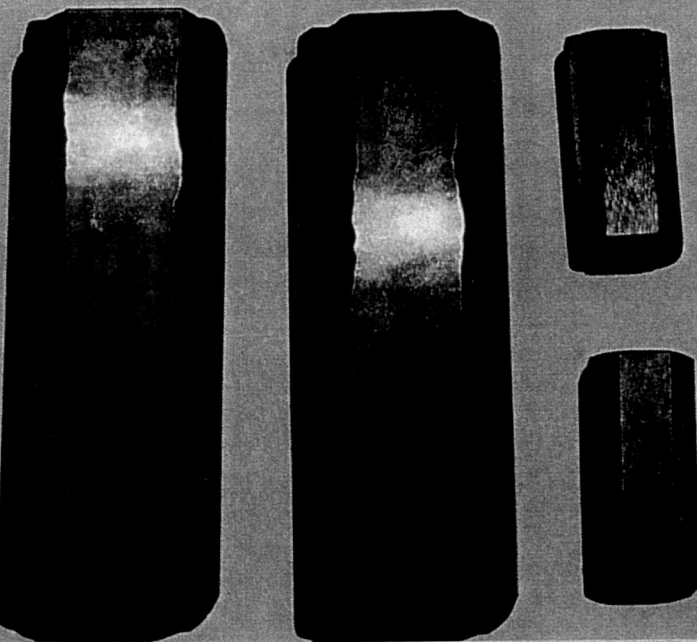
Figure 39. A typical Phase I coefficient of friction trace.

4.1 Friction Testing Naturally Aged Specimens

4.1.1 Phase I Specimens

A typical Phase I friction trace is shown in Figure 39. The highest friction occurs at the beginning of the stroke during these tests. Initially, two undisturbed corroded surfaces are placed against each other, the normal load applied, and the large inner specimens were moved relative to the fixed small outer specimens. The highest friction results from the granular surfaces of the corrosion products interlocking and resisting motion of the specimens. As the specimens are moved relative to each other, the granular surface of the corrosion products is fractured and offers less resistance to further motion. Continued stroking of the specimens relative to each other will increase the fracturing of the granular surfaces and decrease the resistance to motion and the resulting friction. Photographs of typical specimens taken before and after the Phase I friction testing are shown in Figure 40.

Stellite 6 - After 78 Days Free Corrosion
@ 550° F, 100-200 ppb O₂ - No IST



Stellite 6 - After 78 Days Free Corrosion
@ 550° F, 100-200 ppb O₂ - No IST
After Friction Testing

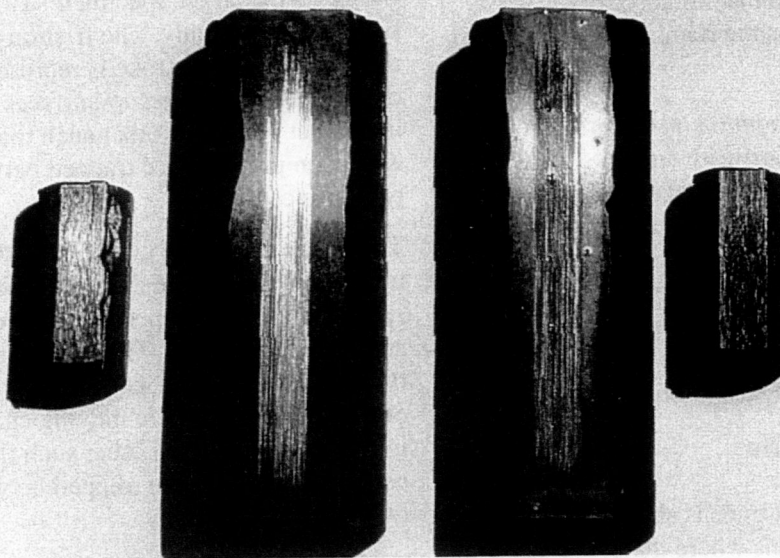


Figure 40. Typical Phase I natural aging specimens before (top) and after (bottom) friction testing.

For the Phase I testing, two friction values are of interest:

- The maximum friction during the stroke. The friction during this portion of the stroke is representative of two initially stationary surfaces that are in contact with each other such that the corrosion products are trapped between the two surfaces.
- The nominal friction during the stroke. The friction during this portion of the stroke is representative of two surfaces that are moving and come into contact with each other such that the corrosion products are trapped between the two surfaces.

During the Phase I testing, seven sets of naturally aged specimens underwent friction testing. The testing included unaged specimens and specimens that had been aged for 2, 10, 20, 40, and 78 days. In addition, friction testing was also performed on specimens that had undergone natural aging combined with simulated valve wedging cycles representing typical in-service testing. These specimens were naturally aged for 78 days with a simulated valve wedging cycle at 25 days and again at 50 days. The results of this friction testing are shown in the following two figures. Figure 41 contains the maximum friction and Figure 42 contains the nominal friction.

These figures show that both the maximum and the nominal friction increase with aging throughout the 78-day testing. These figures also show that the friction during the first stroke, for a given specimen set and a given aging time, is the highest and that the friction decreases with additional stroking, appearing to stabilize after three strokes. These observations will be discussed in greater detail later in this section.

4.1.2 Phase II Specimens

A typical Phase II friction trace is shown in Figure 43. There are two regions where the friction peaks. The first is at the beginning of the stroke, the result of the same phenomenon that influences the Phase I friction trace, an interlocking of the granular surfaces of the corrosion products. Once the two surfaces are moving against each other and the corrosion

products are being fractured the resistance to further motion decreases. However, as the smaller specimen reaches the transition zone, the region where the smaller specimen transitions from riding on the larger specimens two-surfaced region only to riding on the larger specimens single surface region, the friction is again observed to increase. This increase is the result of fresh undisturbed granular surfaces of the corrosion products on both the larger and smaller specimens coming into contact with each other and increasing the resistance to motion. As further motion occurs and the granular surface of the corrosion products is fractured, less resistance to additional motion occurs. Continued stroking of the specimens relative to each other will increase the fracturing of the granular surfaces and decrease the resistance to motion and the resulting friction. Photographs of typical specimens taken before and after the Phase II friction testing are shown in Figure 44.

For the Phase II testing, three friction values are of interest:

- The maximum friction prior to the transition zone where the small specimen is riding on the larger specimen's two-surfaced region only. The friction during this portion of the stroke is representative of two initially stationary surfaces that are in contact with each other such that the corrosion products are trapped between the two surfaces.
- The nominal friction just prior to the transition zone where the small specimen is riding on the larger specimen's two-surfaced region only. The friction during this portion of the stroke is representative of two surfaces that are moving and coming into contact with each other such that the corrosion products are trapped between the two surfaces.
- The nominal friction immediately after the transition zone where the small specimen is riding on the larger specimen's single surface region only. The friction during this portion of the stroke is representative of two surfaces that are moving and coming

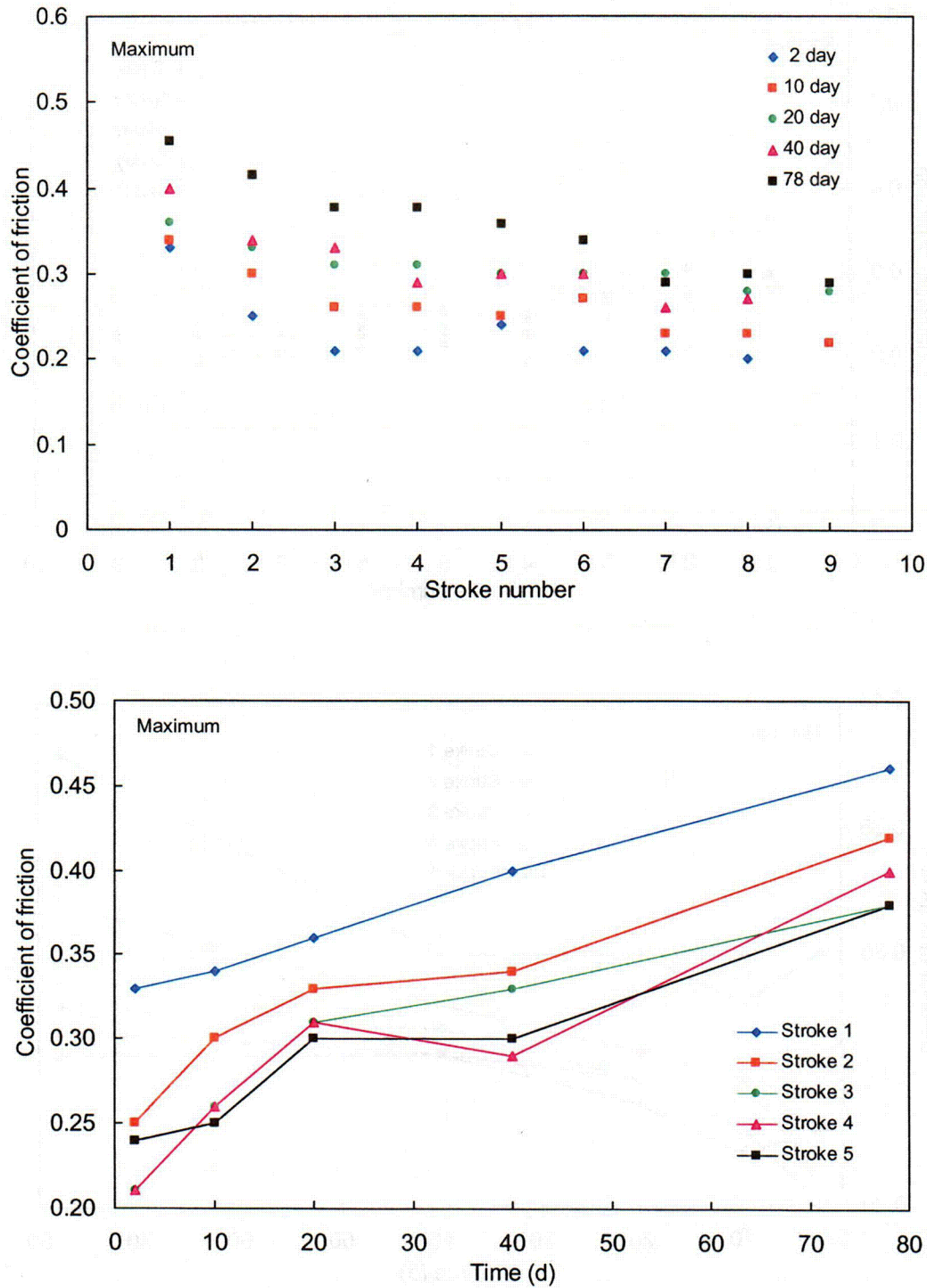


Figure 41. Maximum coefficient of friction for the Phase I naturally aged Stellite 6 specimens; versus stroke (top) and versus aging time (bottom).

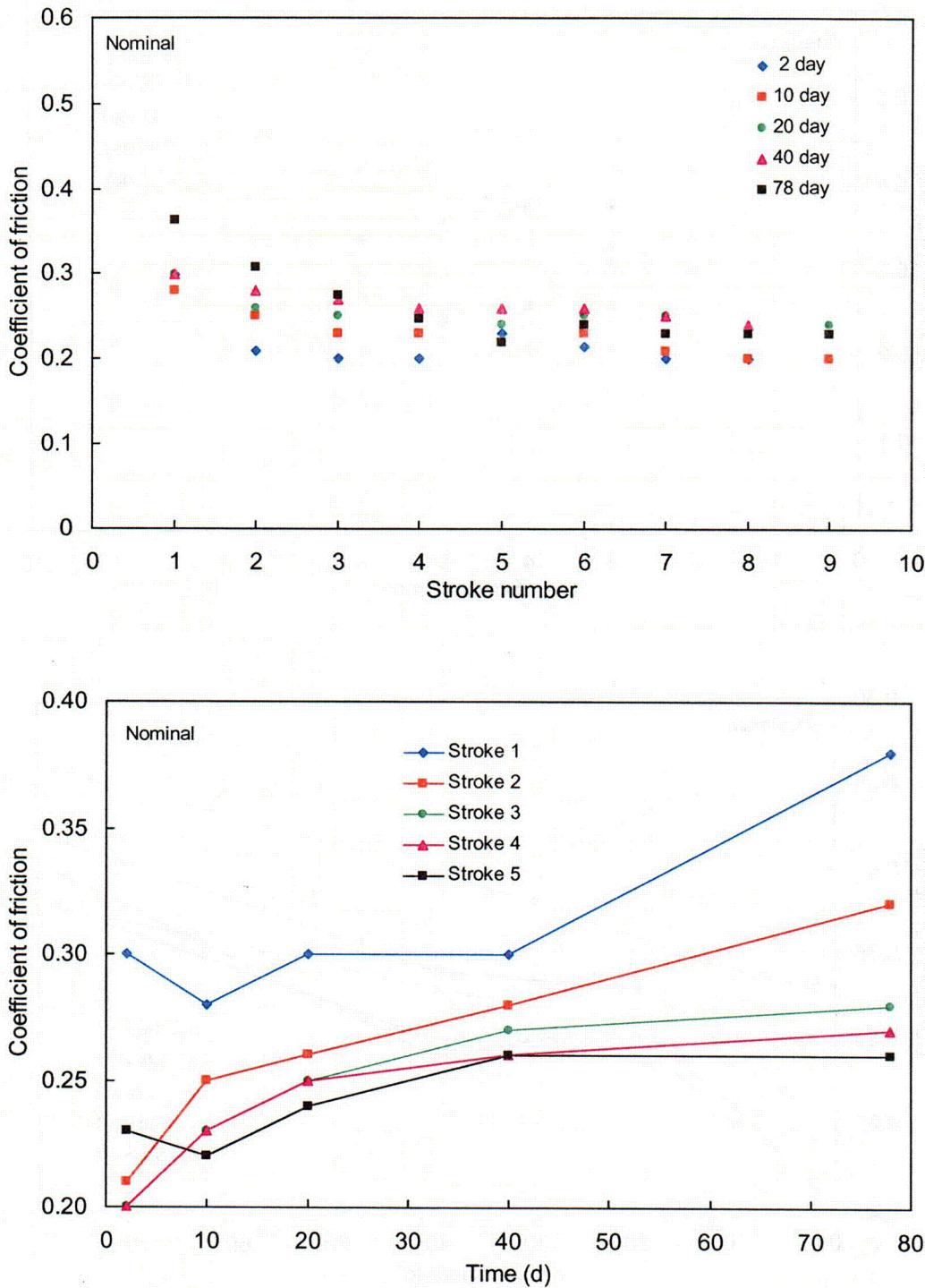


Figure 42. Nominal coefficient of friction for the Phase I naturally aged Stellite 6 specimens; versus stroke (top) and versus aging time (bottom).

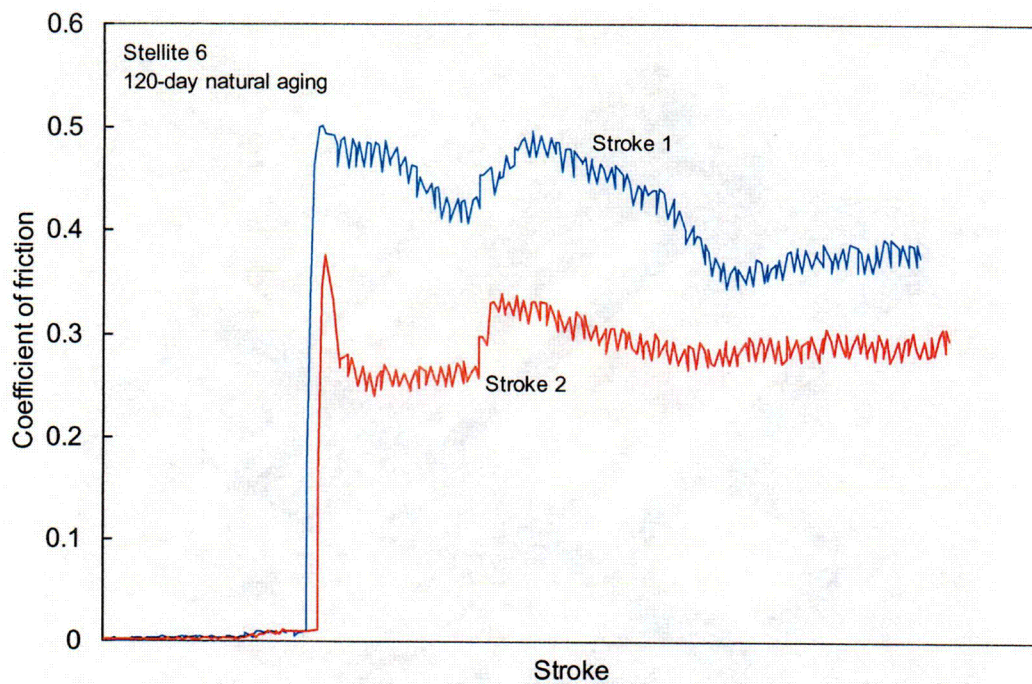


Figure 43. A typical Phase II coefficient of friction trace.

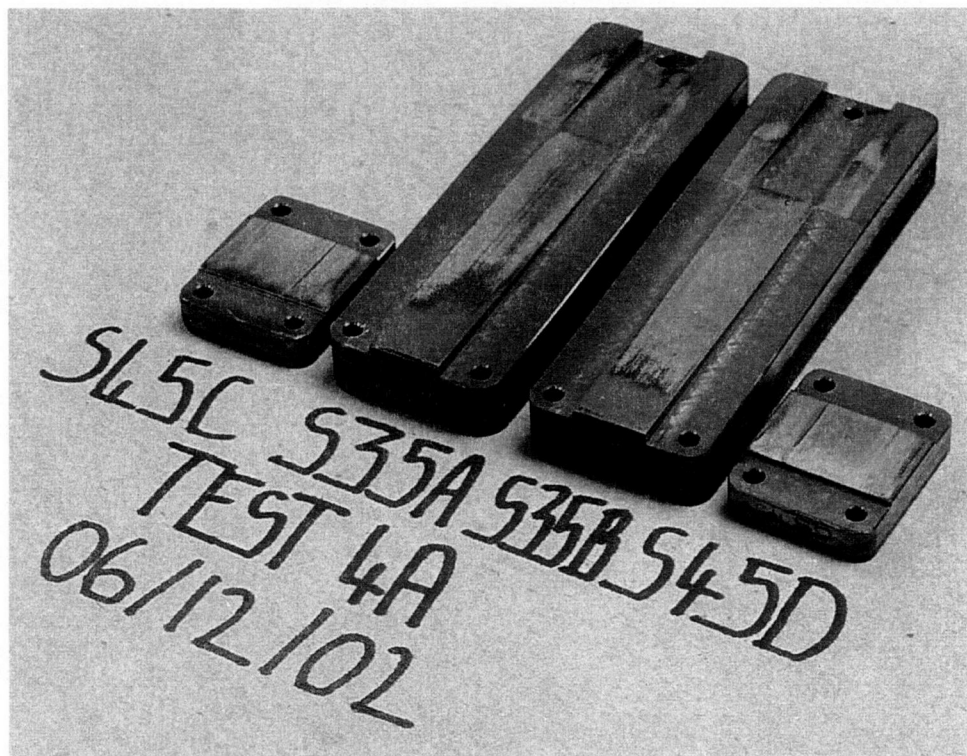
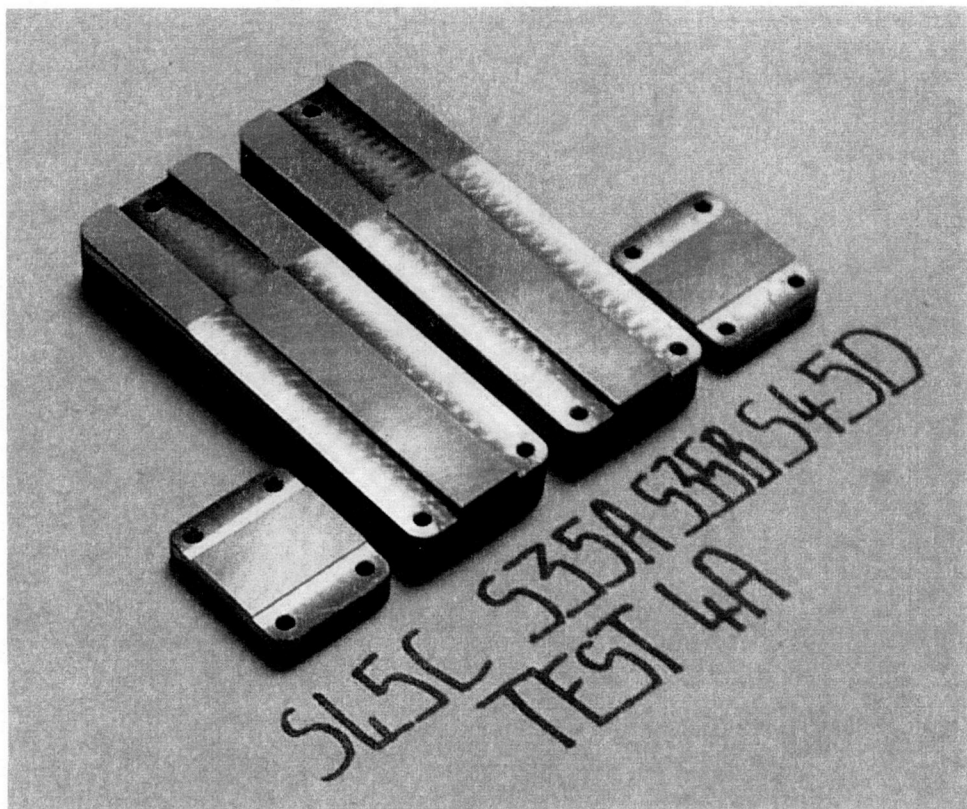


Figure 44. Typical Phase II natural aging specimens before (top) and after (bottom) friction testing.

into contact with each other such that the corrosion products can be pushed out of the way and not trapped between the two surfaces.

The maximum friction at the transition zone is also of interest. Unfortunately, the friction during this portion of the stroke is affected by both the two-surfaced region and by the single surfaced region of the larger specimen. Trapped corrosion products influence the friction when the smaller specimen is riding on the larger specimen's two-surfaced region whereas the single surface region allows the corrosion products to be pushed away and not trapped between the two surfaces. Efforts to separate the total friction into these two effects were not successful.

During the Phase II testing, seven sets of naturally aged specimens underwent friction testing. The testing included unaged specimens and specimens that had been aged for 30, 60, 90, and 120 days. The test matrix included repeat friction testing after 120 days of aging to assess the repeatability of the friction testing results. For this repeat testing, three separate sets of 120-day specimens were aged and then friction tested. The results of the friction testing are shown in the following three figures. Figure 45 contains the maximum friction prior to the transition zone, where the small specimen is riding on the large specimen's two-surfaced region only. Figure 46 contains the nominal friction prior to the transition zone, where the small specimen is riding on the large specimen's two-surfaced region only. Figure 47 contains the nominal friction immediately after the transition zone, where the small specimen is riding on the large specimen's single surface region only.

Due to an unforeseen problem with the new specimen configuration, the specimens were not returned to their original position following the first stroke with the 30-day and the 60-day specimens. As a result, subsequent friction strokes were not performed correctly and the decision was made to repeat the testing with new specimens. Even though the 30-day and the 60-day testing was repeated, the first stroke of the original test was performed correctly. Therefore,

the first stroke of the 30-day and the 60-day friction testing that was ultimately repeated will be included.

These figures show that the maximum and both nominal frictions increase with aging for the first 90 days. After 90 days, the friction appears to stabilize. These figures also show that the friction during the first stroke, for a given specimen set and a given aging time, is the highest and that the friction decreases with additional stroking, appearing to stabilize after three strokes. These observations will be discussed in greater detail later in this section.

4.2 Friction Testing Accelerated Aged Specimens

Four sets of Phase I specimens that were subjected to accelerated anodic aging underwent friction testing. These specimens had been subjected to aging times of (a) 11 days at 0.15 mA/cm^2 (two sets of specimens), (b) 11 days at 0.15 mA/cm^2 followed by 2.5 days at 0.19 mA/cm^2 , and (c) 14 days at 0.35 mA/cm^2 . In addition, two sets of specimens subjected to accelerated high-pH aging (19 days) also underwent friction testing. One set was tested with the zirconium-rich crystals present on the oxide film, and the other set was tested after the crystals had been removed (by cleaning with isopropyl alcohol). Iron-rich crystals remained in the oxide film after cleaning.

Friction data for the specimens aged by the two acceleration methods are presented in Figure 48. The results are discussed in more detail later in this section.

One set of the Phase I specimens that was not subjected to any aging underwent friction testing. The data from this testing, combined with the natural aging data and the accelerated aging data from the Phase I testing presented in Figures 41, 42 and 48, are shown in Figure 49. This figure indicates the presence of friction coefficient "bands" that are characteristic of the three surface conditions: (a) unaged, (b) natural aging, and (c) accelerated aging (both anodic

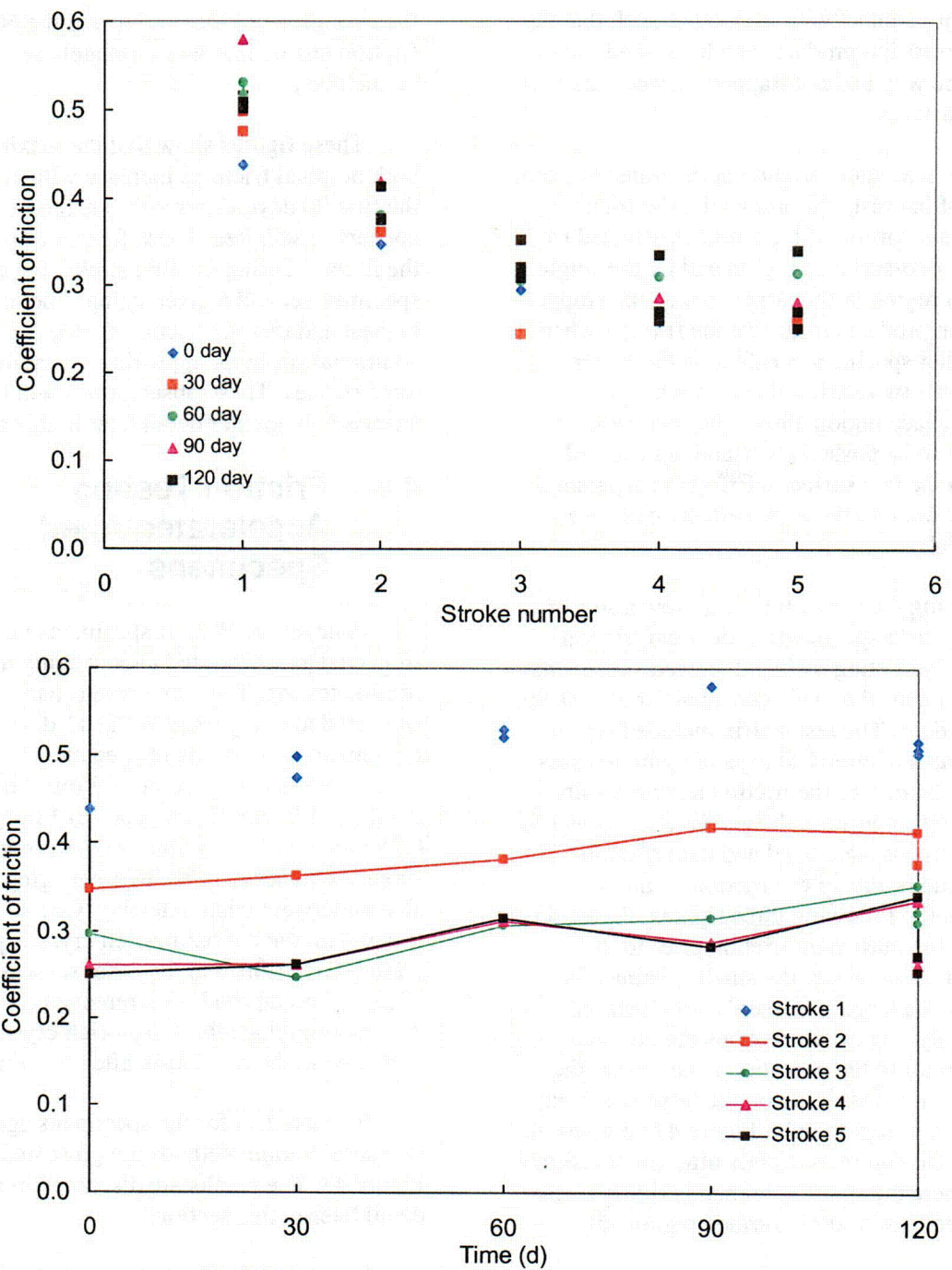


Figure 45. Maximum coefficient of friction prior to the transition zone for the Phase II naturally aged Stellite 6 specimens; versus stroke (top) and versus aging time (bottom).

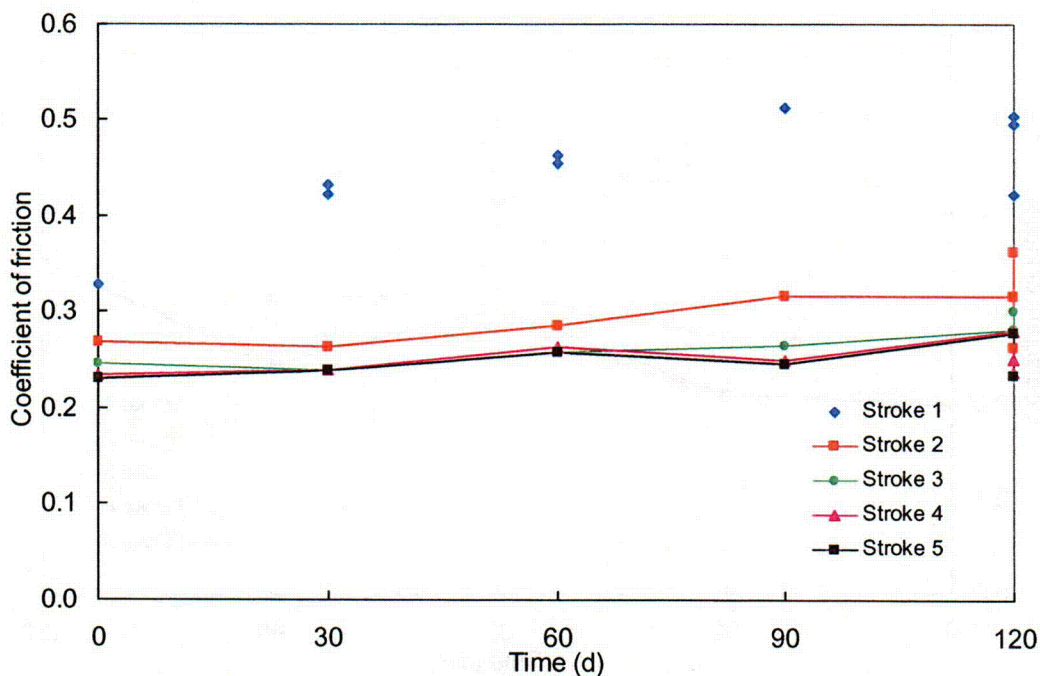
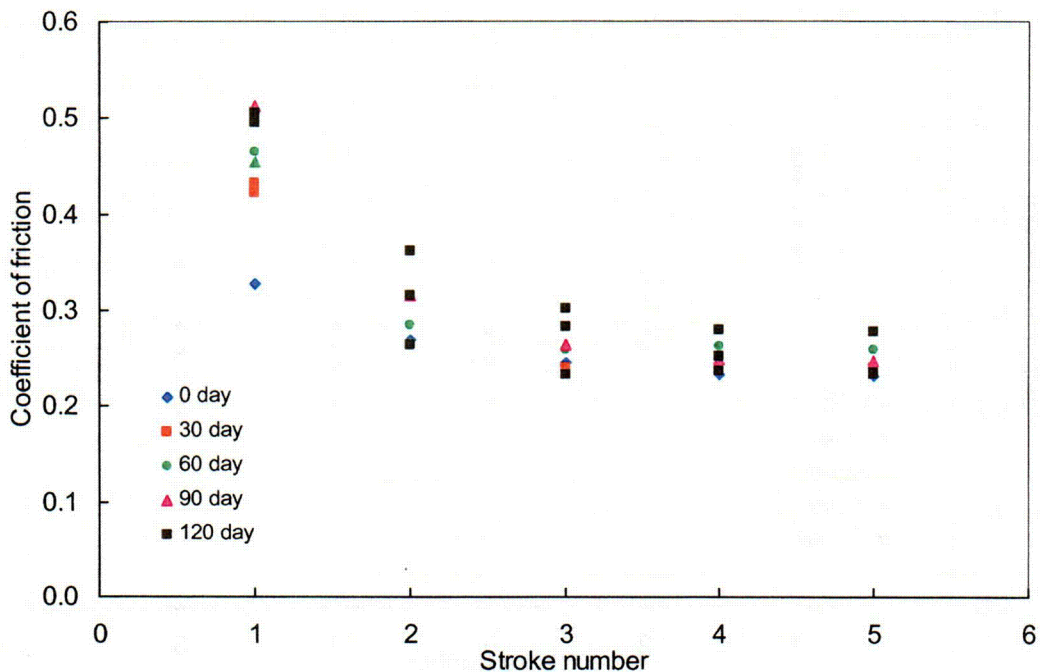


Figure 46. Nominal coefficient of friction just prior to the transition zone for the Phase II naturally aged Stellite 6 specimens; versus stroke (top) and versus aging time (bottom).

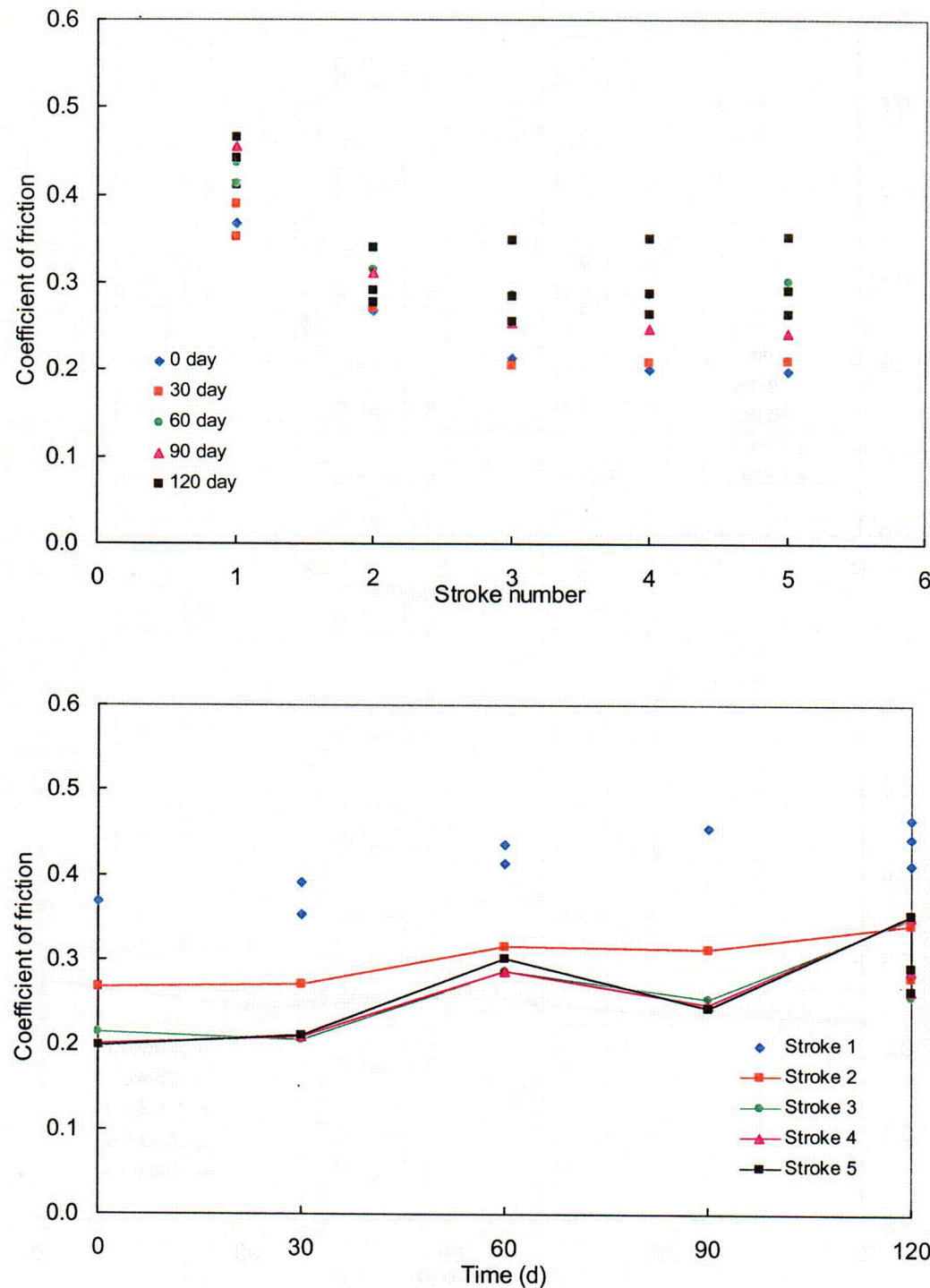


Figure 47. Nominal coefficient of friction immediately after the transition zone for the Phase II naturally aged Stellite 6 specimens; versus stroke (top) and versus aging time (bottom).

and high-pH). Compared with unaged specimens, the bands indicate an increase in friction coefficient of approximately 0.1 for the natural aging specimens, and an increase of 0.2 for the accelerated aging specimens. When moving from one surface condition to another, the bands can be thought of as being moved up or down. As such, the friction would change as an absolute value, not as a fixed percentage, which would distort the shape of the band. For example, the increase in the friction coefficient from 0.2 for condition (a) to 0.3 for condition (b) is simply an increase of 0.1, and should not be regarded as an increase of 50%. Likewise, the increase from 0.2 for condition (a) to 0.4 for condition (c) is simply an increase of 0.2, and should not be regarded as a 100% increase in friction coefficient.

The highest maximum friction values (upper plot, Figure 49) for the first stroke on the accelerated aging specimens is from the high-pH specimens, not the anodic current specimens. The greatest overlap in the bands occurs with the maximum friction in the first stroke, where data from natural aging specimens with longer aging times overlap with data from anodic current specimens.

Overall, the results show that the chemical composition and morphology (presence of crystals or nodules) of the oxide film have a notable effect on the frictional behavior of the Stellite 6 specimens. Successive stroking also affects the frictional behavior. These variables are evaluated in the following discussion.

4.3 Changes in Friction Due to Aging of the Surface

Results from friction testing of the naturally aged Phase I specimens at Battelle are plotted versus aging time in Figures 41 and 42. These figures indicate that both the maximum and the nominal coefficient of friction continue to increase during the first and second stroke as the specimens age. For the third and subsequent strokes, the maximum friction continues to increase with longer aging time, whereas the nominal friction begins to stabilize after 40 days.

Results from friction testing of the naturally aged Phase II specimens at Battelle are plotted versus aging time in Figures 45, 46, and 47. These figures are similar to the results observed on the Phase I testing and indicate that each coefficient of friction continues to increase during the first and second stroke as the specimens age up to 90 days. Thereafter, the friction was observed to stabilize. For the third and subsequent strokes, the friction was relatively stable, showing no significant increase as the specimens continued to age.

Figure 50 shows the friction from the naturally aged specimens plotted against the thickness of the oxide film. This figure shows that the friction is not related to the thickness of the oxide film. One might expect a trend to exist between the time the specimens are naturally aged or the resulting oxide film thickness and the friction. However, the available data do not support such a relationship.

If, however, the change in the maximum friction during the first stroke as the specimens age is plotted against aging time for both the Phase I and the Phase II testing, a very interesting trend emerges as shown in Figure 51. This figure shows that the friction continues to increase during the first 90 days of aging and that the friction increases about 0.15 compared to unaged specimens. After 90 days, the friction was observed to be less. This decrease was consistent for each of the three sets of specimens that were friction tested after 120 days of aging. Again, the friction has peaked prior to 120 days of aging and is no longer increasing. Figure 52 shows similar information except the friction represents nominal values prior to the transition zone. A similar trend is observed, except that the friction increases about 0.20 before starting to show less of an increase. Note also that the trends between the Phase I data and the Phase II data are somewhat different, although both data sets support an increase in the friction as the aging time increases.

If the change in the coefficient of friction after the transition zone is plotted against aging time, a similar trend emerges. The data is shown in Figure 53 and was obtained from the first

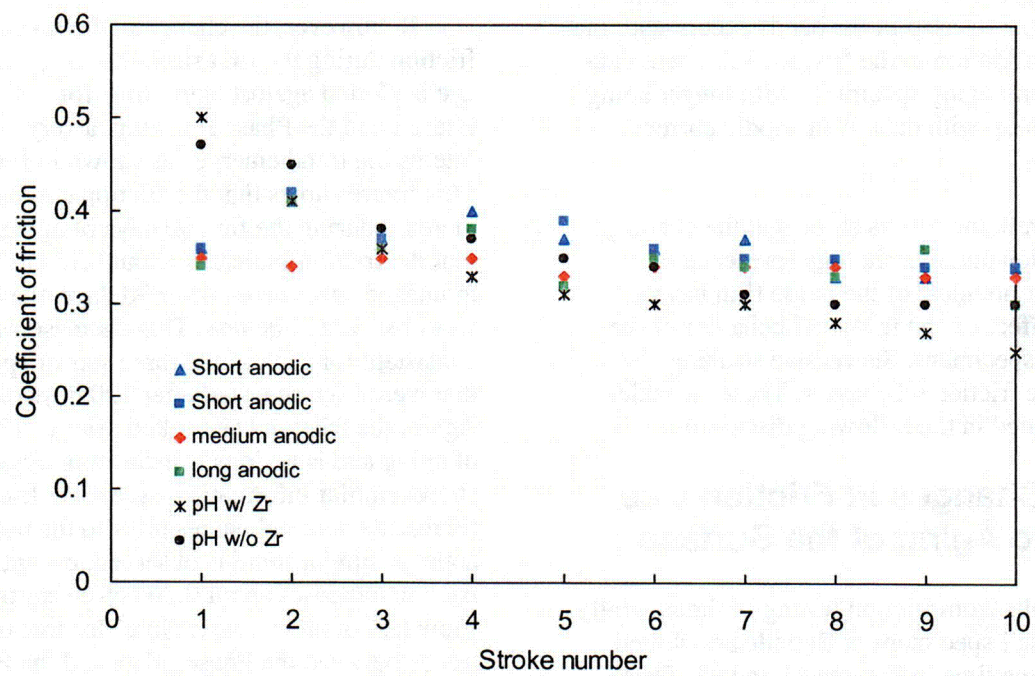
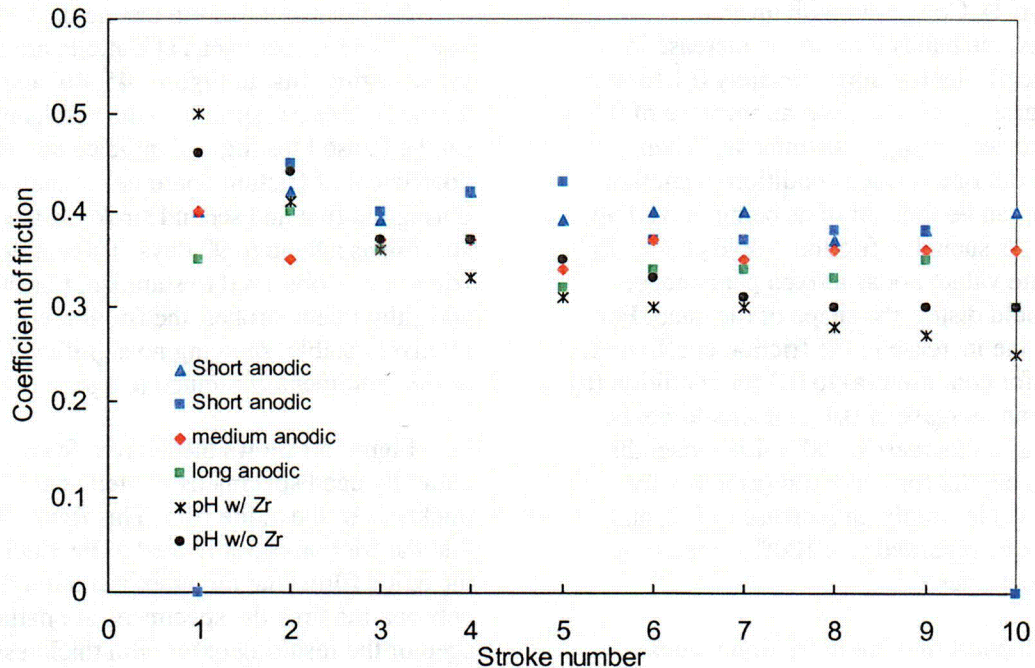


Figure 48. Coefficient of friction versus stroke for Phase I Stellite 6 specimens exposed to accelerated aging conditions; maximum values (top) and nominal values (bottom).

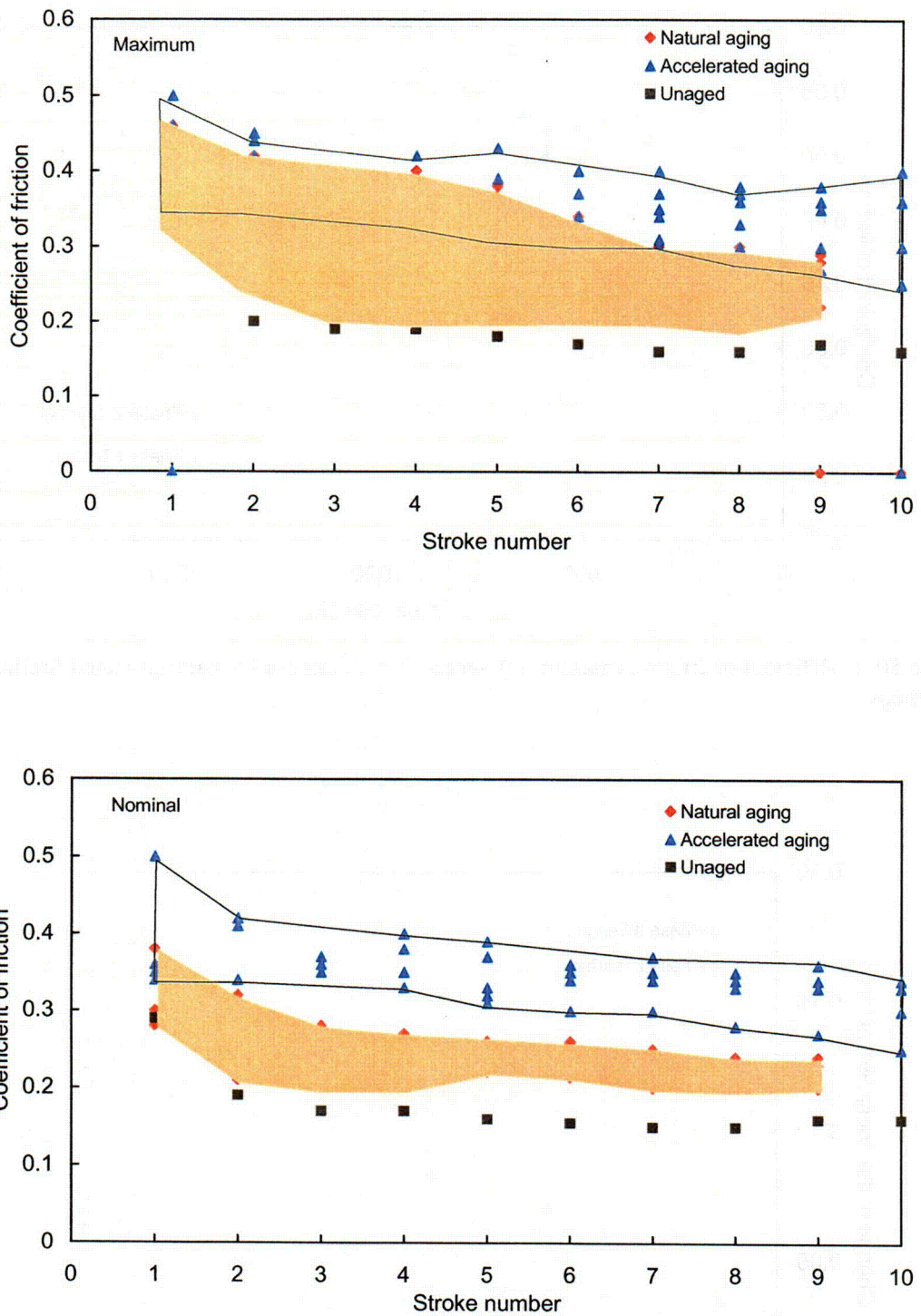


Figure 49. Coefficient of friction versus stroke for unaged and aged Phase I Stellite 6 specimens; maximum values (top) and nominal values (bottom).

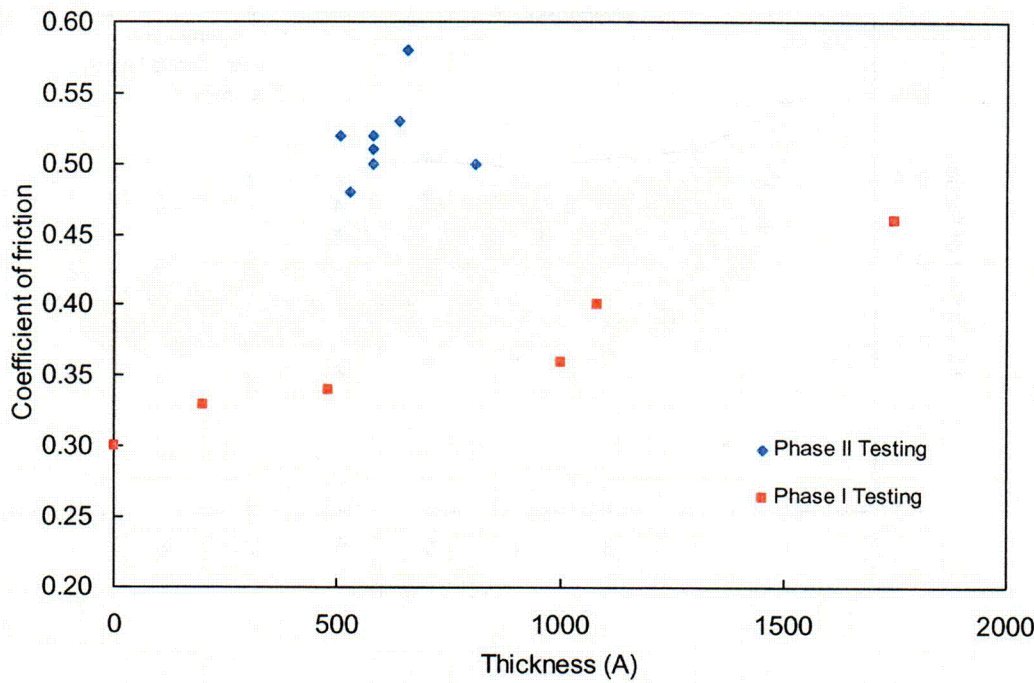


Figure 50. Coefficient of friction (maximum) versus film thickness for naturally aged Stellite 6 specimens.

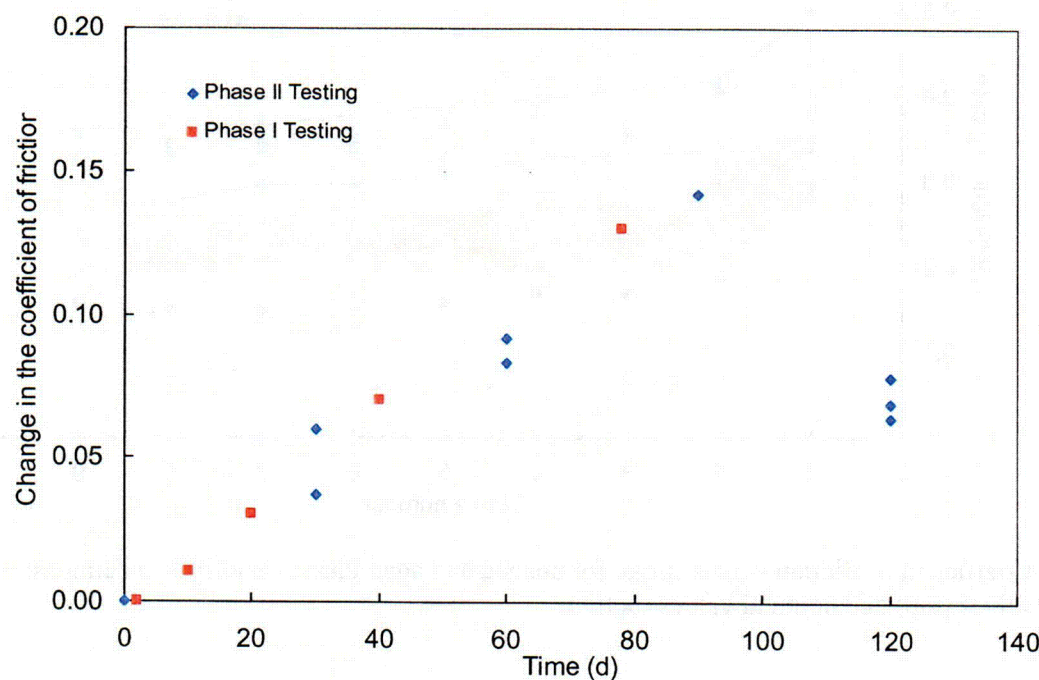


Figure 51. Change in the maximum coefficient of friction during the first stroke versus aging time.

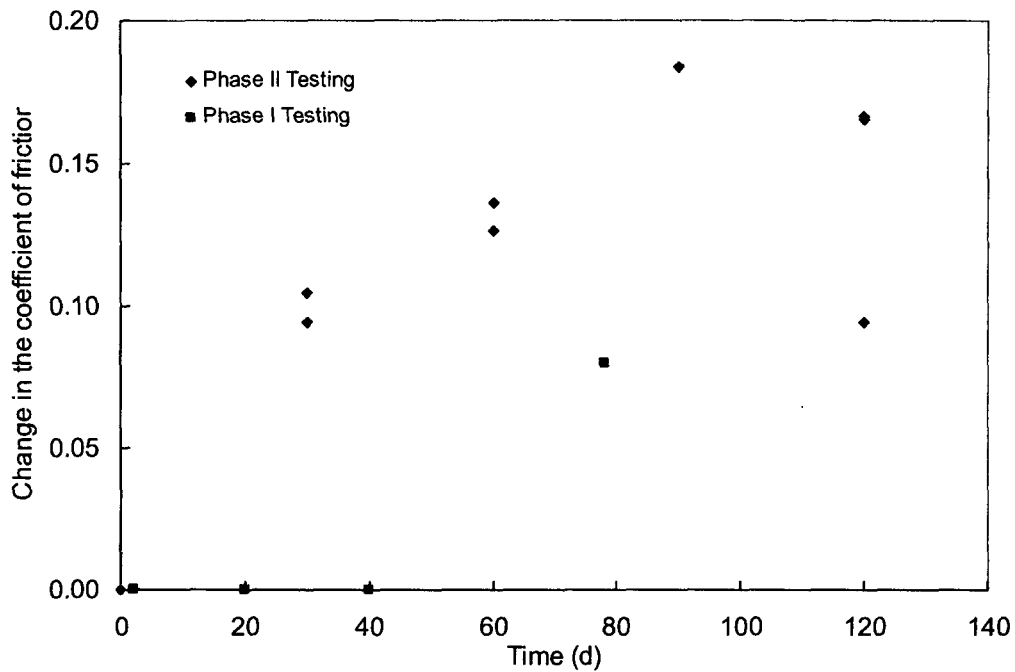


Figure 52. Change in the coefficient of friction just prior to the transition zone during the first stroke versus aging time.

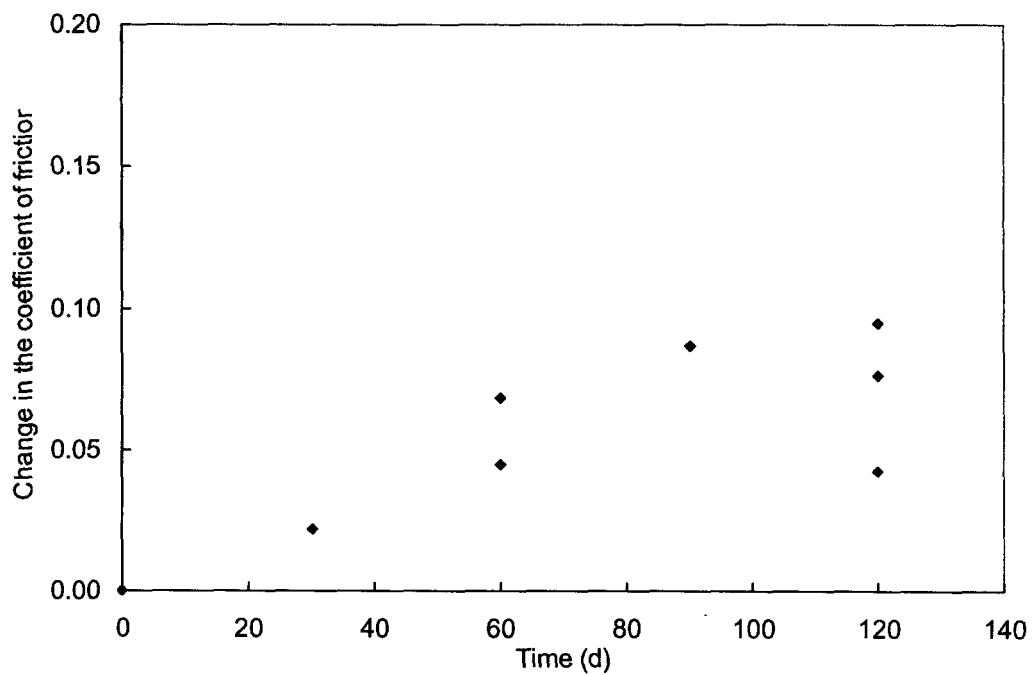


Figure 53. Change in the coefficient of friction after the transition zone during the first stroke versus aging time.

stroke following a period of aging. The friction after the transition zone allows the specimens to push the corrosion products out of the way and was performed during the Phase II testing program only. Again, the friction is observed to increase as the aging time increases. The friction does not increase as much as previously observed; however, the increase does approach 0.1. Again, the friction has peaked prior to 120 days of aging and is no longer increasing.

4.4 Changes in Friction Due to Chemical Composition and Surface Structure

The increase in friction with greater aging of the specimens is the result of the growth characteristics of the oxide film. In particular, as the surface ages, the crystalline solids in the oxide film grow larger. Oxide films of different ages can be compared to pieces of sandpaper with different degrees of roughness. The grains on the sandpaper are analogous to the crystalline solids, and as the surface of the Stellite 6 ages, the crystals become larger, similar to rougher sandpaper, corresponding with coarser grit or larger grains. The composition of the crystalline solids was not determined, but we expect them to be chromium oxide, cobalt oxides, or carbides. Such crystalline solids are, in general, very abrasive. When two such surfaces are placed against each other, the friction can be quite high, especially during the first stroke. With subsequent stroking, the crystalline solids will either plastically deform or fracture as the two surfaces pass each other. As such, the friction should decrease with continued stroking until the friction of the bulk Stellite 6 material is reached. This is similar to two pieces of sandpaper rubbing against each other. During the first stroke, the surface grains are intact and offer the most resistance to motion. As the surface grains are fractured, the resistance to motion decreases, approaching a friction value

representing the two pieces of paper backing rubbing against each other.

The larger crystals (from high-pH exposure) or nodules (from anodic polarization) found on the surface of the accelerated aging specimens appear to have a significant contribution to the high friction, especially during the first stroke. In these cases, it is probable that the larger crystal size and different chemical composition of the crystalline structure contribute to this higher friction. As with the naturally aged specimens, it appears that harder particles on one surface plastically deformed or fractured areas on the other surface as they pass. We also note that the removal of the zirconium-containing crystals on the high-pH specimens lowered the corresponding coefficient of friction. However, the remaining iron-rich particles, and incorporation of iron and iron oxide through the oxide film, were sufficient to cause the friction coefficient to be higher than that measured on the specimens exposed to natural aging conditions. We speculate that the mechanical properties of this iron-rich film, and the large crystalline structure observe on the micrographs of the surface, were largely responsible for the difference.

While there may be an effect on the friction due to the film thickness, it is of significantly lower magnitude than the effect due to composition and morphology. In other words, beyond a minimum oxide film thickness, the mechanical properties of the oxide film have a far greater effect on whether a valve can operate safely. This effect is evident in Figure 54, which compares friction results from the high-pH specimens (Figure 48) with the results from the 20- and 40-day natural aging specimens (Figure 41). The film thickness was approximately the same (1100 \AA) for these specimens, yet the friction coefficient was at least 0.1 higher with the high-pH specimens than with the natural aging specimens.

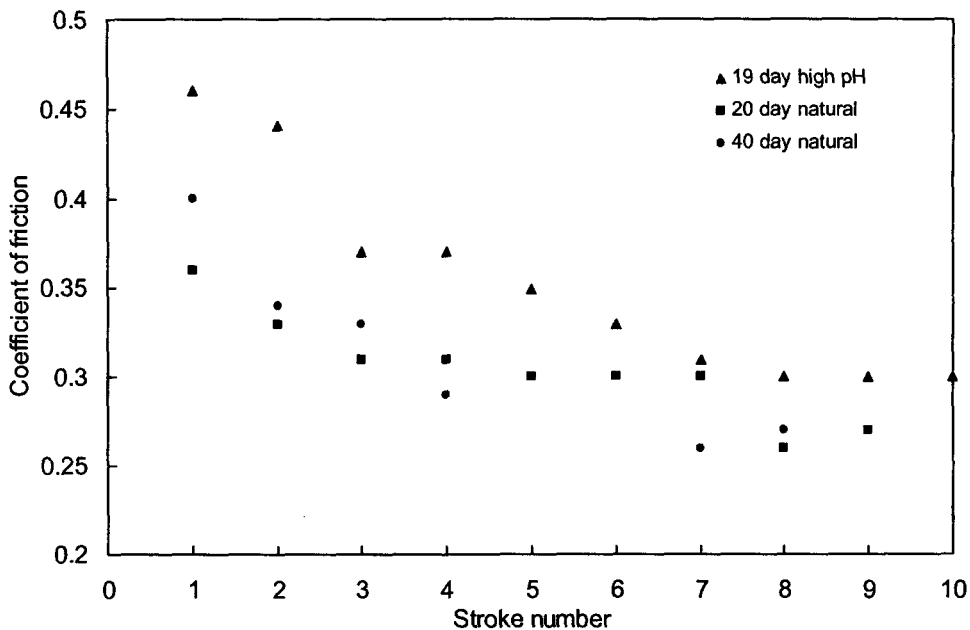


Figure 54. Coefficient of friction versus stroke for 20- and 40-day naturally aged and high-pH accelerated aging Phase I Stellite 6 specimens.

4.5 Changes in Friction with Stroking

In general, the first stroke shows higher friction than succeeding strokes. The difference is greater for some specimens than for others. The decrease in the friction coefficient with continued stroking is probably caused by a change in the surface condition of the specimens due to plastic deformation or fracturing of the crystals. The results indicate that the first stroke a valve experiences after it has been allowed to age and establish an oxide film will result in the highest coefficient of friction and therefore require the highest stem thrust to successfully operate the valve. This result has important implications for valves being subjected to in-plant testing: such in-plant tests need to collect data from the very first stroke a valve experiences following a period of inactivity, and data from subsequent strokes will be less relevant to valve operability and plant safety.

The presence of any oxide film, combined with the crystalline structure of the film, caused a significant increase in the friction coefficient, as compared to unaged specimens. The appearance of lower friction in subsequent

strokes (as compared to the first stroke) was a phenomenon that manifested even for the very thin films produced after 2 and 10 days of natural aging (Figures 41 and 42). Even for these specimens, the friction decreased significantly between the first and second strokes and again between the second and third strokes.

Interestingly, the friction coefficient was high during the first stroke for the unaged specimens, too, about the same as for the 2- and 10-day aged specimens (Figure 49). During the next few strokes, the friction coefficients for the unaged specimens are only a little lower than for the 2- and 10-day specimens. These results indicate the possible presence of an extremely thin oxide film (with small, hard granules) on the “unaged” specimen. This very thin film most likely would have formed during the several hours it took to heat up the friction autoclave. If such a film was present, it was worn or smeared away during the first stroke, just as the very thin film on the 2-day natural aging specimens was apparently worn away during the first two strokes, as indicated by the response of the friction coefficient.

This decreasing friction trend is a different outcome than we observed in earlier valve

testing, specifically the gate valve blowdown testing performed by the INEEL in 1989 and early 1990 (DeWall and Steele, 1989; Steele et al., 1991). In those tests, fully equipped full-scale gate valves were subjected to blowdown flows and tested for their ability to close (or open) against the resulting high differential pressure loads. The first several differential pressure strokes were opening strokes against very little flow. Typically, the first few full differential pressure strokes were performed cold (ambient temperature), followed by several strokes at elevated temperature. The results from those tests showed very little change in the friction coefficient from stroke to stroke under elevated temperature conditions. In contrast, the friction tests that are the subject of this report showed a decreasing trend with subsequent strokes.

The difference in the outcome is due to basic differences in the test parameters. The 1989-90 flow tests were designed to test new and refurbished valves, absent any effect (oxide film) due to aging. Before the tests, the valves were verified to be leak tight, and if necessary, the sealing surfaces were machined to achieve a leak tight condition. In addition, between each of the tests, the valves were exposed to the atmosphere; they were not maintained in an environment that was conducive to the formation of an oxide film. As such, the testing represented design basis testing on new valves, not valves that had been allowed to age at BWR coolant conditions. The consistency of the friction coefficient indicates that no significant oxide film had developed on the sealing surface, and certainly not one that would be indicative of an aged valve. In contrast, the friction tests documented in this report were deliberately designed to produce an oxide film on the surfaces of the Stellite 6 specimens, and the decreasing friction trend is evidence of the effects of repeated stroking on the oxide film.

4.6 Changes in Friction Due to Surface Contact

Part of the work performed by NIST was to evaluate the testing process in comparison with

the operation of an actual valve. As part of this evaluation, NIST identified a difference that might be important. Specimens prepared for friction testing were installed into the friction autoclave in full face to face contact without any relative motion. The friction autoclave was heated and pressurized to BWR conditions, and then the normal 10-ksi contact stress was applied for 10 to 20 seconds before the actual friction test began. Based on this operation of the friction autoclave, all of the oxide film would be trapped between the surfaces before the specimens began moving relative to each other.

In an actual valve, however, the surfaces are moving before they contact each other; the surfaces come into contact as the valve nears flow isolation. When the surfaces first touch each other, it is possible that the leading edges might shear the oxide film from the surface, whereas the trailing surfaces would tend to trap the oxide film in a manner similar to what occurs in the friction autoclave. Whether an actual valve shears most of the oxide film off or traps most of the oxide film would depend on how and when the valve disc contacts the valve body seats.

To investigate the effect the contact method has on the resulting friction between the valve disc and the valve body seat, NIST performed additional friction testing on 10-day and 50-day specimens. The testing used either a 0.5-inch steel ball or a 0.125-inch steel ball moving against the flat surface of a Stellite 6 specimen so that the oxide film would not be trapped between the surfaces, but rather it could be pushed aside by the ball. This testing was performed at ambient temperature and pressure and yielded friction values in the range of 0.15 to 0.17. When the contact geometry was changed to a small 1.8 mm^2 flat surface against the flat surface of a Stellite 6 specimen, such that the oxide film would be trapped between the surfaces, friction values in the range of 0.30 to 0.35 were observed. By comparison, the friction testing performed by Battelle at BWR coolant conditions produced maximum friction values in the range of 0.35 to 0.40.

This additional testing implies that trapping the corrosion products between two moving surfaces can have a significant effect on the friction. Thus, the contact mode between the valve disc and the valve body seats can be very important. In the event the disc tips and contacts the valve body seats such that the oxide film is scrapped off and not trapped between the two surfaces, the resulting friction values are likely to be lower than the values produced by our friction tests at Battelle. However, the friction values will not be as low as the results from the testing with a steel ball on the flat Stellite 6 surface. In the event the disc drops flat onto the valve body seats near valve isolation and traps the oxide film between the surfaces, the friction values reported here for the naturally aged specimens are very reasonable (qualified, of course, for the short duration of the aging times.).

This concern can be evaluated further using the Phase II data. The nominal friction representative of surfaces that initially trap the corrosion products (Figure 46) can be compared to the nominal friction representative of surfaces that allow the corrosion products to be pushed out of the way (Figure 47). Based on this data, the friction between surfaces that initially trap the corrosion products is higher than between surfaces where the corrosion products can be pushed out of the way. This trend is consistent with the results of the NIST friction testing. However, the difference between the two frictions at a given stroke and aging time is typically 0.05 or less.

4.7 Changes in Friction Due to Valve Wedging

Figure 55 presents the maximum and nominal friction coefficients for specimens subjected to simulated valve wedging, compared to specimens not subjected to simulated valve wedging, both sets having undergone 78 days of natural aging. A slightly lower value in both the maximum and nominal friction was observed during the first stroke for specimens that had undergone the simulated valve wedging, with

nominal friction coefficients of 0.36 versus 0.38 and maximums of 0.43 versus 0.46.

During subsequent strokes, the effect of the simulated valve wedging on the resulting friction coefficient was either negligible or varied from stroke to stroke.

The friction behavior of each successive stroke appears to be influenced by changes in the condition of the surface due to previous strokes. As such, only the first stroke would be strongly influenced by the simulated valve wedging. Although the single data point obtained in this study suggests that valve wedging cycles will decrease the expected friction, the difference is small. Before a definitive claim can be made as to either a small decrease in the coefficient of friction, or no effect due to the simulated valve wedging, it would be prudent to perform further testing to obtain additional data that would verify the direction and magnitude of the effect.

4.8 Changes in Friction Due to Temperature

Previous gate valve blowdown testing performed by the INEEL in 1989 and early 1990 (DeWall and Steele, 1989; Steele et. al., 1991) indicated that the friction varied with the temperature of the fluid and of the Stellite 6 surfaces. In particular, the friction was observed to decrease as the temperature increased. Conversely, the friction was observed to increase as the temperature decreased. During the Phase II testing, we also observed this trend. Figure 56 contains two friction traces; both obtained from the same specimens that had been aged for 120 days. One trace represents the friction during the last friction test while the friction autoclave was at temperature. The other trace represents the friction during the first stroke following cooldown of the friction autoclave. The friction during the cold test was observed to increase dramatically. Fortunately, this phenomena has previously been observed and is currently being accounted for when estimating the thrust demands of a gate valve.

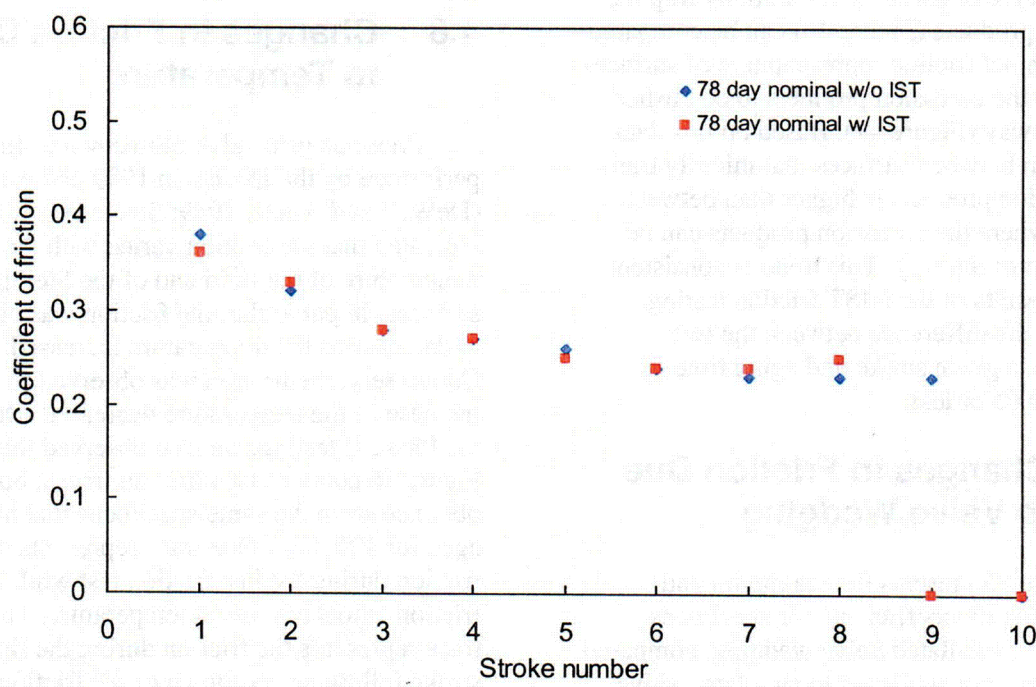
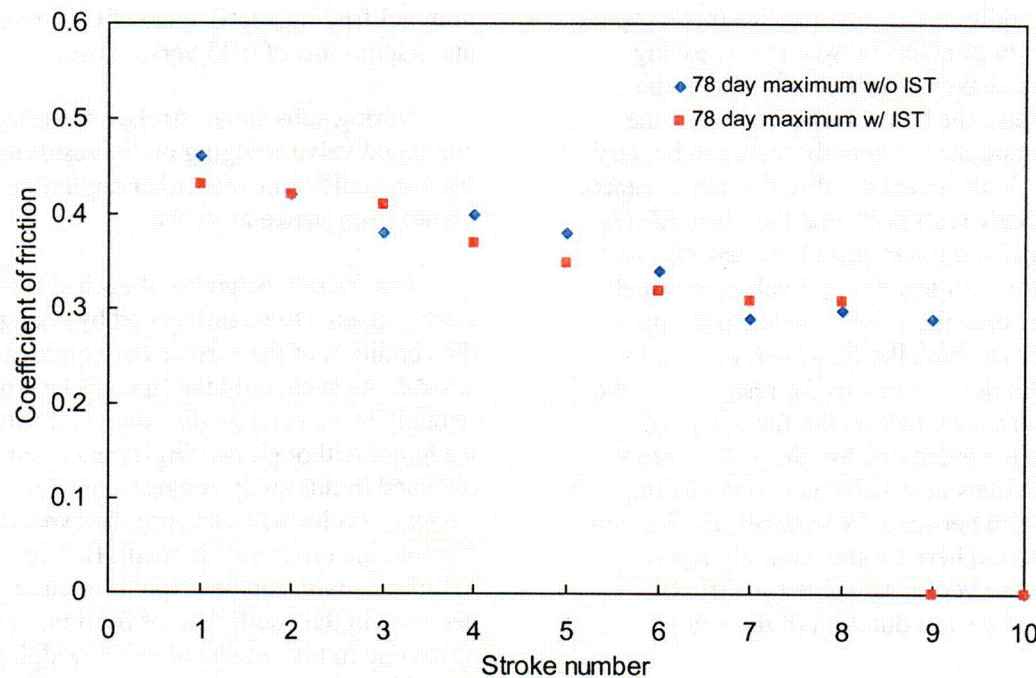


Figure 55. Coefficient of friction versus stroke for naturally aged Phase I Stellite 6 specimens and Phase I Stellite 6 specimens subjected to in-service testing; maximum values (top) and nominal values (bottom).

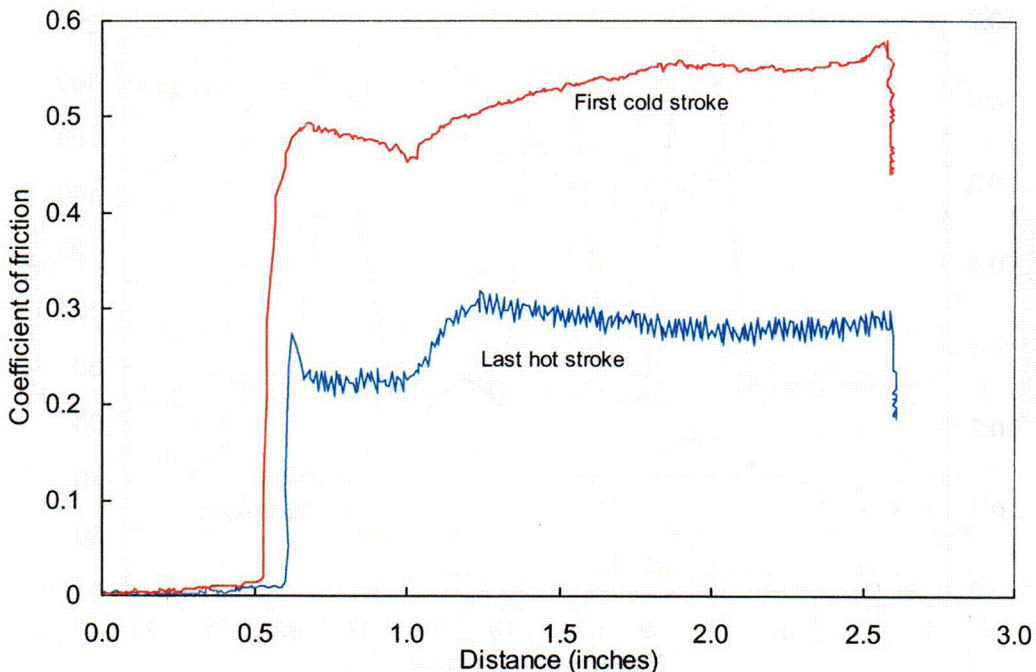


Figure 56. Change in the coefficient of friction of Phase II Stellite 6 specimens while hot and immediately upon cooldown.

4.9 Changes in Friction Due to Exposure to Air

All of the natural aging and accelerated aging was done in a corrosion autoclave. Following the aging, the specimens were removed from the corrosion autoclave and transferred to the friction autoclave. During this transition, the specimens were exposed to air. Some concern has been expressed about the exposure of the specimens to air and the reliability of the subsequent friction testing. The exposure of the Stellite 6 specimens to air following their removal from the corrosion autoclave is not expected to influence the results of the friction testing. If the testing were being performed at cold or room temperature conditions, previous testing has shown that exposure to air will affect the friction testing, resulting in abnormally low friction values until the surfaces are stroked repeatedly which returns the friction to nominal values. This effect is well understood and is referred to as preconditioning the surfaces. However, the friction testing discussed in this report is being performed at the BWR primary temperature,

550°F, and the results of previous valve testing has shown that if the temperature of the specimens is increased prior to the friction testing, the exposure to air will not affect the friction testing.

Previous gate valve pressure locking testing performed by the INEEL in 1997 and early 1998 (DeWall et al., 1998) investigated the effect exposing the internals of a valve to air had on the friction. Figure 57 shows the results of such testing. Note that the friction during the first six strokes is very low when the valve is cold and after the valve internals had been exposed to air, although the friction is observed to increase slightly as the valve is stroked. This phenomenon is known as the preconditioning effect and has been observed during other valve testing. Following the six strokes with the valve cold, the valve was heated to approximately 200°F. Note that the friction immediately increases. This effect has been shown in other testing. Because the friction increases immediately upon increasing the temperature, we do not believe that exposure of either the Phase I or the Phase II Stellite 6 specimens to air

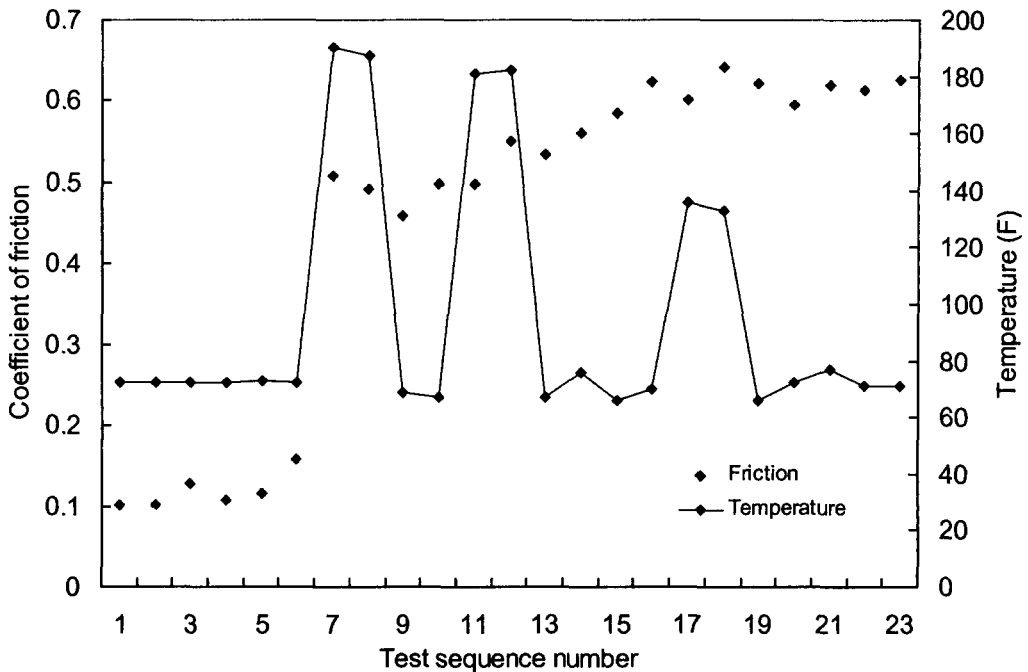


Figure 57. Effect of temperature on the coefficient of friction of Stellite 6 following exposure to air.

during the time the specimens were being transferred from one autoclave to the other has any affect on the friction.

This testing was performed by subjecting a gate valve to pressure locking conditions, as opposed to subjecting small specimens of the valve material to pressure locking loads. The testing also operated the gate valve in the opening direction only. Nonetheless, the response of Stellite 6 following exposure to air (stroke number 1 through 6) and the subsequent increase in the frictional characteristics of the material following heating (stroke number 7 and greater) demonstrate that friction testing at an elevated temperature will immediately increase the friction and avoid the need to repeatedly cycle the valve surfaces in order to stabilize the friction.

4.10 Changes in Friction Due to Magnetite

Both types of accelerated aging methods produced oxide films with either distinct nodules or crystals on the surface. The crystals present in the high-pH case were identified as iron-rich,

and although the crystals appear to be present discretely on the specimen (Figure 20), the presence of iron was detected through the film thickness. For this reason, we postulate a possible dissolution or precipitation mechanism. Based on the AES results shown in Figure 30, we expect that the oxide film developed on specimens aged using an anodic current would be iron-rich as well, probably in the form of magnetite (Fe_3O_4). The presence of iron in the oxide films of these accelerated aging specimens corresponds with higher friction coefficients, as compared with the natural aging specimens. The cause/effect relationship suggested here is likely, though not certain.

If it is possible for magnetite to form in the corrosion autoclave at accelerated aging conditions, and then to precipitate on the Stellite 6 surfaces as the oxide film grows, then it is also possible that in a BWR plant, where there is a measurable amount of magnetite flowing in the system (there are filters to remove it), magnetite could precipitate on the valve seats and become embedded in the oxide film. The presence of magnetite precipitant would cause some increase in the valve operating

requirements as a result of the increased friction coefficient. Indeed, this effect may explain some of the reported discrepancies between valve tests in the plant and laboratory data generated in very clean environments.

There is some information in the literature regarding the solubility of magnetite as a function of pH and temperature (Takamatsu et al., 1990; Sweeton and Baes, 1970). This information indicates that if there are local differences in fluid temperature or chemistry (pH), magnetite can dissolve at some locations and precipitate at other locations.

From the results to date, we conclude that the maximum friction obtained during the first stroke of the naturally aged specimens should be considered most applicable to RWCU valves in BWRs. The applicability of the friction coefficients for the oxide films grown under accelerated aging conditions depends on the extent to which iron-rich particles or other stray particles are present on in-plant valves. We know of no currently available data on the composition of the oxide film for in-plant Stellite 6 surfaces. However, since there is a measurable amount of magnetite flowing in BWR systems, the presence of magnetite in the oxide film is possible and should be considered.

5. SUMMARY OF TEST RESULTS

The results of the aging tests show the presence of a very thin oxide film after very short exposure times of only a few days. The results of the friction tests show that even a very thin oxide film causes an increase in friction. Although the thickness of the oxide film may influence the friction, the key to being able to safely operate a valve is not necessarily based on the thickness or thinness of the oxide film, but rather on the mechanical properties of the oxide film as the Stellite 6 surface ages.

The results of both the Phase I and the Phase II testing show that the friction increases as the specimens age. The friction during the Phase I testing showed no evidence of stabilizing after 78 days of aging. However, the friction during the Phase II testing did stabilize prior to 120 days of aging.

In general, the first stroke shows higher friction than succeeding strokes. The difference is greater for some specimens than for others. The decrease in the friction coefficient with continued stroking is probably caused by a change in the surface condition of the specimens due to plastic deformation or fracturing of the crystals. The results indicate that the first stroke a valve experiences after it has been allowed to age and establish an oxide film will result in the highest coefficient of friction and therefore require the highest stem thrust to successfully operate the valve. This result has important implications for valves being subjected to in-plant testing: such in-plant tests need to collect data from the very first stroke a valve experiences following a period of inactivity, and data from subsequent strokes will be less relevant to valve operability and plant safety.

The results of the AFM and X-ray diffraction analyses at NIST indicate that the surface of the oxide film contains crystalline solids within an amorphous substrate. The composition of the solids was not determined, but is expected to be chromium oxides, cobalt

oxides, or carbides. Crystalline solids in general are very abrasive and can result in high friction between the moving surfaces, analogous to rubbing two pieces of sandpaper together. Longer aging times correspond with larger crystalline grains and higher friction.

Although the single data point obtained in this study suggests that the simulated valve wedging would slightly decrease the expected friction, the difference is small. Before a definitive claim can be made as to either a small decrease in the friction, or no effect due to the simulated valve wedging, it would be prudent to obtain additional data to verify the direction and magnitude of the effect.

The composition and surface structure of the oxide films grown using acceleration techniques (anodic current and high pH) differ from those formed during natural aging. Large granular structures, iron enrichment, cobalt in the film, and additional oxide particles were observed in the accelerated tests. Considering these differences, oxide films produced by the acceleration methods are not representative of those produced by natural aging in the laboratory. However, the oxide films grown using acceleration techniques may be considered relevant to plant operations if highly oxidizing potentials can occur in the plant, if pH excursions can occur, or if magnetite or other stray particles are deposited on and incorporated into the oxide films on the Stellite 6 sealing surfaces of the valves.

The results from the high-pH test indicate that precipitation of aging products on valve sealing surfaces from aging elsewhere can increase the friction, a phenomenon that might occur in a plant environment. We know of no currently available data on film composition or thickness for in-plant Stellite 6 surfaces, but the presence of magnetite on the oxide film on valve hardfacing is possible and should be considered.

6. CONCLUSIONS

This report describes a series of tests that investigate the frictional characteristics of Stellite 6 surfaces as they age. Stellite 6 specimens were aged in a corrosion autoclave, the oxide films were examined and characterized, and the specimens were subjected to friction testing in a friction autoclave. A very thin oxide film formed after only a few days of natural aging. Even a very thin oxide film caused an increase in friction. The surface structure of the oxide film was dominated by a hard crystalline structure, such that the frictional response was analogous to rubbing two pieces of sandpaper together. The friction of the naturally aged specimens was observed to increase initially, but eventually stabilize.

Based on this research, the following conclusions should be considered when evaluating the effectiveness of long term valve programs.

1. The exposure of Stellite 6 surfaces to a BWR reactor coolant system environment

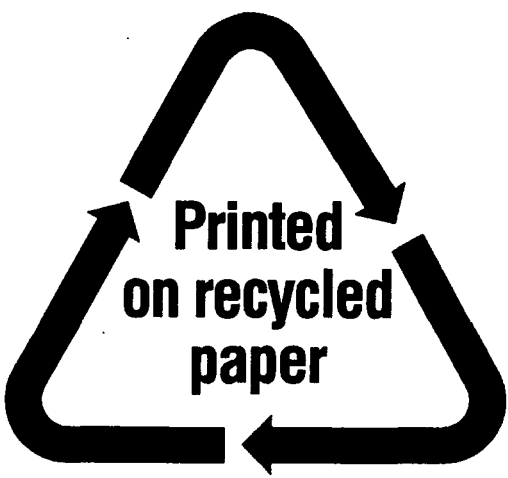
causes the oxide film to grow. The growth of the oxide film in turn causes the friction to increase. The friction was observed to increase during the initial 90 days in the reactor coolant system environment and stabilize prior to 120 days.

2. The initial valve stroke after a period of inactivity will have the highest friction. The friction will be reduced during subsequent strokes as the oxide film is removed.
3. Periodic valve operation does not appear to have a significant effect on friction. However, such periodic valve operation will have an impact if performed shortly before a measured test.
4. Accelerated aging techniques were investigated, however the resulting oxide films were not representative of the oxide film produced during natural aging.

7. REFERENCES

- DeWall, K. G. and R. Steele, Jr., 1989, BWR Reactor Water Cleanup System Flexible Wedge Gate Isolation Valve Qualification and High Energy Flow Interruption Test, NUREG/CR-5406, EGG-2569.
- DeWall, K. G., J. C. Watkins, M. G. McKellar, and D. L. Bramwell, 1998, Results of Pressure Locking and Thermal Binding Tests of Gate Valves, NUREG/CR-6611, INEEL/EXT-98-00161.
- Honda, T., E. Kashimura, K. Ohashi, and Y. Furutani, 1987, "Corrosion of Ferrous Materials and Deposition of Trace Metal Ions in High Purity Water at High Temperature," Corrosion Engineering 36, No. 5, pp. 257-266.
- Steele, R. Jr., K. G. DeWall, J. C. Watkins, 1991, Generic Issue 87: Flexible Wedge Gate Valve Test Program, NUREG/CR-5558, EGG-2600.
- Sweeton and Baes, 1970, "Solubility of Magnetite and Hydrolysis of Ferrous Ion in Aqueous Solutions at Elevated Temperatures," Journal of Chemical Thermodynamics 2, p. 479.
- Takamatsu, H., K. Matsueda, K. Onimura, K. Arioka, S. Tokunaga, and K. Katsura, 1990, "IGA/IGSCC Propagation Behaviors of Alloy 600," Proceedings of the 4th International Degradation of Materials in Nuclear Power Systems - Water Reactors.

NRC FORM 335 (2-89) NRCM 1102, 3201, 3202		U.S. NUCLEAR REGULATORY COMMISSION BIBLIOGRAPHIC DATA SHEET (See Instructions on the reverse)	1. REPORT NUMBER (Assigned by NRC, Add Vol., Supp., Rev., and Addendum Numbers, if any.) NUREG/CR- 6807 INEEL/EXT-02-01021
2. TITLE AND SUBTITLE Results of NRC-Sponsored Stellite 6 Aging and Friction Testing		3. DATE REPORT PUBLISHED MONTH YEAR March 2003	4. FIN OR GRANT NUMBER W6593
5. AUTHOR(S) J. C. Watkins, K. G. DeWall		6. TYPE OF REPORT Technical	7. PERIOD COVERED (Inclusive Dates)
8. PERFORMING ORGANIZATION - NAME AND ADDRESS (If NRC, provide Division, Office or Region, U.S. Nuclear Regulatory Commission, and mailing address; if contractor, provide name and mailing address.) Idaho National Engineering and Environmental Laboratory P.O. Box 1625 Idaho Falls, ID 83415-3129			
9. SPONSORING ORGANIZATION - NAME AND ADDRESS (If NRC, type "Same as above"; If contractor, provide NRC Division, Office or Region, U.S. Nuclear Regulatory Commission, and mailing address.) Division of Engineering Technology Office of Nuclear Regulatory Research U.S. Nuclear Regulatory Commission Washington, DC 20555-0001			
10. SUPPLEMENTARY NOTES Jerry E. Jackson, NRC Project Manager			
11. ABSTRACT (200 words or less) This report documents the results of recent tests sponsored by the Nuclear Regulatory Commission (NRC) and performed by the Idaho National Engineering and Environmental Laboratory (INEEL). These tests investigate the changes that occur in the friction as the Stellite 6 surfaces age and develop an oxide film. Stellite 6 specimens were aged in a corrosion autoclave, the oxide films were examined and characterized, and the specimens were subjected to friction testing in a friction autoclave. The results of the aging tests show the presence of a very thin oxide film after very short exposure times of only a few days. The results of the friction tests show that even a very thin oxide film causes an increase in friction. Although the thickness of the oxide film may influence the friction, the key to being able to safely operate a valve is not necessarily based on the thickness or thinness of the oxide film, but rather on the mechanical properties of the oxide film as the Stellite 6 surface ages. The results of both the Phase I and the Phase II testing shows that the friction increases as the specimens age. The friction during the Phase I testing showed no evidence of stabilizing after 78 days of aging. However, the friction during the Phase II testing did stabilize prior to 120 days of aging.			
12. KEY WORDS/DESCRIPTORS (List words or phrases that will assist researchers in locating the report.) Motor-operated valve (MOV), Stellite 6, friction, aging		13. AVAILABILITY STATEMENT Unlimited	14. SECURITY CLASSIFICATION (This page) Unclassified (This report) Unclassified
		15. NUMBER OF PAGES	16. PRICE



Federal Recycling Program

UNITED STATES
NUCLEAR REGULATORY COMMISSION
WASHINGTON, DC 20555-0001

OFFICIAL BUSINESS
PENALTY FOR PRIVATE USE, \$300